Use of comatuslactone to modulate microbial biofilms

Von der Fakultät für Lebenswissenschaften

der Technischen Universität Carolo-Wilhelmina zu Braunschweig

zur Erlangung des Grades einer

Doktorin der Naturwissenschaften

(Dr. rer. nat.)

genehmigte

D i s s e r t a t i o n

von Maira Peres de Carvalho
aus Porto União, Brasilien

1. Referentin: Prof. Dr. Petra Dersch
2. Referent: Prof. Dr. Dietmar Schomburg
eingereicht am: 16.12.2013
mündliche Prüfung (Disputation) am: 01.04.2014

Druckjahr 2015

Vorveröffentlichungen der Dissertation

Teilergebnisse aus dieser Arbeit wurden mit Genehmigung der Fakultät für Lebenswissenschaften, vertreten durch die Mentorin der Arbeit, in folgenden Beiträgen vorab veröffentlicht:

Publikationen

Carvalho, M. P. and Abraham, W.R. Antimicrobial secondary metabolites from fungi. *In*: Natural Antimicrobials in food safety and quality. Cambridge: CAB international 1: 105-113 (2011).

De Carvalho, M. P. and Abraham, W.R. Antimicrobial and Biofilm Inhibiting Diketopiperazines. Current Medicinal Chemistry 19: 3564-3577 (2012).

Tagungsbeiträge

Carvalho, M.P. & Abraham, W.R. Use of Basidiomycotina fungi to modulate microbial biofilms. (Vortrag). NTH Bottom up Symposium, Clausthal-Zellerfeld, Germany (2011).

Carvalho, M.P. & Abraham, W.R. Use of comatuslactone to modulate microbial biofilms.(Poster). Internationale Drei-Länder-Tagung, Deutsche Gesellschaft für Mykologie, Drübeck, Germany (2012).

Carvalho, M.P. & Abraham, W.R. Use of comatuslactone to modulate microbial biofilms.(Vortrag). COST Action [CM0804] event: Management Committee Meeting an Final Workshop, CM0804, Natural Products and the Biological Context, Izmir, Turkey (2013).

Gedruckt mit Unterstützung des Deutschen Akademischen Austauschdienstes

Acknowledgments

I am truly indebted and thankful to my supervisor Dr. Wolf-Rainer Abraham, who gave me the opportunity to work in his group with my beloved fungi, guiding me during the course of this work. To Dr. Gabriella Molinari, for her valuable advices. To Dr. Stephanie Libnow, who spent a considerable time introducing me to the HPLC, as well as for providing coffee and cookies, warming up the winter days. To Dr. Heinrich Lünsdorf and Ingeborg Kristen, for generating the electron microscopy images. To Christel kakoschke for the NMR measurements. To Dr. Maximiliano Gutierrez, Dr. Cristiane Carvalho and Dr. Cristina Vazquez for the directions concerning the handling of the confocal microscope. To Dr. Florenz Sasse, Bettina Hinkelmann and Raimo Franke for performing the cytotoxicity assays and the bioinformatics evaluations. To Dr. Melissa Wos-Oxley and Dr. Rolf Kramer for their assistance regarding the statistical analysis. To Dr. Amélia Silva, for her help and advices about some molecular biology methods.
I am also grateful to the examiners of this work, for their responsiveness and time: Prof. Dr. Dietmar Schomburg, Prof. Dr. André Fleißner, Prof. Dr. Petra Dersch and Prof. Dr. Marc Stadler.
Also, I would like to acknowledge the CMIK or ex-CMIK colleges, in special Esther Surges, Bettina Klug, Enno Michaelis and Dr. Andréia Estrela for all the technical support, fruitful discussions and good work atmosphere. To the students and scholars Linn, Daniel and Florentin, who contributed to this project. To the Brazilian trainees Matheus Weiler do Amaral and Patrick Türck, who helped me with the experiments, always showing interest and willing to learn.
I wish to thank my family, particularly my parents, for all the support during these years in Germany. Special thanks to the TT group, especially Márcia, Marina, Alexito and Giuseppe for the fun and relaxed moments. Thanks to my friends, Marina, Mariana, Rafael and my cousin Geórgia, for the virtual support. I am also very thankful to Alexander Börries, for his patience, dedication and help.
I am obliged to DAAD, for financial support.

Abstract

Biofilms are structured microbial communities where microorganisms are embedded in a matrix of extracellular polymers (EPS) and can adhere to inert and living surfaces. The interfaces where biofilms can form include several medical devices, such as heart valves, catheters and implants. The failure of medicine to treat emergent infectious diseases caused urgent seeking for alternative therapies. Furthermore, pathogens organized in biofilms are much more resistant to antibiotics than planktonic ones. Biofilms are recognized to be involved in more than 80% of all microbial infections, being characterized by persistent inflammation and tissue damage. These infections are caused by pathogenic or opportunistic microorganisms combined with a chronic disease.

A number of essential elements, indispensable for biofilm formation and maintenance have been evaluated as targets for the development of new drugs. As a result of an ancient co-existence with prokaryotes, it is reasonable to hypothesize that some eukaryotes, such as plants and fungi, have developed protection systems based on secondary metabolites capable of modulating biofilm formation and QS systems. Therefore, fungi collected in Germany were subjected to a screening for biofilm modulators.

Within this work, a small lactone produced by *Coprinus comatus* was purified and its structure elucidated. This compound, comatuslactone, showed a broad spectrum bacteriostatic activity. When biofilms of *Pseudomonas aeruginosa* and *Staphylococcus aureus* were treated with comatuslactone a severe damage as well as *P. aeruginosa* biofilm dispersal could be visualized using confocal laser scanning microscopy with live/dead®staining. Although no inhibition on biofilm formation could be proved, experiments carried out using reporter strains based on homoserine-lactone *quorum sensing* systems, revealed that this compound influences bacterial communication by blocking *quorum sensing* in the homoserine-lactone pathway. Additionally, this compound inhibited pyocyanin and rhamnolipid B production. Moreover, 6 roridins and fusidic acid were purified from *Calcarisporium arbuscula* cultivation. Their structures were solved using NMR and their biological activities have been assessed.

Zusammenfassung

Biofilme sind strukturierte mikrobielle Gemeinschaften, in denen die Mikroorganismen in einer Matrix aus extrazellulären Polymeren eingebettet sind und die an unbelebte und belebte Oberflächen binden können. Die Oberflächen, an denen sich Biofilme bilden können, umfassen auch viele Medizinprodukte wie Herzklappen, Katheter oder Prothesen. Die zunehmenden Probleme der Medizin, neu auftretende Infektionskrankheiten zu bekämpfen, verursacht eine breite Suche nach neuen Therapiemöglichkeiten. Hinzu kommt, dass in Biofilmen organisierte Pathogene viel resistenter gegenüber Antibiotika sind als planktonische. Bei etwa 80% aller mikrobiellen Infektionen nimmt man an, dass Biofilme beteiligt sind, was zu persistierenden Entzündungen und Gewebeschäden führt. Solche Infektionen werden durch pathogene oder opportunistische Mikroorganismen in Kombination mit chronischen Erkrankungen verursacht.

Eine Reihe essentieller Mechanismen, unerlässlich für die Biofilmbildung oder dessen Erhaltung wurden als Ziele für die Entwicklung neuer Medikamente untersucht. Es ist vernünftig anzunehmen, dass einige Eukaryoten wie Pflanzen oder Pilze als Ergebnis der uralten Ko-existenz mit Prokaryoten Schutzmechanismen entwickelt haben, welche auf Sekundärmetaboliten beruhen, die Biofilmbildung und quorum-sensing Systeme beeinflussen. Daher wurden in Deutschland gesammelte Pilze auf solche Biofilm-Modulatoren untersucht.

In dieser Arbeit wurde ein kleines, von *Coprinus comatus* gebildetes Lakton aufgereinigt und in seiner Struktur charakterisiert. Diese Verbindung, Comatuslakton, zeigte ein breites Spektrum von bakteriostatischen Aktivitäten. Wenn Biofilme von *Pseudomonas aeruginosa* oder *Staphylococcus aureus* mit Comatuslakton behandelt wurden, wurden schwere Schäden, bzw. bei *P. aeruginosa* auch die Auflösung des Biofilms im konfokalen Laser-Rastermikroskop bei live/dead®Färbung beobachtet. Obwohl keine Inhibierung der Biofilmbildung beobachtet wurde, zeigten Experimente mit Reporter-Stämmen, dass die Verbindung die bakterielle Kommunikation über die Blockade des *quorum-sensing* auf dem Homoserinlakton-Wege bewirkt. Weiter blockiert Comatuslakton die Pyocyanin und rhamnolipid B Produktion. Ausserdem wurden sechs Roridine und Fusidinsäure aus *Calcarisporium arbuscula* Kulturen gereinigt, die Strukturen mittels NMR aufgeklärt und die biologischen Aktivitäten bestimmt.

Contents

List of Figures

List of Tables

List of abbreviations

^{1}H - NMR	Hydrogen nuclear magnetic resonance
^{1}H - ^{1}H COSY	H - H correlation spectroscopy
^{13}C-NMR	Carbon nuclear magnetic resonance
^{1}H - ^{13}C COSY	H - C correlation spectroscopy
3-oxo-C_6-HSL	N-oxohexanoyl-L-homoserine lactone
3-oxoC_{12}-HSL	N-3-oxododecanoyl-L-homoserine lactone
ACN	Acetonitrile
AHL	N-acyl homoserine lactone
APS	Ammonium persulfate
BAF	Biotin aneurin folic acid
BHI	Brain heart infusion
CASO	Casein soja pepton
CCD	Charged coupled device
CD_3OD	Deuterated methanol
$CDCl_3$	Deuterated chloroform
CLSM	Confocal laser scanning microscopy
DAD	Diode array detector
DAPI	4,6-diamino-2-phenylindole
DMEM	Dulbecco's modified Eagle media
DMSO	Dimethyl sulfoxide
DNA	Deoxyribonucleic acid
dNTP	Deoxynucleotide triphosphate
ESI	Electrospray ionization
EtBr	Ethidium bromide
EtOAc	Ethyl acetate
HTS	High throughput screening
ITS	Internal transcribed spacer
MNM	Melin Norkrans modified
MOPS	3-(N-morpholino) propanesulfonic acid
MRM	Multiple reaction monitoring
MS	Mass spectrometry
MS/MS	Tandem mass spectrometry
MTT	3-(4,5-dimethylthiazol-2-yl)-2,5-diphenyltetrazolium bromide
Na_2- EDTA	Ethylenediamine tetraacetic acid disodiumsalt dehydrated

NMR	Nuclear magnetic resonance
PB	Phosphate buffer
PBS	Phosphate buffered saline

Chapter 1

Introduction

1.1 Biofilms

Bacteria are frequently found living in highly organized and complex communities instead of single cells. In fact, most of them show a preference in existing in these peculiar associations and are capable to switch among two different lifestyles: individual cells (planktonic state) and biofilms. Transition between one state to the other is regulated by a variety of physiological and environmental features, such as bacterial cell density, shear forces and nutrients availability [1, 2].
Biofilms are defined as microbial cells, attached irreversibly to biotic or abiotic surfaces. They usually occur as communities and are enclosed in a highly hydrated self-produced slime matrix, named extracellular polymeric substances (EPS matrix), constituted of exopolysaccharides, proteins, surfactants, glycolipids, membrane vesicles, extracellular DNA and ions such as Ca^{2+}. Bacterial biofilms are composed of a dry volume of approximately 10% of cells and 90% of the EPS matrix varying with environmental conditions. They represent a protected mode of growth that allows bacterial survival in a hostile environment and can involve a single microbial species or several species. Global transcriptomic profiling has shown that growing in biofilms cause bacteria to change their gene expression and behavior when compared to the planktonic cells [1, 2, 3, 4, 5].
Solid-liquid interfaces provide optimal environmental conditions for the attachment, colonization and growth of microorganisms. Therefore, bacteria growing on biofilms are recognized as a severe threat to the medical, industrial, engineering and agricultural sectors of the economy, causing billions of dollars losses annually [4, 5, 6, 7]. On the other hand biofilms are very useful, e. g. in cleaning rivers, processing our wastewater in sewage plants, degrading our food in the gut or in protecting our skin against pathogens.

1.1.1 Biofilm structure and development

The structure of a biofilm shows a substantial complexity, even resembling tissues of eukaryotic organisms. Knowledge about the biofilm complex architecture was first achieved through confocal scanning laser microscopy (CSLM) experiments. Hereby, bacterial cells growing inside the EPS matrix, interspersed with water channels could be observed [2, 5].
A biofilm development is a high elaborated process, which starts from surface recognition,

is regulated by bacterial communication and ends on colonization of new environments. This process undergoes several steps, which are commonly seen to occur in the following sequence (Fig. 1.1):

- Step 1. Initial cellular attachment to the surface (reversible attachment) - this stage is characterized by a loose interaction between cells and surface. The cells are surrounded by a small amount of EPS, and independent movement can still be noticed, such as twitching and gliding. Some cells leave the surface again and adopt the planktonic lifestyle [3, 8, 9].
- Step 2. Irreversible attachment. Here the cells produce a higher amount of EPS matrix, which is a variable element and its composition differs according to the species of microorganisms and environmental factors. In a general aspect, the EPS matrix
  - promotes cellular adhesion to the colonized surfaces
  - enables bacterial cells assemblage and maintains biofilm stability
  - captures organic and inorganic nutrients
  - digests exogenous macromolecules, as also the EPS matrix itself, due to its enzymatic activity
  - improves genetic information exchange
  - retains water by hydrogen bonding, protecting the biofilm against dehydration
  - shields the biofilm, conferring protection against oxidants, pH shifts, toxins, predators, host defenses during infection, antimicrobial agents and disinfectants [8, 9].
- Step 3. Development of biofilm architecture. After the irreversible attachment, the biofilm starts to grow acquiring either a flat or a mushroom shape [9].
- Step 4. Biofilm maturation. During this stage, the development of the typical complex architecture of biofilms is achieved, containing water channels and pores, together with the further spreading of bacteria inside the EPS matrix, away from the surface. The architecture of mature biofilms can vary from flat, homogenous to highly structured biofilms, characterized by empty spaces and towers of cells confined in the EPS matrix. Water channels improve organic and inorganic nutrient uptake and transport and assure metabolic waste and toxic products removal. Several factors have been shown to influence biofilm architecture, including motility, EPS matrix components and surfactant (e. g. rhamnolipid) production [8, 9, 10].
- Step 5. Dispersion. Mechanical damage or physiological processes, such as *quorum sensing* can induce biofilm detachment. Essentially, biofilm dispersal is a natural mechanism which allows the bacteria to colonize other environments. Three particular biofilm dispersal patterns can be recognized: a) swarming dispersal: individual bacterial cells simply leave the biofilm after dissolving the EPS, adopting

the planktonic lifestyle until another surface is recognized; b) clumping dispersal: bacterial aggregates are released and start a new colonization (sloughing) and c) surface dispersal: biofilm moves over the already colonized surface, increasing its area [6, 8, 9, 10].

Cells growing in biofilms are physiologically distinct from planktonic cells, and also vary from each other according to the biofilm development. In a mature biofilm, exclusive niches can be established, which arise from nutrients chemical gradients, metabolic activities of bacteria, waste and toxic products, as also signaling compounds. Bacteria living inside a biofilm change their gene expression and physiological processes. Hence, they adapt to particular regions within the biofilm, and are able even to select for advantageous mutant phenotypes that can preferably survive under a certain environmental condition [1].

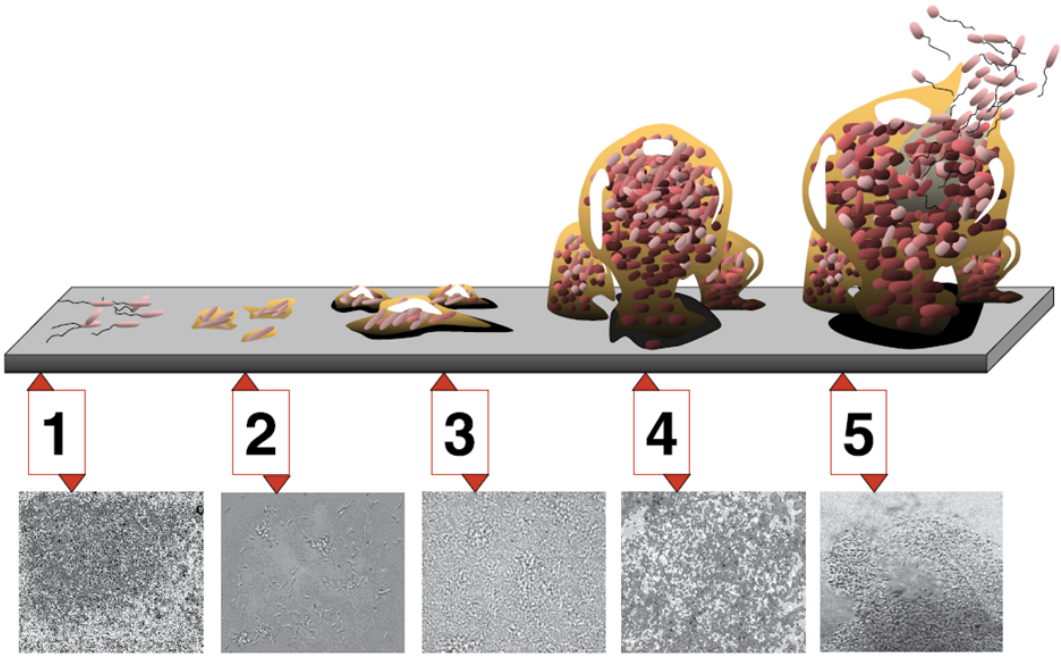

Figure 1.1: Steps of biofilm formation. Source: Monroe *et al.* 2007 [11].

1.1.2 *Quorum sensing* (QS)

In 1970, Nealson *et al.* [12] after studying bacterial bioluminescence, showed that light emission does not initiate immediately after media inoculation, but after the presence of a considerable number of bacterial cells. Afterwards, in 1981, Eberhard *et al.* [13], isolated and identified the compound N-(3- oxododecanoyl)-L-homoserine lactone, postulating that this molecule could work as a specific genetic regulator, which acts after its own excretion and accumulation into the culture medium. The terminology *quorum sensing* (QS) was proposed by Fuqua *et al.* 1994 [14], to explain the phenomenon of bacterial cooperative behavior. QS is a communication mechanism used by many bacterial species to perceive and respond to a multitude of environmental factors. Among the several QS systems known to date, the QS mediated by the production and subsequent recognition

of the small molecules called autoinducers - e. g. N-acyl homoserine lactone (AHL), for Gram-negative and small oligopetides for Gram-positive bacteria - are the most studied (Fig. 1.2) [15].

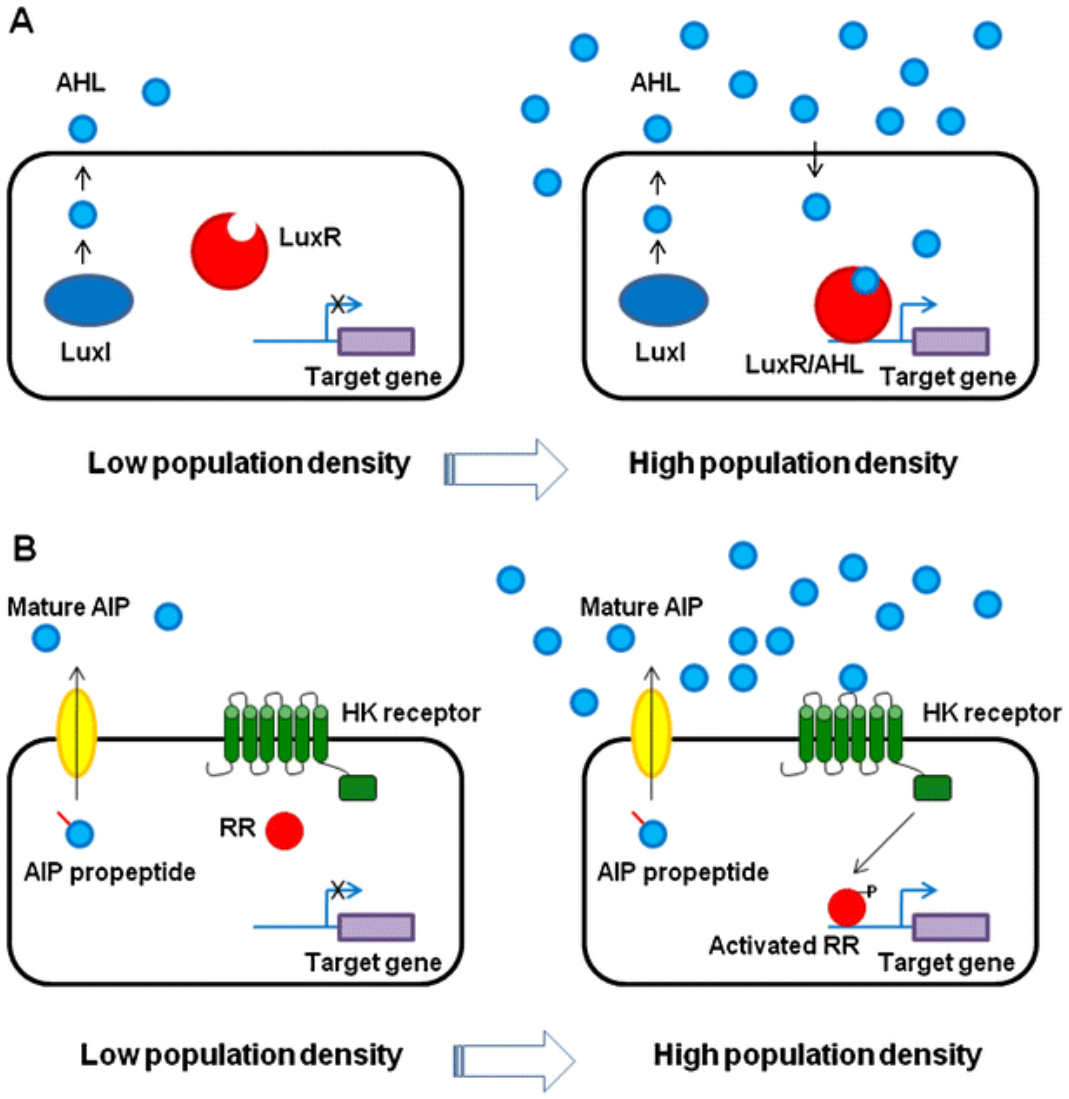

Figure 1.2: Bacterial (QS) systems. A. Gram-negative QS. AHLs are secreted to the environment, initiating the expression of target genes after the achievement of a threshold concentration. B. Gram-positive bacteria QS systems. Small peptides are used as autoinducers [16].

Concerning the AHLs structures, the homoserine lactone ring is conserved and binds to the acyl moiety through an amine. Differences occur in the length and in the substituents at the 3-position of the acyl chain, which varies between 4 and 16 carbons, generally by addition of two-carbon moieties. The acyl chain can bear at C-3 a carbonyl, a hydroxyl group or be fully reduced. This AHL diversity arises from an abundance of AHL synthases in the bacterial world, therefore some microorganisms produce only one type of AHL, while other species produce a large variety of these compounds [17, 18].

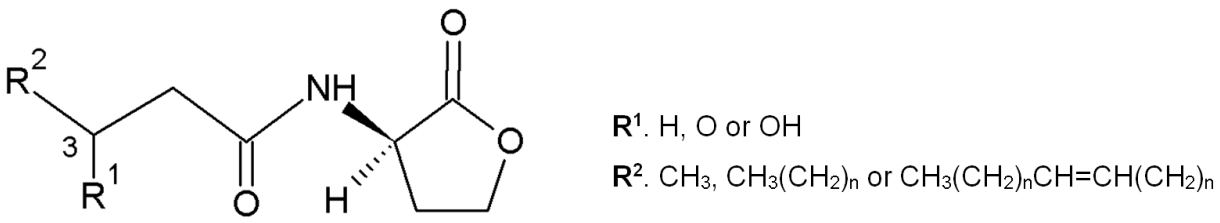

Figure 1.3: Structure of AHLs. Adapted from Churchill *et al.* 2011 [18].

Small, linear or cyclic peptides, are used in QS systems of Gram-positive bacteria (Fig. 1.3). These peptides are secreted actively via an ATP-Binding Cassette (ABC) transporter complex. When a threshold concentration is achieved in the environment, the autoinducer peptides bind to a histidine kinase sensor, located on the bacterial membrane, causing its auto-phosphorylation. Next, the phosphate group is transferred to a regulator response protein, which has the capability of binding to DNA, therefore initiating the expression of QS controlled genes [19, 20].

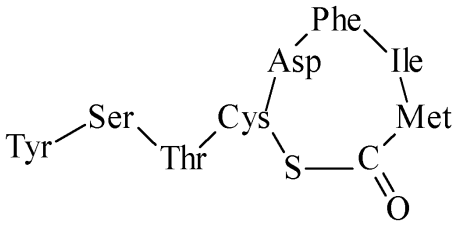

Figure 1.4: Example of an oligopeptide autoinducer, used by *Staphylococcus aureus* [20].

Changing gene expression allows bacteria to perform particular behaviors only when existing in a community but not when living alone as a single cell. The majority of the behaviors controlled by QS systems are productive only when a group of bacteria express them in synchrony; these behaviors include bioluminescence, EPS matrix production, sporulation, conjugation, pigment and antibiotic production [14, 15, 16]. However, in pathogenic microorganisms these changes in gene expression allow bacteria also to coordinate the expression of virulence factors, such as enzymes and toxins. A number of molecules, produced via QS systems have the ability of minimizing the impact of the host immune system until a proper number of microorganisms develops in order to establish infection [15, 21].

1.1.3 Clinical relevance of biofilms

Biofilms are recognized to be involved in more than 80% of all microbial infections, being characterized by persistent inflammation and tissue damage. These infections are caused by pathogenic or opportunistic microorganisms combined with a chronic disease. A large number of diseases are related to the presence of biofilms, and some examples are dental

caries, periodontitis, chronic infection of the middle ear, chronic rhinosinusites, chronic tonsillitis, endocarditis, fasciite, wound infections in burned patients, urinary and biliary tract infections, osteomyelitis, pneumonia, including the majority of cases of patients with cystic fibrosis [22, 23, 24, 25]. Macfarlane and Dillon 2007 [26] and Rosenvinge *et al.* 2013 [27] discussed in reviews the role and implications of biofilms on gastrointestinal conditions and cited several diseases which could be related to biofilm formation and persistence.
Bacteria growing as biofilms are often associated with medical devices, characterizing a new disease named chronic polymer-associated infection. *Staphylococcus* spp. followed by *Pseudomonas aeruginosa* are commonly related with infections on artificial bone implants, intravenous catheters, heart valves, pacemakers, ventricular assist devices, synthetic vascular grafts and stents, urinary and orthopedic prostheses and contact lenses [3, 28].
One of the major challenges in the clinics is providing an assertive diagnosis between an infection caused by a biofilm or by planktonic cells. Culture dependent methods are often not sufficient to detect chronic biofilm infections, occasionally showing a negative result even when severe symptoms related to bacterial infections are diagnosed. Molecular methods, which are demonstrated to be high sensitive to accurate cases of a biofilm infection, should be conducted always when an infection suspicion is present [23, 24, 25, 28]. Therefore, several criteria were proposed by Hall-Stoodley and Stoodley 2009 [24], Parsek and Singh 2003 [25] and Fux *et al.* 2003 [29] to a better distinction between infections caused by planktonic cells or biofilms. According to these criteria, an infection caused by a biofilm, should: a) be caused by microorganisms associated to biotic or abiotic surfaces, including several types of epithelium and/or medical devices; b) show the presence of aggregated cells in clusters or inside a EPS matrix, visible through direct examination of the infected tissue; c) be restricted to a particular site in the host; d) be recalcitrant to antibiotic treatments; e) show culture-negative results despite strong infection symptoms; e) have an ineffective host clearance, evidenced by the presence of bacterial aggregates associated with inflammatory cells in the host tissue.
Since bacterial presence stimulates immune response, biofilm infection symptoms may be present, although they usually originate from planktonic cells or microbial metabolites, such as toxins. The immune mediated response leads to damage of the surrounding tissues, but generally the host defense mechanisms fail to resolve biofilm infections [24, 25].
Conventional antibiotics therapy typically shows some efficacy against biofilms infections, usually improving the symptoms caused by detached cells or aggregates. Nevertheless, eradication of biofilm infections using conventional antibiotic therapies generally fails, and recurrent symptoms are common, even after cycles of antibiotic therapy. The results of this colonization are persistent infections that are hard and even impossible to treat, leading to severe health complications and longer hospital stays [29, 30].

1.1.4 Antibiotic resistance of biofilms

Antibiotic sensitive bacteria can extremely reduce their susceptibility when growing inside a biofilm. Experiments of biofilms grown *in vitro* , also demonstrated an elevated reduction on antibiotic susceptibility, suggesting that resistance is not achieved through mutations or mobile genetic elements, nor connected with host factors. When bacteria restore the planktonic lifestyle, the sensitivity against antibiotics is also rapidly restored, show-

ing that biofilms possess peculiar resistance mechanisms. Compared with free-swimming cells, biofilms resist clearance by the host immune system and display increased resistance to antimicrobial agents. Up to 1000-fold resistance (compared to planktonic cells) against antibiotics, heavy metals and disinfectants have been reported. Hence, the necessary doses of antibiotics to eradicate a biofilm infection will frequently exceed the maximum tolerable doses, making the treatment, in most of the cases, not feasible [3, 5, 28].
Several concomitant factors occur in order to confer biofilm resistance against antibiotics:

- the biofilm EPS matrix may work as an adsorbent or reactant, reducing the amount of antibiotic available for interaction with the bacterial cells, mostly with the bacteria that are located in the center of a biofilm. As biofilms are mainly constituted by water, relatively small compounds, with the molecular weight of antibiotics can freely pass through the matrix. However, antibiotics can be inactivated by enzymes present in the EPS matrix, such as beta-lactamases, or be sequestered by binding, in the case of aminoglycosides [31, 32].

- reduced metabolic and growth rates exhibited by bacteria which are growing in biofilms, particularly those deep inside the community. On the surface of a biofilm, the oxygen concentration is higher than in its core. This induces the generation of chemical gradients, which leads to an increase of slow growing and persistent cells. Under convenient environmental conditions, persistent cells can repopulate a biofilm. Moreover, gradients in pH, caused by accumulation of acidic metabolic products may have a negative impact on antibiotic efficacy [32, 33].

- biofilm cells are physiologically distinct from planktonic bacteria, and express specific protective factors, such as multidrug efflux pumps, upregulation of porin proteins expression and stress responses. Bacterial cells adapt themselves to local variations inside a biofilm, changing their gene expression and consequently their physiological activities. Cell growth, protein synthesis, and metabolic activities are stratified within a biofilm and mutation or recombination arises [1, 32].

Therefore, the majority of antibiotics which are capable to eradicate actively growing and dividing bacterial cells failed completely against persistent and slow growing cells. This coupled with the protection that the EPS matrix displays may explain the failure of most of the available antibiotics treatment on clearing a biofilm infection.

1.1.5 Preventing and treating a biofilm

Preceding aggressive antibiotic administration and impregnation of medical devices with antimicrobial agents are conventional approaches used in the clinics to prevent bacterial attachment to surfaces and subsequent biofilm formation. For example chlorhexidine/silver sulfadiazine showed to decreased microbial medical devices colonization in clinical trials [33, 34].
When a biofilm is already established in the host, chronic suppressive antibiotic treatment and removal of the infected device are the main strategies used in the clinics to control the infection. In particular cases, medical devices removal is possible, but monetary investments and complication risks of a surgery have to be carefully evaluated. On

the other hand, prostheses, pacemakers and cardiac implants are difficult and sometimes even impossible to replace, putting emphasis on the need of optional and more effective therapies. Moreover, the treatment of a biofilm infection requires combinations of multiple antibiotics, which are administrated in elevated doses for a prolonged period of time, often causing severe side effects. A short treatment with minimal antibiotic doses, usually applied to control acute infections, is greatly discouraged due to the risk of resistance induction. Within this statement, a correct diagnostic, differentiating a biofilm from an infection caused by planktonic microorganisms, is crucial to a successful treatment approach decision [31, 32, 33, 34].

1.1.6 Research Strategies for controlling biofilm infections

A number of essential elements, indispensable for biofilm formation and maintenance have been evaluated as targets for the development of new drugs [35, 36, 37]. Therefore, several approaches have been proposed to control such infections: a) use of antimicrobial peptides - several peptides have the property of disrupting membrane stability, showing a potential to target the slow growing cells which are found inside the biofilms; b) antiadhesion agents - some compounds possess the ability of blocking bacterial attachment to surfaces, consequently preventing biofilms formation (e. g. pilicides); c) bacterial polysaccharides - a number of bacterial exopolysaccharides have the characteristic of inhibiting and/or dispersing biofilms assembled by other species; d) *quorum sensing* inhibition, a phenomenon called *quorum quenching* (QQ) - interrupting bacterial communication prevents the expression of virulence factors, biofilm architecture and maintenance and in some bacterial species, even biofilm formation. A combined administration of an antibiotic for killing the dispersed organisms and a *quorum sensing* inhibitor could be successful; e) chelating agents destabilize biofilm architecture; f) D-amino acids and norspermidine - both are shown to work synergistically to disassemble biofilms, acting through different mechanisms; g) phage therapy - specific phages lyse bacterial cells and produce enzymes, more specifically, polysaccharide depolymerases which have the ability on degrading the biofilm EPS matrix; h) vaccines and antibodies - both are being evaluated aiming the prevention of biofilm infections. Many antibodies are in distinct stages of clinical trials; i) high-throughput screening (HTS) processes and chemical libraries screening are also being performed in order to identify new candidates which display activity against biofilms [35, 36, 37, 38, 39, 40].
In addition already approved antibiotics also have shown to inhibit elements necessary for biofilm formation. One example is azithromycin, which is inactive against planktonic *P. aeruginosa*, but is able to delay biofilm development and to affect bacterial cell communication. Gentamicin was proved to be effective against persistent cells, but only when administrated in combination with fructose, glucose, manitol and pyruvate. A gentamicin and mannitol, when applied synergistically, showed to be effective on treating urinary biofilms infections in a mice model. Combinations of rifampicin and vancomycin, daptomycin or levofloxacin have been successfully evaluated *in vitro* , but the high doses necessary to eradicate a biofilm remain a constant concern [41, 42, 43, 44].
The currently available methods used for the treatment of biofilm infections are insufficient and demonstrate a high failure rate. Improvements in this field, including new therapies which specifically prevent biofilm formation or actively eradicate already exist-

ing biofilms, are urgently needed. Besides these numerous interesting research strategies, infections caused by biofilms still prevail as a critical threat to human health. Furthermore, no small molecules targeting formation and/or eradication of biofilms are currently on clinical trials [38, 39].

1.2 Natural products

The discovery of bioactive microbial secondary metabolites and their introduction into the clinic caused a revolution in the medical field. In the past decades, population longevity increased and pain and suffering caused by several diseases diminished. Numerous natural products and their respective synthetic derivatives were successfully generated for medical use, covering many therapeutic fields. They are the most important agents applied on the treatment of infectious diseases, providing a multitude of chemical structures coupled with an abundance of biological activities. Due to co-evolution processes, the lead molecules originated from natural products frequently display an increased activity and adaptation to biological systems than the ones arising from pure laboratorial synthetic chemistry approaches [39, 40, 45, 46, 47, 48].
Although new chemical entities and promising bioactive lead molecules candidates are being continuously discovered, most of the big pharmaceutical companies have restraint their programs on natural products discovery. Synthetic combinatorial chemistry allied with HTS technologies were believed to be a preferred strategy to discover unknown and useful molecules for medicinal use. A number of companies invested heavily in these approaches, and, without the expected success, finished their activities on natural products development. The result we have nowadays is a crisis in the field of anti-infective agents, with a lower rate of this type of medicines introduced in the market combined with a higher rate of bacterial resistance. Notably, the research on anti-infective agents is still being performed by a few pharmaceutical companies, small biotechnology companies, research institutes and academic laboratories worldwide [48, 49, 50, 51].

1.2.1 Eukaryotes as a natural source of biofilm modulators

As a result of an ancient co-existence with prokaryotes, it is reasonable to hypothesize that some eukaryotes, such as plants and fungi, have developed protection systems based on secondary metabolites capable of modulating biofilm formation and QS systems. Following this rational, a number of natural products which exhibit the capacity of inhibiting or dispersing bacterial biofilms were already identified [52, 53, 54]. In 1993, de Nys *et al.* [55] isolated halogenated furanones from the macroalga *Delisea pulchra* (Rhodophyta). These compounds possess several biological activities and are capable of inhibiting a number of QS-controlled phenotypes, including swarming motility of *Serratia liquefaciens*, toxin production of *Vibrio harveyi* and bioluminescence of *Vibrio fischeri*. Furanones (Fig. 1.5) can also inhibit QS systems in *P. aeruginosa*, and it has been demonstrated that a derivative (C-30) (Fig. 1.2B) downregulates expression of more than 80% of the QS-regulated genes, many of them encoding virulence factors [53, 54, 55]. The marine alga *Laminaria digitata* produces and secretes the oxidized halogenated compounds hypochlorous and hy-

pobromous acids, which react with AHLs, destroying the signaling molecule [57].

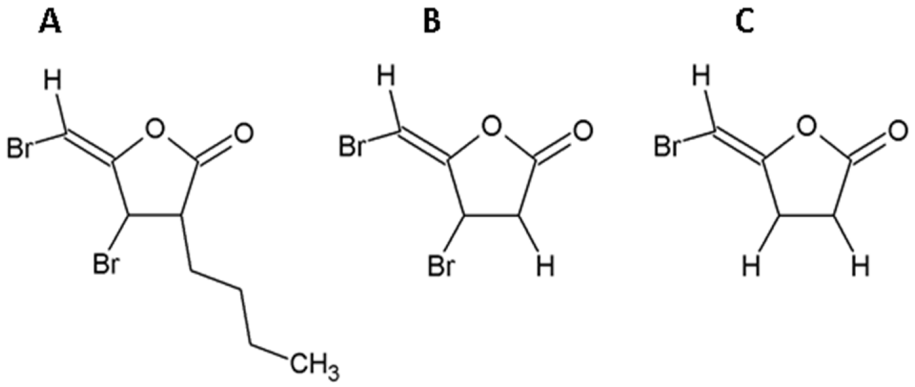

Figure 1.5: Chemical structures of furanones. A. Natural furanone, isolated from the algae *D. pulchra*; B and C. Synthetic furanone derivatives [55, 57].

Plants such as carrots, garlic, habanero (chili), and water lily produce compounds that interfere with bacterial QS systems. Garlic extracts were demonstrated to be able to clear pulmonary *P. aeruginosa* infections in mouse models, and ajoene was recognized as the major QS inhibitor. Allicin, a very well-known antibacterial compound extracted from garlic, did not show any interference with QS systems of *P. aeruginosa*. The result of interference with QS systems are dispersed and thinner biofilms, more accessible to antibiotic therapies and to the host immune system. Moreover, a decrease in the production of virulence factors such as pyocyanin and rhamnolipids was demonstrated in the presence of QQ compounds. Furthermore, cranberry extracts were also shown to inhibit biofilm formation of Gram-positive and Gram-negative bacteria [52, 58, 59, 60, 61, 62, 63, 64, 65]. Furanones, compounds from garlic, polymers and many other molecules capable of inhibiting QS systems have been used as a scaffold for synthetic combinatorial chemistry libraries. Modifications on the acyl chain substituents, on the lactone ring and synthesis of analogues are the most common used approaches to generate compounds effective against QS systems of bacteria [66].

1.2.2 Bioactive metabolites from fungi

Fungi are capable of producing a broad range of molecules, which vary from simple to high complex structures. Normally, these metabolites are biosynthesized for specialized physiological, social or protective reasons, conferring environmental advantages to the producer. Mycelia and fruiting bodies contribute differently to the life cycle of a fungus, where the vegetative mycelia responsible for substrata colonization and nutrient uptake and the fruiting bodies, usually short-lived forms, for the reproduction. Mycelia are exposed to nutrient and space competitors, including bacteria and other fungi, whereas the fruiting bodies need protection against parasites, insects, mammals and other kind of predators. Consequently, these both entities need to secure themselves against environmental animosities. Therefore, fungi have evolved several chemical defense mechanisms, which confer protection against the threats of the environment [67, 68, 69, 70].

Since the discovery of penicillin the importance of fungal metabolites in the search for new drugs has been demonstrated. Beside the enormous biodiversity of fungi, they possess peculiar and uncommon biosynthetic pathways, generating complex and new chemical scaffolds. A number of products from these pathways are important compounds used in the clinics and are also lead molecules for a semisynthetic approach: (i) beta-lactams antibiotics, such as penicillins, cephalosporins, monobactams and carbapenems; (ii) antifungal agents, like griseofulvin, echinocandins and pneumocandins; (iii) the antihelmintic PF1022A; (iv) antilipidemic statins, such lovastatin, mevastatin and their synthetic analogs and the immune-supressive cyclosporine [71, 72, 73].
Besides these molecules which are used for medical treatments, numerous others structures, belonging to diverse chemical classes and displaying several kinds of biological activities have been isolated from fungal sources. Here, a few examples, grouped according on their building blocks, leading to three classes, are given [45, 74].

- Polyketides
  Polyketides comprise the most abundant class of secondary metabolites produced by fungi, possessing from simple to highly diverse and complex structures. They are synthesized by sequential reactions catalysed by polyketide synthases, assembling carboxylic acids monomers, usually acetate and propionate. Alterations on the carbon skeleton can develop previously, on the course and subsequently of chain assemblage, giving rise to the vast array of fungal polyketide structures. The outcome compound depends mostly on type and amount of biosynthetic precursors applied in the reactions [46, 71, 75, 76].
  Both beneficial, used for human health and agricultural proposals, and harmful compounds, such mycotoxins are present in this class. Moreover, several secondary metabolites displaying a variety of biological activities have been continuously isolated from fungal sources, such as polyacetylenes, styrylpyrones, lactones and azaphilones (Fig. 1.6) [71, 75, 76, 77, 78, 79].

Biformin

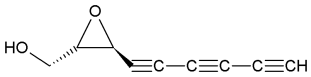

Antibacterial activity

Producer: *Polyporus biformis a* [80, 81].

10-Hydroxy-undeca-2,4,6,8-tetraynamide

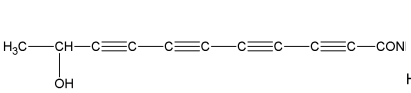

Antibacterial, antifungal, cytotoxic activity

Producer: *Mycena viridimarginata* [82, 83, 84].

Agrocybin

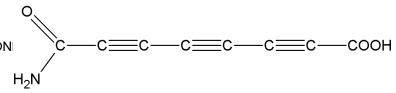

Cytotoxic, trypanocidal, immunosuppressive

Producer: *Agrocybe dura Marasmius* [84, 85, 86].

Frustulosin

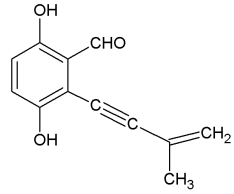

Antibacterial activity

Producer: *Stereum frustulosum* [81, 84, 87, 88].

Hispolon

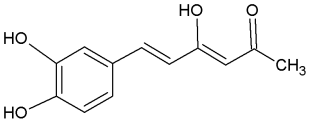

Antiviral activity

Producer: *Inonotus hispidus* [81, 84, 87].

Chrysodin

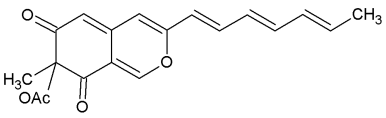

Antifungal activity

Producer: *Sepedonium chrysospermum* [91, 92].

Strobilurin A

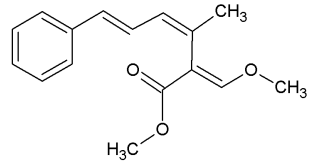

Fungicide

Producer: *Agaricus* sp., *Mycena* spp., *Strobilurus* spp. [84, 93].

Agaricoglycerides A and B

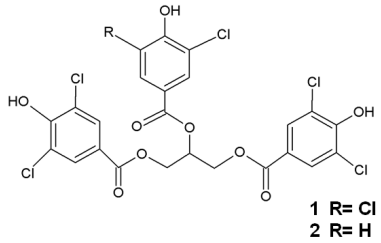

Analgesic properties

Producer: *Agaricus* spp., *Hebeloma* spp.*Psathyrella* spp.*Stropharia* spp. [94].

Bulgarialactones 1 and 2

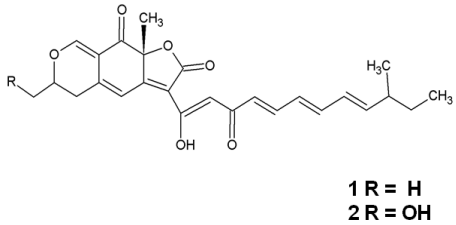

Antibacterial activity

Producer: *Bulgaria inquinans* [95].

L-1

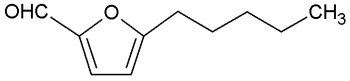

Nematocidal activity

Producer: *Irpex lacteus* [84, 96].

Cinnabarin

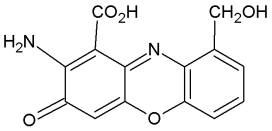

Antibacterial, antiviral, antioxidant activities

Producer: *Pycnoporus sanguineus* [81, 97, 98].

Figure 1.6: Examples of polyketides produced by fungi.

- Nonribosomal peptides (NRPs).
  A large number of fungal secondary metabolites are non-ribosomally assembled pep-

tides, generated by multimodular enzymes, the non-ribosomal peptide synthetases. NRPs are differentiated from the other chemical classes by the wide range of amino acids incorporated into their structures. Numerous biological activities, like antimicrobial, QS regulators, immunosuppressive (cyclosporine) and antiviral were linked to compounds from this group of natural products. β-lactam antibiotics, diketopiperazines, siderophores, peptaibols and the ergot alkaloids comprise some examples of this type of compounds (Fig. 1.7) [74, 99, 100].

Mca

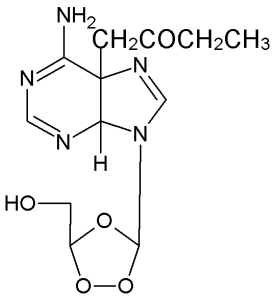

Antiviral activity

Producer: *Macrocystidia cucumis* [101].

Nebularine

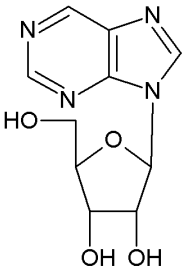

Activity against *Mycobacterium* spp.

Producer: *Clitocybe nebularis* [84].

Cylindrocyclin A

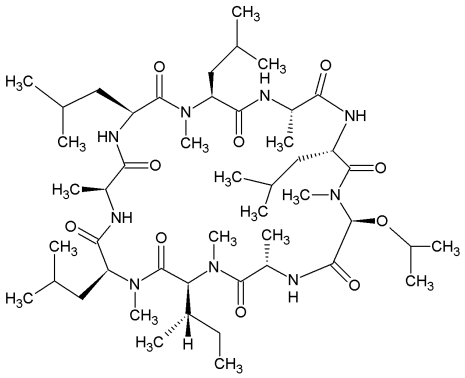

Cytotoxic activity

Producer: *Cylindrocarpon* sp. [102].

L-α-aminoadipyl-L-cysteinyl-D-valine

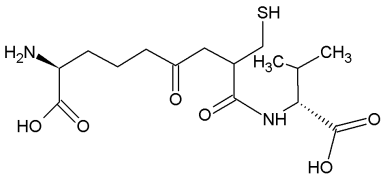

ÎŠ-lactam antibiotics precursor

Producer: *Penicillium chrysogenum (Acremonium chrysogenum)* [74].

Epicoccin G

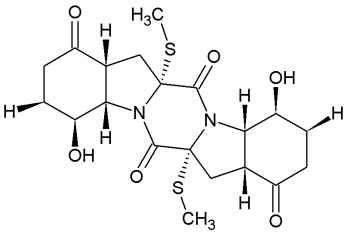

Antiviral activity

Producer: *Epicoccum nigrum* [103].

Cyclo(Pro-Val)

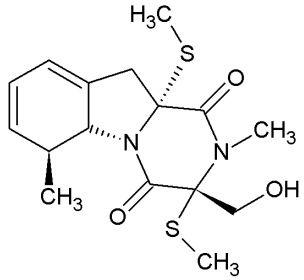

Antibacterial activity

Producer: *Colletotrichum gloeosporioides* [104, 105].

Figure 1.7: Examples of NRPs produced by fungi.

- Terpenoids
  Terpenes are composed of C_5 isoprene units, linked in a "head-to-tail manner". Their classification is based on the number of isoprene units: monoterpenes (C_{10}), sesquiterpenes (C_{15}), diterpenes (C_{25}), triterpenes (C_{30}) and tetraterpenes (C_{40}).

Their structures can be linear, cyclic, saturated or unsaturated and the isoprene units can also be linked to another type of carbon skeleton. Terpenes diversity is due to the large amount of terpene synthases. This class of compounds demonstrates numerous biological activities, including antibacterial, antifungal, antiviral and cytotoxic (Fig. 1.8) [74, 106].

Collybial

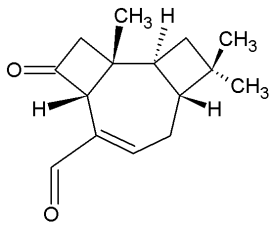

Antiviral and antibacterial activity

Producer: *Collybia confluens* [84, 106, 107].

Wickerol A and B

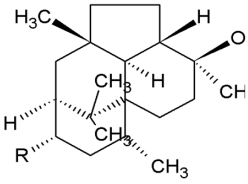

1 R = H
2 R = OH

Antiviral activity

Producer: *Trichoderma atroviride* [108].

Phellodonic acid

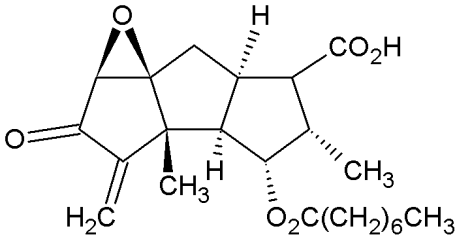

Antibacterial, antifungal, algicidal

Producer: *Phellodon melaleucus* [84, 109].

Ganoderic acid

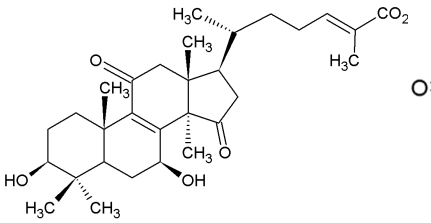

Antiviral activity

Producer: *Ganoderma lucidum* [81, 110].

Hypnophilin and Desoxyhypnophilin

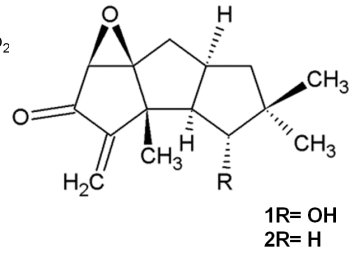

1R= OH
2R= H

Antibacterial and antiparasitic activity

Producer: *Lentinus crinitus, L. strigosus, Pleurotellus hypnophilus* [84, 106, 111, 112, 113].

Cheimonophyllal

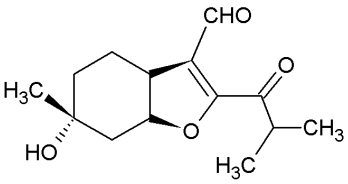

Nematocidal activity

Producer: *Cheimonophyllum candidissimum* [84, 114].

Enokipodin C

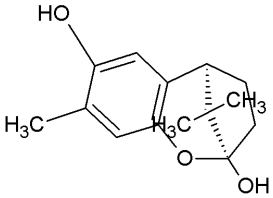

Antibacterial activity

Producer: *Flammulina velutipes* [115].

Sterelactone C

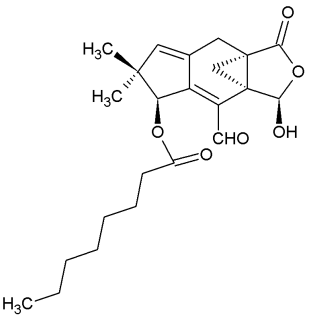

Antibacterial, antifugal and cytotoxic activity

Producer: *Stereum* sp. [116].

Lentinellic acid

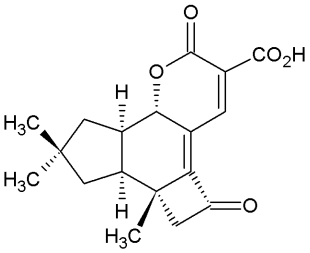

Antibacterial and cytotoxic activity

Producer: *Lentinellus omphalodes, L. ursinus* [84, 106, 117].

Figure 1.8: Examples of terpenoids produced by fungi.

1.2.3 Fungi as biofilm modulators

Information about fungi metabolites capable of inhibiting QS and biofilm formation are scarce in the literature. Following the lessons learned from the past concerning the genus *Penicillium* as a prolific source of secondary metabolites, fifty strains were screened for compounds which could modulate *P. aeruginosa* QS systems, leading to the identification of patulin and penicillic acid as inhibitors. In 2012, Scopel *et al.* [118] showed that *Staphylococcus epidermidis* biofilm could be inhibited by the presence of the diketopiperazine cis-cyclo(Leucyl-Tyrosyl), isolated from a marine *Penicillium* sp. Ophiobolins, sesquiterpenes isolated from the marine fungus *Emericella variecolor* could inhibit *Mycobacterium bovis* (BCG) and *M. smegmatis* biofilm formation. Moreover, QS inhibitors were found in mushrooms extracts, were a screen of crude extracts of 14 Basidiomycotina species was performed [119, 120].
The proofed ability to produce a wide variety of bioactive compounds, and the lack of information about metabolites capable to interfere with QS and biofilm formation, makes fungi obvious candidates for screening for quorum-quenching secondary metabolites. Since these organisms may produce such compounds to defend themselves against their natural enemies, it can be expected that this group of organisms produce metabolites which are capable to inhibit bacterial *quorum sensing*. Therefore, the task of this work was to cultivate Basidimycotina collected in Germany and search for compounds able to inhibit biofilm formation.

Chapter 2

Hypothesis and rationale

Bacteria growing on biofilms are recognized as a serious menace to human health, causing chronic and severe diseases. The failure of conventional medical treatments against emerging infectious diseases together with the increasing incidence and severity of such infections has urged seeking for alternative therapies. Within this context, several approaches with the aim of finding more efficient treatments have been discussed.
Since decades, fungi have been demonstrated to be a prolific source of bioactive secondary metabolites, producing a wide range of chemical structures. Their fruiting bodies are exposed to rain and moist climate periods, especially in the German fall, offering an ideal substratum for the establishment of biofilm communities. On the other hand, fungal vegetative mycelia have to compete with several kinds of organisms present in the environment for nutrients and space. It is clear that fungi have self-defense mechanisms which are crucial to efficient substrata colonization and reproduction. Aiming at products used for chemical defense, we exploited compounds from fungal origin for their possible applications for controlling bacterial pathogenic biofilms.

Chapter 3

Objective and specific aims

The main objective of this study was to investigate the biofilm modulatory properties of fungal secondary metabolites. The specific aims were:

- Assessment of microbial communities on surfaces of Basidiomycotina fungi fruiting bodies collected in Germany using the SSCP technique.
- Cultivation of these fungi, taxonomic and molecular identification of the isolates.
- Preliminary screening of crude extracts for antimicrobial and antibiofilm activities.
- Purification of active fractions, identification and characterization of these compounds by NMR and mass spectrometry.
- Evaluation of QS systems inhibitory properties of the isolated compound.
- Assessment of the toxicity of active compounds in eukaryotic tissue culture.

Chapter 4

Material and Methods

4.1 Chemicals

4.1.1 Organic solvents

Acetonitrile (ACN) and methanol (MeOH) - HPLC grade -, acetone, chloroform, dichloromethane, ethanol, ethyl acetate (EtOAc), isopropanol and heptane were purchased from J.T Baker®(Deventer, Holland). Butanol was purchased from Sigma-Aldrich (St. Louis, Missouri, USA). Deuterated chloroform ($CDCl_3$) and methanol (CD_3OD) were purchased from Deutero GmbH (Kastellaun, Germany), acetic acid and formic acid from Carl Roth GmbH (Karlsruhe, Germany).

4.1.2 Organic reagents

Bacteriological agar, malt extract, peptone, tryptone and yeast extract were purchased from Difco (Sparks, Maryland, USA). 3-(4,5-dimethylthiazol-2-yl)-2,5-diphenyltetrazolium bromide (MTT), 3-(N-morpholino) propanesulfonic acid (MOPS), 4',6-diamidino-2-phenylindole (DAPI), bromophenol blue, crystal violet, folic acid, lead citrate, sodium cacodylate, uranyl acetate, xylene cyanol were purchased from Sigma-Aldrich®. Biotin, dimethylsulfoxide (DMSO), ethidium bromide (EtBr), ethylenediamine tetraacetic acid disodiumsalt dihydrated (Na2- EDTA), formamide ($CHONH_2$), formaldehyde (CH_2O), glycine, paraformaldehyde, sodium carbonate (Na_2CO_3), tris HCl and Triton were purchased from Carl Roth GmbH. Bind silane and repel silane were purchased from GE Healthcare life sciences (Uppsala, Sweden). Inositol and thiamine HCl were purchased from Calbiochem (Darmstadt, Germany). N-3-oxododecanoyl-L-homoserine lactone (3-oxoC_{12}-HSL), N-oxohexanoyl-L-homoserine lactone (3-oxo-C6-HSL) and pyocyanin were purchased from Cayman Chemical (Denver, Colorado, USA). Glucose and glutardialdehyde came from Merck (Darmstadt, Germany), tetramethylethylenediamine (TEMED) from Amresco®(Solon, Ohio, USA) and agarose from Lonza (Basel, Switzerland).

4.1.3 Media and antibiotics

Brain heart infusion (BHI), casein-soya-peptone broth (CASO) and potato dextrose broth (PDB) were purchased from Carl Roth GmbH, Mueller Hinton (MH) agar and potato dextrose agar (PDA) from Difco, Dulbecco's modified Eagle Media (DMEM) from Lonza and RPMi-1640, gentamycine and tetracycline from Sigma-Aldrich®.

4.1.4 Antibodies and enzymes

Anti- α-tubulin was purchased from Sigma-Aldrich®and anti-mouse Alexa Fluor 488 from Molecular Probes®, Life Technologies GmbH (Darmstadt, Germany). RNAse was purchased from Macherey-Nagel (Düren, Germany), proteinase K from AppliChem (Darmstadt, Germany) and lambda exonuclease from New England Biolabs (Schwalbach, Germany).

4.1.5 Primers

Primer sets used for fungal identification were purchased from Eurofins MWG Operon GmbH (Huntsville, Alabama, USA). Phosphorylated primer set used for SSCP analysis was purchased from Invitrogen™, Life Technologies GmbH.

4.1.6 Inorganic reagents

Boric acid (H_3BO_3), chlorhydric acid (HCl), magnesium chloride, hexahydrated ($MgCl_2$ x 6 H_2O), heptahydrated magnesium sulphate and anhydrous ($MgSO_4$ x 7 H_2O and $MgSO_4$), manganese sulphate ($MnSO_4$), silver nitrate ($AgNO_3$), sodium chloride (NaCl), phosphoric acid (H_3PO_4), potassium chloride (KCl), disodium hydrogen phosphate (Na_2HPO_4), sodium thiosulfate ($Na_2S_2O_3$), potassium dihydrogen phosphate (KH_2PO_4) and sodium hydroxide (NaOH) were purchased from Carl Roth GmbH. Hexahydrated Ferric chloride ($FeCl_3$ x 6 H_2O), sodium phosphate (Na_3PO_4), osmium tetroxide (OsO_4) and heptahydrated zinc sulphate ($ZnSO_4$ x 7 H_2O) were purchased from Sigma-Aldrich®. Dihydrated calcium carbonate ($CaCl_2$ x 2 H_2O) was purchased from Merck, ammonium persulfate (APS) from Amresco®.
All kits used in this work and chemicals which are not listed above are mentioned together with the supplier in the correspondent method.

4.2 Biological material

4.2.1 Basidiomycotina collection

Fifteen Basidiomycotina species were collected in Braunschweig, Göttingen and Köris, Germany. A tissue fragment from the inner part and from the skin covering the pilleus of the fruiting bodies was frozen in Tris EDTA (TE) Buffer (10 mM Tris, 1 mM EDTA, pH 8.0) for DNA extraction, sequencing and bacterial community analysis.

4.2.2 Bacterial strains

Bacillus cereus DSM 626, *Escherichia coli* DSM 498, *Micrococcus roseus* DSM 20447 and *Staphylococcus aureus* DSM 1104 were purchased from the German collection of microorganisms and cell cultures (DSMZ). *Streptococcus mutans* UA159 was kindly provided by Prof. Irene Wagner-Döbler, *P. aeruginosa* PA14 by Dr. Mathias Müsken, *E. coli* MT102 (pSB403) and *Pseudomonas putida* F117 (pKR-C12) by Prof. Kathrin Riedel.

4.2.3 Yeast strains

Candida albicans DSM 11225, *Candida guilliermondii* DSM 70052, *Candida krusei* DSM 6128, *Candida parapsilosis* DSM 5784, *Candida tropicalis* DSM 70151, *Rhodotorula glutinis* DSM 70398 and *Yarrowia lipolytica* DSM 70561 were purchased from DSMZ.

4.2.4 Eukaryotic cell line

Mouse fibroblast L-929 DSMZ ACC2 was purchased from DSMZ.

4.3 Isolation of fungi

4.3.1 Isolation and mycelia development in different media

Small tissue fragments from the inner part of the collected fruiting bodies were excised and placed on three solid medium: a) Melin-Norkrans Modified (MNM); b) biotin aneurin folic acid agar (BAF) and c) yeast and malt extract agar (YEM), for mycelia isolation. After fungal growth, small pellets were cut and placed into cryotubes containing PDB with 20% of glycerol. The stocks were kept at - 80°C. Mycelia development in four solid medium (BAF, MNM, PDA and YEM) pH 5.0, 7.0 and 9.0 was measured in order to set up the screening conditions. BAF, MNM and YEM components are listed in table 5.12. PDA was obtained commercially.

Table 4.1: Chemical composition of the media used for fungal isolation.

	BAF	**MNM**	**YEM agar**
glucose	30 g	10 g	-
malt extract	-	3 g	20 g
yeast extract	0.2 g	-	3 g
peptone	2 g	-	-
$(NH_4)_2HPO_4$	-	0.25 g	-
KH_2PO_4	0.5 g	0.5 g	-
$MgSO_4.7H_2O$	0.5 g	0.15 g	-
$FeCl_3.6H_2O$	0.01 g	0.012 g	-
NaCl	-	0.025 g	
$ZnSO_4.7H_2O$	0.001 g	-	-
$MnSO_4.4H_2O$	0.005 g	-	-
$CaCl_2.2H_2O$	0.1 g	0.067 g	-
thiamin HCl	50 μg	30 μg	-
biotin	1 μg	-	-
folic acid	100 μg	-	-
inositol	50 μg	-	-
water	1000 mL	1000 mL	1000 ml
agar	15 g	15 g	15 g

4.4 Molecular methods

4.4.1 Fungal identification

DNA from fungal colonies and fruiting bodies was used for PCR amplification and sequencing reaction in order to identify the isolates. DNA was extracted from mycelia and fruiting bodies fragments (10 - 50 mg) using the kit NucleoSpin®PlantII (Macherey-Nagel), as recommended for fungal DNA extraction. Fungal material was incubated in ethanol overnight and cell lysis was performed using sea sand (Merck) and a Fastprep® (MPbiomedicals, Santa Ana, USA) instrument (running time: 45 s, speed: 4.0 m sec^{-1}). Samples were incubated with 10 μl of RNase and proteinase K (10 mg ml^{-1}) for 1 h (optional step). The specific fungal primers set ITS1F - CTTGGTCATTTAGAGGAAGTAA and ITS4 - TCCTCCGCTTATTGATATGC was used for PCR amplification [121].
Amplification was performed in an Eppendorf Mastercycler in a 50 μL reaction mixture containing 5 μL 10 x PCR buffer, 2.5 mM $MgCl_2$, 10 mM dNTP Mix (2.5 mM each), 1 μM of each primer, 35.5 μL Milli-Q®water, 2 μL (15 ng) of DNA template and 0.5 μL Taq polymerase (5000 U ml^{-1}). The following program was used: 35 cycles, initial denaturation: 94°C for 05 min, melting: 94°C for 40 s, annealing: 55°C for 45 s, extending: 72°C for 1 min 30 s, final extension 72°C for 07 min. PCR products were run on a 2% agarose gel for 2.5 h at 100 V using a horizontal gel system (Starlab International, Ahrensburg, Germany). Molecular weight marker IV (Bioline GmbH, Luckenwalde, Germany) was used for fragments size determination. The gels were stained in an EtBr bath for 20 min and visualized under UV light using E.A.S.Y Win32 gel documentation system (Herolab,

Wiesloch, Germany). The bands were excised and purified with a NucleoSpin®ExtractII kit (Macherey-Nagel).
A sequence reaction was performed using the DYEnamic ET Terminator cycle sequencing kit (Amershan Biosciences, Freiburg, Germany) and both primers. The product was purified with a Dye Ex Spin Kit (Qiagen, Hilden, Germany). Amplicons were sequenced at HZI on an Applied Biosystems 377 genetic analyser. The software Sequencher 4.10.1 was used to analyse the obtained sequences.

4.4.2 Evaluation of microbial communities on basidiomas using single strand conformation polymorphism (SSCP) fingerprint

A FastDna®Spinkit for Soil (MPbiomedicals) was used to extract DNA from a fragment of the skin covering the mushroom pilleus. PCR reactions were performed using the eubacterial primers 27F - AGAGTTTGATCMTGGCTCAG- and 521R - Ph - ACCGCGGCTGCTGGCAC, in order to access the bacterial communities through SSCP fingerprint [122, 123]. Amplification was performed in a Eppendorf Mastercycler in a 50 μL reaction mixture containing 05 μL 10 x PCR buffer, 2.5 mM MgCl2, 10 mM dNTP Mix (2.5 mM each), 1 μM of each primer, 35.5 μL Milli-Q®water, 2 μL of DNA template (15 ng) and 0.5 μL Taq polymerase (5000 U ml^{-1}). The following program was used: 30 cycles, initial denaturation: 95°C for 3 min , melting: 95°C for 1 min , annealing: 56°C for 40 s , extension: 72°C 40 s, final extension 72°C for 10 min. PCR products were analysed on a 1.5% agarose gel stained with EtBr.
After purification of PCR reactions using a MiniElute kit (Qiagen) as recommended by the manufacturer, amplicons were digested according to the following reaction: 10 μl of amplicons in elution buffer (EB) were incubated with 2.5 μl of lambda exonuclease buffer (New England Biolabs) and 2.5 μl of lambda exonuclease (5000 U ml^{-1}) at 37°C for 1 h. The resulting phosphorylated single strand was further purified using the same kit. A NanoDrop spectrophotometer (PEQLAB GmbH Biotechnologie, Erlangen, Germany) was used to quantify the DNA obtained from the reaction. A solution containing 100 ng of the single strand DNA, 4 μl of Milli-Q®water and 4 μl of SSCP loading buffer (47.5% formamide, 5mM NaOH, 0,12% bromophenol blue and 0.12% xylene cyanol) was subjected to electrophoresis on a polyacrylamide gel (table 5.13).

Table 4.2: Composition of polyacrylamide gels.

Polyacrylamide gel preparation	
10 x TBE Buffer	6 mL
(891.5 mM tris-base; 889.5 mM boric acid; 22.4 mM Na2 EDTA)	
Bi-destilated water	36 mL
MDE	18 mL
10% APS	240 μL
TEMED	24 μL

Two previous cleaned glass plates were respectively coated with: a) a solution of 3 ml

ethanol p.a.; 30 μl of acetic acid and 30 μl of Bind-silane) and b) 500 μl of Repel-silane. The gel was poured between the glass plates and allowed to polymerize for 2.5 h. Gels were run at 400 V for 16 h at 20°C in a PEQLAB electrophoresis unit and subsequently silver stained, according to Bassam *et al.* 1991 [124]. Briefly, the gel was fixated with a 10% acetic acid solution during 30 min and washed 3 times during 5 min with bi-destilated water. An aqueous solution of 0.1% $AgNO_3$ and 500μl of formaldehyde was used to stain the gel, for 30 min. After washing, the gel was developed using a 2.5% Na_2CO_3 with 500 μl of formaldehyde and 500 μl of a 2% $Na2S_2O_3$ solution. To stop the reaction, the gel was allowed to stand for 10 min in a 2% glycine and 0.5% EDTA aqueous solution. The last step consisted of gel impregnation, using a solution of 10% glycerol during 10 min. A polyester backing paper was used to cover the stained gel. All solutions were prepared using 500 mL of bi-destilated water. Single bands were excised from the polyacrylamide gels and eluted in an SSCP extraction buffer (10 mM Tris-buffer, 5 mM KCl, 1.5 nM $MgCl_2$ x 6 H_2O, 0.1% Triton x 100, pH 9.0) at 95°C for 15 min. The DNA template in this solution was used for a PCR with the 27F-521R primers set. PCR reaction was cleaned with the MiniElute kit and a sequence reaction was performed in the same fashion as described in the 4.4.1.

4.5 Screening for bioactive secondary metabolites

4.5.1 Production of secondary metabolites

The fungi strains BS_HZI4, BS_HZI14, BS_BP1, GÖ_W13, GÖ_W19 and KÖ_S3 showed appropriate growth rate in the tested conditions and were chosen for the secondary metabolites screening. After growth in Petri dishes with YEM agar at 22°C, 5 x 5 mm pellets sized were transferred to 100 ml Erlenmeyer flasks filled with 35 ml of BAF, PDB and YEM broth, pH 9.0, pH 7.0 and pH 5.0. After 14, 21, 28, 35 and 42 days of static incubation, at 20°C and 25°C, in the dark, mycelia were separated from the liquid medium by filtration under vacuum using a Whatman paper n°1. The obtained aqueous extracts were concentrated using a lyophilisator (Martin Christ Gefriertrocknungsanlagen GmbH, Osterode am Harz, Germany), then resuspended in 1.1 ml of Milli-Q®water and tested for their biological activities. Freeze dried culture media was used as control. A total of 121 extracts showed biological activity and the compounds were extracted with organic solvents. Extracts obtained were compared using RP-HPLC/MS and the producing fungi were incubated in 5 L of media in order to obtain a larger amount of the active compounds for structure elucidation and testing.

4.5.2 Liquid - liquid extraction

The obtained supernatant was extracted three times with ethyl acetate, followed by washing with an aqueous sodium chloride saturated solution. In the end, anhydrous $MgSO_4$ was added to the organic fraction, to complete removal of residual water. The remaining aqueous solution was re-extracted using 2-butanol. Extracted fresh autoclaved media were used as background control.

4.5.3 Extraction from mycelia and fruiting bodies

Mycelia obtained from the cultivation of the strains BS_HZI4, GÖ_W13 and GÖ_W19 and fruiting bodies from *Boletus* spp. and *Coprinus* spp. were freeze dried and macerated. The obtained powder was scaled and first extracted with heptane during 7 h, followed by an overnight extraction using ethyl acetate and finishing with an 8 h extraction using methanol. The volume of organic solvent used corresponded to 20% of sample dry weight. Extracts obtained according to 4.4.2 and 4.4.3 items were submitted to solvent organic evaporation at 40°C, on a rotary evaporator and tested for their biological activities.

4.5.4 Reverse Phase-High Performance Liquid Chromatography /Mass Spectrometry (RP-HPLC/MS)

RP-HPLC/MS was carried out on an Agilent 1200 series system (Agilent Technologies, Santa Clara, California, USA), using a C18 analytical column (Nucleosil®125 x 20 mm, Macherey-Nagel), on a gradient condition. A 6460 TripleQuad with electrospray ionization (ESI) was used for Mass Spectrometry. The running conditions were: (solvent A) Milli-Q®water: formic acid (0.1 %) and (solvent B) acetonitrile: formic acid (0.1 %), the gradient started with 5% B at 0 min and 100% B at 15 min; UV absorbance was detected using a diode array detector (DAD) at 210, 230, 254, 260 and 400 nm; flow rate: 0.3 mL min^{-1}. Ionization was performed in the positive and negative modes with the following ion source parameters: N2 flow 9 L min^{-1} and temperature 300°C, nebulizer pressure 25 psi, sheath gas flow 7 L min^{-1} and temperature 300°C, capillary voltage 5000 V and charge voltage 1000 V. The fragmentor voltage was tested from 0 to 150 V, and set on 100 V. An MS scan was performed from 20 to 2000 atomic units. Chromatograms were analysed using Qualitative Analysis Mass Hunter Software (Agilent Technologies).

4.5.5 Fractionation strategies

4.5.5.1 Fractionation using Reverse Phase-High Performance Liquid Chromatography (RP-HPLC)

RP-HPLC fractionation was carried out on an Agilent 1100 series system, coupled with a fraction collection accessory, using a C18 analytical column (Nucleosil®125 x 20 mm) on a gradient condition. Fractions were collected each 0.15 s, on a microtiter plate. The running conditions were set according to 4.5.4. The microtiter plates were allowed to dry under N2 stream. After complete solvent removal, microbiological tests were performed. If chromatograms showed a lack of peak separation or if the biological activity was no further detected, the following fractionation approaches were tested.

4.5.5.2 Fractionation using solid phase extraction (SPE)

C18 (A) and SiOH (B) (Macherey-Nagel) cartridges were eluted using (A) methanol: water (85 : 15), methanol: water (50 : 50), methanol (100); (B) heptane (100), ethyl acetate (100), ethyl acetate: methanol (50 : 50) and ethyl acetate: methanol (30 : 70).

4.5.5.3 Fractionation through molecular weight

The crude extracts were fractionated using Sephadex LH-20 (GE Healthcare) as stationary phase and eluted with methanol. All obtained fractions were tested for their biological activities. Active fractions were analysed using RP-HPLC/MS.

4.6 Purification

4.6.1 Thin layer chromatography (TLC)

Pre-coated glass silica plates (silica gel 60 F264 1 mm, 20 x 20 cm, Macherey-Nagel) were used for normal phase TLC. The solvent system dichloromethane: MeOH (98 : 4) was used to develop the plates. The chromatographic plates were visualized under UV light at 264 nm. Bands were scraped and the compounds extracted with dichloromethane: MeOH (90 : 10).

4.6.2 Semi preparative RP-HPLC

Purification of compounds was carried out on an Agilent 1200 series system, using a C18 column (Varian, Agilent Technologies 250 x 100 mm) and a specific guard column. The method was adjusted according to the results obtained from the analytical experiments and set as follows: for the extract obtained from BS_HZI4 the running conditions were: (solvent A) Milli-Q®water and (solvent B) acetonitrile, the gradient starting with 90% of A at 0 min and 20%B at 20 min. For a fraction obtained from BS_HZI14 a gradient condition was applied using the following running conditions: (solvent A) Milli-Q®water and (solvent B) acetonitrile, the gradient starting with 30% of A at 0 min and 100%B at 15 min. The pure isolated compounds were subject to mass spectrometry and nuclear magnetic resonance (NMR) to elucidate their structures.

4.7 Structure Elucidation

NMR spectra were recorded on a Bruker 400 MHz spectrometer, in $CDCl_3$ and CD_3OD using a 5mm tube (Norell®, Deutero GmbH). Structures were elucidated with ^{1}H- and ^{13}C-NMR including ^{1}H-^{1}H- and ^{1}H-^{13}C-COSY. The already known structures had their ^{1}H spectra recorded and were compared to data from literature.

4.8 Biological activity

4.8.1 Antimicrobial activity

4.8.1.1 Disk diffusion test

C. albicans, E. coli, *P. aeruginosa*, *S. aureus*, were used as target microorganism to assess the antimicrobial activity of the organic extracts and fractions. Antimicrobial susceptibility tests were performed using the Kirby-Bauer method [125]. Briefly, bacteria

were inoculated on Luria Bertani (LB) (10 g.L^{-1} yeast extract, 5 g.L^{-1} tryptone and 10 g.L^{-1} NaCl) and incubated overnight. The broth was further diluted in sterile Phosphate Buffered Saline (PBS) (NaCl 137 mM, 2.68 mM KCl, 10.1 mM Na_2HPO_4, 1.76 mM KH_2PO_4) and inocula adjusted to 0.5 according to the McFarland scale. With a sterile swab (Heinz Herenz, Hamburg, Germany), a plate containing MH agar for bacteria and PD agar for yeasts was uniformly inoculated. A paper disk containing 10 μl of the organic extracts or fractions diluted in 1 mL MeOH was placed in the center of the plate. A disk containing 10 μl of MeOH was used as control. The plates were incubated at 37°C for bacteria and 30°C for yeasts and the inhibition zones were measured after 24 h.

4.8.1.2 Minimal inhibitory concentration (MIC)

Minimal inhibitory concentrations were defined for yeasts and bacteria mentioned in sections 4.2.2 and 4.2.3, using the method of micro-dilution. Briefly, 1x10^8 cells were inoculated in RPMI-1640 and LB medium, for yeasts and bacteria, respectively. After addition of the isolated compounds, serial dilutions were performed in round-bottom, non tissue treated polystyrene microtiter plates (Falcon®Micro Test™). Compound concentrations ranged from 300 μg mL $^{-1}$ to 0.3 μg mL $^{-1}$. MeOH was used as control. After 24 - 48 h of incubation for yeasts and 16 - 24 h for bacteria, 10 μl of each well was inoculated on PD and LB agar to determine antibiotic or static activity.

4.8.1.3 Preparation of bacterial cells for transmission electron microscopy (TEM)

TEM was performed in order to investigate ultrastructural changes in bacterial cells submitted to the active compound. *P. aeruginosa* and *S. aureus* were grown overnight in LB, at 37°C. Tubes were centrifuged and the pellet was washed with PBS. Pellets were resuspended in new media containing the active compound MIC and the controls in a new media with 5 μl of MeOH. After overnight incubation, the tubes were centrifuged and pellets washed with PBS. Cells were fixed in 2.5% glutardialdehyde, buffered with phosphate buffer (PB) (20 mM Na_3PO_4, 150 mM NaCl, pH 7.2), at room temperature for 30 min.

4.8.1.4 Embedding and ultrathin sectioning

After washing in 0.1 x PB, the cells were post-fixed with 1 % OsO_4, in 0.1 M sodium cacodylate, pH 7.0, overnight at 4°C. Cells were immobilized in 2% Difco agar in PB. Dehydration in an acetone series (30, 50, 70, 90 and 100%) was done at room temperature, requiring 20 min for each dehydration step. Infiltration with ERL resin [126] as a resin + acetone mixture (1 + 1) was done at ambient temperature overnight, followed by pure resin infiltration overnight again and finally for 4 h. Probes were transferred into a gelatin capsule and filled with resin monomer. Polymerization was done for 8 h at 70°C. Ultrathin sections were cut with a diamond knife using the Leica Ultracut ultramicrotome (Leica, Heidelberg, Germany) and were picked up with Formvar-coated grids (300 mesh, Cu). Sections were post-stained for 10 min with 3 % aqueous uranyl acetate and for 5 min with 0.5 % lead citrate [127, 128].

4.8.2 Inhibition of biofilm formation

P. aeruginosa, *S. aureus* and *S. mutans* were used in this assay. The experiments were performed in 96-well, flat bottom, polystyrene, non tissue treated microtiter plates (Falcon®Micro Test™, Becton Dickinson labware, Franklin Lakes, USA). After overnight incubation at 37°C, *P. aeruginosa* and *S. aureus* were inoculated in CASO broth, with the inocula adjusted to 0.5 according to Mcfarland scale. For S. mutans, BHI broth was used, and the strain was allowed to grow for 24 h with 5% of CO_2 tension. 100 μl of media containing bacterial cells were pipetted into a microtiter plate with the addition of 50 μl of the aqueous extracts. 4 wells were employed to each aqueous extract. When organic extracts and fractions were used, extracts were diluted in 1 mL MeOH and 10 μl were added to 140 μl of medium. Fresh freeze dried media and media with 5 μl of MeOH were used as control.
The microtiter plates were covered with a sterile adhesive porous paper (Kisker Biotech GmbH, Steinfurt, Germany) and incubated at 37°C for 18 h. After the incubation time, the medium was discharged, the plates washed with PBS and stained for 15 min with a 0.1% crystal violet aqueous solution. The residual stain was removed with successive washing, the plates were air-dried and the biofilm suspended in a solution containing 30% of acetic acid. A plate reader was used to determine the amount of biofilm in the wells, at the absorbance of 595 nm [129]. The amount of biofilm was calculated as follows: Biofilm amount (%) = (Control-Blank)-(Sample-Blank).

4.8.3 Activity on bacterial biofilms

P. aeruginosa and *S. aureus* were incubated overnight and the cell concentration adjusted to $1x10^8$, in CASO broth. Inoculated media (200 μL) was pipetted into the wells on an 8-well glass chamber system (Nunc, Thermo Fisher Scientific, Rochester, New York, USA) for *S. aureus* and an 8-well Permanox chamber system (Nunc, Thermo Fisher Scientific) for *P. aeruginosa*. After 16 h of incubation, wells were washed with PBS and fresh medium with serial dilutions of the active compound was added. Concentration ranged from 300 μg mL^{-1} to 15 μg mL^{-1} for *P. aeruginosa* and from 150 μg mL^{-1} to 15 μg mL^{-1} for *S. aureus*. Fresh medium with 10 μL of MeOH was used as control. The chambers were incubated at 37°C for 18-20 h.
After this period, medium was discharged and the samples washed with PBS to remove planktonic cells. Live/dead®BacLight™bacterial viability kit (Invitrogen™) was used according to the manufacturer instructions. The chambers were detached and the slides visualized under a confocal laser scanning microscope.

4.8.4 *Quorum sensing* inhibition

P. putida F117 (pKR-C12) [130] and *E. coli* MT102 (pSB403) [131] were used to test the isolated compounds against QS systems. *P. putida* F117 (pKR-C12) is based on the *las* QS-system of *P. aeruginosa*, responding to long chain AHLs. *E. coli* MT102 (pSB403) is a strain reporter for genes *lux* of *Vibrio fischeri*, responding to short chain AHLs. After overnight incubation in LB with the respective antibiotics at 30°C, 5 mL of media containing the sensor strains was added to 20 mL of fresh media. Homoserine

lactones were added to the 20 mL of media (50 nM 3-oxoC_{12}-HSL for F117 and 100 nM of 3-oxo-C_6-HSL for MT102), and 5 mL was used as background control. 100 μl were added to the wells of a black microtiter plate (Greiner Bio One GmbH, Frickenhausen, Germany). Serial dilutions of the isolated compounds were performed, within a range of concentration from 250 μg mL $^{-1}$ to 0.025 μg mL $^{-1}$. MeOH was used as control. The plates were incubated at 30°C, and fluorescence and bioluminescence were measured on a multi-mode Synergy 2 plate reader (Bio TeK Instruments GmbH, Bad Friedrichshall, Germany) after 4 and 8 h of incubation. QS inhibition was calculated relative to the control.

4.8.5 Pyocyanin and rhamnolipid B quantification

P. aeruginosa PA14 was allowed to grow overnight. Thereafter, 1 x 10^8 cells were inoculated in LB media, in a microtiter plate. Serial dilutions of the isolated compounds were performed, on a concentration range of 300 μg mL $^{-1}$ to 0.3 μg mL $^{-1}$. MeOH was used as control. After 30 h of incubation, at 37°C, 1 mL of the treated media was extracted with EtOAc (3 times). Control was submitted to the same procedure. Pyocyanin and rhamnolipid B were quantified using HPLC - MS/MS. Here, the target parent ions (211 m/z [M + H]$^+$ for pyocyanin and 652 m/z [M + H]$^+$ for rhamnolipid B) were selected and fragmented with collision energy of 30 V. The two most intense product ions from each selected parent ion were monitored in the multiple reaction monitoring (MRM) mode. Curves using a pyocyanin commercial standard were generated and used to calculate compound concentration by the Quantitative Analysis MassHunter software (Agilent Technologies). Rhamnolipid B concentration was calculated relative to the control.

4.9 Cytotoxicity assays

4.9.1 MTT test

The cytotoxicity of purified compounds was measured using the mouse fibroblast cell line L-929 (DSMZ ACC2). First, cells were grown at 37°C in a humidified 5% CO2 tension incubator in Dulbecco's modified Eagle Media (DMEM) supplemented with 10% fetal bovine serum, during 3 days. Serial dilutions were performed in 96 - well microtiter plates, inoculated with 5 x 10^4 cells and a starting concentration of 30 μg mL^{-1} of the tested compounds. Blank and solvent controls were incubated under the same conditions. After five days of incubation at 37°C, MTT was used to measure growth and viability of cells, which were capable of reducing it to a violet formazan product. Therefore, MTT was dissolved in PBS and added to the each well, giving a final concentration of 0.5 g L^{-1}. The plate was incubated at 37°C during 2 h, the precipitate of the formazan crystals was centrifuged, and the supernatant was discarded. The precipitate was washed with PBS and dissolved in isopropanol containing 0.4% HCl. The microplates were gently shaken for 20 min to ensure a complete dissolution of the formazan, and finally measured at 595 nm using an ELISA plate reader. All experiments were carried out in two parallel experiments. Activity values were calculated as the mean with respect to the controls, which were set to 100% [132].

4.9.2 Impedance measurements

The impedance measurements were performed with small modifications on a RT-CES system (xCelligence) from Acea Biosciences (Roche), which has been described previously [133, 134, 135]. For time-dependent cell response profiling, 60 μL of media was added to a 96-well E-Plate (ACEA biosciences, San Diego, CA, USA) to obtain background readings followed by the addition of 120 μL cell suspension of L-929 cells. After each step, the E-Plates were incubated for 30 min at room temperature and then placed on the reader in the incubator for continuous recording of impedance as reflected by cell index. After 24 h of incubation the cells were treated with the compounds. To prepare the compounds for screening each stock solution (10 mM in DMSO) was diluted with cell media to get a final test concentration of the IC_{90} and less than 0.1 % DMSO. 1 μL of each prepared solution was then transferred into the 96-well E-Plate. Each E-plate contained also wells only with DMSO as a solvent control. All measurements were performed in triplicates and run for 5 d. The time-dependent cellular response profiles (TCRP) were recorded by the Roche RTCA Software, Version 1.2. Data processing and mining workflow was implemented in the statistical programming language R, Version 2.12.2 (R Development Core Team, 2011). The following additional R packages were used in addition: class [136], gplots [137] and MASS [136]. For the development of the R code the integrated development environment R Studio, Version 0.94.92, was used. The workflow starts by importing the raw impedance data which is provided by the RTCA software as cell index (CI) data. The CI is already background corrected and is calculated as follows (Eq. 1) [138]:

$$CI(t) = \frac{R_t - R_b}{Z_n} \tag{4.1}$$

where $CI(t)$ is the cell index at time point t, R_t is defined as measured electrode impedance of the well with the cells in the medium at a certain time point and R_b as measured background impedance of the well with the cell medium alone. Z_n is a frequency factor which corrects for different frequencies of the alternating voltage the xCelligence system can use, the standard setting is $Z_n = 15$. The raw data were imported into R and normalized as suggested by Abassi *et al.* by dividing the cell indices for each time point after compound addition by the cell index at a reference time point (Eq. 2) [135]. As reference time point, the last measurement before compound addition was taken. For further analysis, only the measurements starting at the reference time point (with normalized cell index = 1) and later were considered.

$$NCI = \frac{CI_t}{CI_{t(reference)}} \tag{4.2}$$

The reference compounds and the test compounds with unknown mode of action were measured as triplicates randomly distributed over the microtiter plates (using sampling without replacement in R) to avoid batch effects.

Detection and removal of outliers was carried out using the median polishing procedure. The central idea of the data mining concept is to use cubic smoothing splines for the approximation of the impedance data and as dimension reduction technique. This approach has the benefit of avoiding the curse of dimensionality and the Runge phenomenon that occurs for high polynomials, while keeping the complexity of the data set. The smooth spline function of R was used for TCRP approximation. As set of descriptors, the basis

spline coefficients were extracted to construct a distance matrix that was used for hierarchical cluster analysis. A heatmap was constructed that displays the Z-transformed values of the 22 descriptors (= basis spline coefficients). Hierarchical cluster analysis of the reference compounds together with the compound of unknown mode of action was carried out. Co-clustering of the compound of unknown mode of action with reference compounds with known activity class label was used to predict the mode of action [139].

4.9.3 Eukaryotic cell staining

Cells were grown on cover slips in 4-well plates, test compounds were added after the cells had become semi-confluent and incubated for 24 h. Cells were fixed with 3.7% paraformaldehyde (followed by 0.1% Triton-X 100 treatment for 5 min) or ice cold methanol: acetone (50:50) for 10 min and then washed with PBS. For α-tubulin staining, anti-α-tubulin was added, incubated for 45 min and washed with PBS. Afterwards, anti-mouse Alexa Fluor 488 was added to the cells and incubated for further 45 min. After washing with PBS, 4,6-diamino-2-phenylindole (DAPI) was added and kept at room temperature for 5 min. Cover slips were mounted in anti-fade mounting medium (Molecular Probes®, Life Technologies) and the samples observed under a fluorescence microscope.

4.10 Microscopy methods

4.11 Confocal laser scanning microscopy (CLSM)

CLSM was performed using a Leica TCS SP1 (Leica, Heidelberg, Germany) and Leica Confocal software, version 2.5, Build 1347d. The instrument was equipped with the following laser lines: 405 nm UV line, a multiline Argon laser, a 561 nm yellow diode-pumped solid state laser and a 633 nm HeNe laser, attached to an upright microscope. Biofilm samples were observed with 20 x 0.5 NA and 63 x 0.9 NA oil immersible lenses, using the laser lines 488 nm and 561 nm.
Thickness of biofilms were defined using Z-stacking, where the Z values are set for the beginning and end of a sample. Biofilm damaging was calculated according to the area covered by green or red cells, using the softwares ImageJ and Fiji.

4.11.1 Transmission electron microscopy (TEM)

The samples were examined using an in-column energy-filter transmission electron microscope Libra120plus (Zeiss, Oberkochen, Germany), operated in the elastic bright-field mode with anobjective aperture-set of 60 μm, 120 kV acceleration voltage and an energy-slit set to 12 eV. Micrographs were recorded with a cooled bottom-mount 2048x2048 CCD-camera (Sharp: Eye; Tröndle, Moorenweis, Germany) within the range of x 3000-x 30000 magnification.

4.11.2 Fluorescence microscopy

Images were taken with CCD (charged coupled device) camera attached to a Zeiss Axiophot fluorescence microscope (Carl Zeiss GmbH), using appropriate filter sets.

4.12 Statistical methods

Standard deviation was calculated using the software Origin 9 (Originlab Corporation, Northhampton, MA, USA). Non-parametric multivariate statistical analysis was performed using PRIMER (v.6.1.6, PRIMER-E, Plymouth Marine Laboratory, UK) [140, 141]. A sample-similarity matrix was generated using the modified Bray-Curtis coefficient by comparing presence/absence of bacterial phylotypes.

Chapter 5

Results

5.1 Fungal isolates classification

Basidiomycotina fruiting bodies were collected in Braunschweig, Göttingen and Köris, Germany. Pure cultures were obtained from eleven fungal species. The isolates were classified according to fruiting bodies macroscopic features and sequence analysis of the region containing ITS1, ITS2 and the 5.8S rRNA genes. The identities of the consensus sequence obtained from fungal mycelia were confirmed using BLAST search to known sequences (table 5.14). The strain BS_HZI14 was classified as *Russula emetica*, but the sequence obtained from the mycelia showed 99% of similarity with *C. arbuscula*. *C. arbuscula*is a parasitic fungus, being commonly found in the inner tissues of *Russula* spp. and *Lactarius* spp. [142].

Table 5.1: Classification of the Basidiomycotina fungi according to fruiting bodies macroscopic features and the sequences obtained with ITS1F-ITS4 primers set.

Isolate	**Morphological analysis**	**Sequence (ITS1F-ITS4)**
BS_HZI4	*Coprinus comatus*	*Coprinus comatus*
BS_HZI14	*Russula emetica*	*Calcarisporium arbuscula*
BS_HZI30	*Boletus edulis*	*Boletus edulis*
BS_HZI23	*Boletus aestivalis*	*Boletus aestivalis*
BS_HZI27	*Boletus luridus*	*Boletus luridus*
BS_BP1	*Laetiporus sulphureus*	*Laetiporus sulphureus*
BS_BP5		*Hebeloma incarnatulum*
GÖ_W13	*Macrolepiota* sp.	*Macrolepiota fuliginosa*
GÖ_W19	*Pholiota* sp.	*Pholiota lenta*
GÖ_W29	*Macrolepiota rhacodes*	*Macrolepiota rhacodes*
KÖ_S3	*Macrolepiota procera*	*Macrolepiota procera*

5.2 Bacterial communities associated with mushrooms

The rationale of this work was based on fungi self-defense mechanisms to control bacterial biofilms. Compounds production by these organisms is reported, while there is a lack on the information about bacterial communities related with Basidiomycotina fruiting bodies. Thus, within this work, single strand conformation polymorphism (SSCP) fingerprint was employed to analyze the bacterial composition of those communities. Therefore, 49 fruiting bodies were collected in Braunschweig (BS), Drübeck (DRÜ), Göttingen (GÖ) and Köris (KÖ) and identified according to their morphological characteristics. One individual of each fungal species was submitted to ITS region sequencing. The identified fungi with their respective abbreviation and collection year are shown in table 5.2.

Table 5.2: Fungal species used in the SSCP analysis, together with their respective abbreviation, venue and year of collection.

Fungal Species	**Abbreviation**	**Collection venue/year**
Coprinus comatus	CC1	BS - HZI/2009
C. comatus	CC2	BS - HZI/2010
C. comatus	CC3	BS - Bürgerpark/2010
C. comatus	CC4	BS - Bürgerpark/201
C. comatus	CC5	BS - Bürgerpark/2011
C. comatus	CC6	BS - HZI/2012
C. comatus	CC7	BS - HZI/2012
C. comatus	CC8	BS - HZI/2012
C. comatus	CC9	BS - HZI/2012
C. comatus	CC10	BS - HZI/2012
C. comatus	CC11	GÖ/2010
C. comatus	CC12	DRÜ/2012
C. comatus	CC13	DRÜ/2012
C. comatus	CC14	BS - HZI/2012
C. comatus	CC15	BS - HZI/2012
C. comatus	CC16	BS - HZI/2012
C. comatus	CC17	BS - HZI/2012
Coprinopsis atramentaria	CA1	BS - HZI/2012
C. atramentaria	CA2	BS - HZI/2012
C. atramentaria	CA3	BS - HZI/2012
C. atramentaria	CA4	BS - HZI/2012
C. atramentaria	CA5	BS - HZI/2012
C. atramentaria	CA6	BS - HZI/2012
Coprinopsis picacea	CP1	DRÜ/2012
C. picaceus	CP2	DRÜ/2012

Fungal Species	Abbreviation	Collection venue/year
Macrolepiota fuliginosa	MF	GÖ/2009
Macrolepiota procera	MP	KÖ/2011
Macrolepiota rhacodes	MR	DRÜ/2012
Boletus aestivalis	BA1	BS - HZI/2009
B. aestivalis	BA2	BS - HZI/2009
B. aestivalis	BA3	BS - HZI/2010
B. aestivalis	BA4	BS - HZI/2011
B. aestivalis	BA5	GÖ /2010
B. aestivalis	BA6	GÖ /2010
B. aestivalis	BA7	GÖ /2011
B. aestivalis	BA8	KÖ/2011
B. aestivalis	BA9	KÖ/2011
Boletus aureus	BAu	BS- HZI/2010
Boletus edulis	BE1	BS - HZI/2009
B. edulis	BE2	BS - HZI/2010
B. edulis	BE3	GÖ/2009
Laetiporus sulphureus	LS1	BS - Bürgerpark/2011
L. sulphureus	LS2	BS - Bürgerpark/2011
L. sulphureus	LS3	BS - Bürgerpark/2011
Amanita sp.	AM1	BS - HZI/2010
Amanita sp.	AM2	BS - HZI/2010
Stropharia sp.	SI	BS - HZI/2009
Russula emetica	RE1	BS - HZI/2009
R. emetica	RE2	BS - HZI/2011

To analyze the bacterial communities associated with the collected fruiting bodies, DNA was extracted from the skin which covers the mushrooms hat, and quantified using a NanoDrop spectrophotometer. Herein, DNA concentration varied between 15 ng μl^{-1} and 50 ng μl^{-1}. A PCR reaction was performed using the bacterial universal primers set 27F-521R [126], generating a fragment of approximately 500 bp. The reaction was repeated several times, until the concentration of 100 ng μl^{-1} was achieved. Although displaying enough DNA yields, 18 fungal strains did not show any bacterial DNA amplification and were excluded from the SSCP analysis. With the other 31 samples, a SSCP was performed and silver stained. From those 31 samples, all the bands observed in the SSCP gels were numbered and quantified. SSCP fingerprint allowed the quantification of a maximum of 9 bacterial phylotypes among the mushrooms samples (Fig. 5.1). For phylogenetic and statistical analysis, fungal samples were divided into 5 groups, representing: a) *Coprinus comatus* and *Coprinopsis* spp., b) *Boletus* spp., c) *Macrolepiota* spp., *Russula emetica* and e) mixed genera.

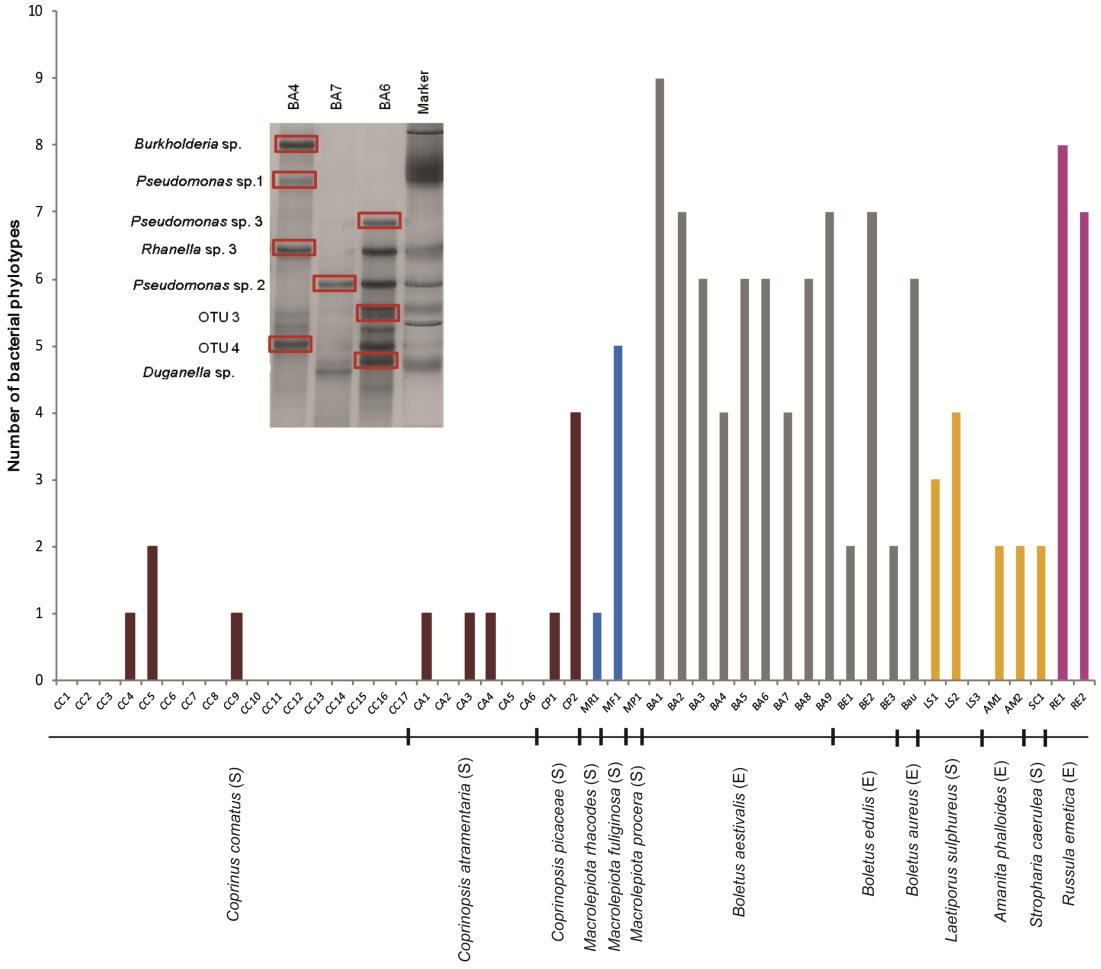

Figure 5.1: Number of bacterial phylotypes detected on 31 mushrooms hats. (S) - Saprophytic species and (E) - ectomycorrhizal ones. A detail of a SSCP gel is shown in the insert.

To identify the members of the bacterial community, SSCP bands were excised and subjected to a new PCR reaction followed by 16 rRNA fragment sequencing. Sequences were analysed using the software Sequencher 4.10. The identity of the consensus 16S rRNA obtained sequences was confirmed using the Seqmatch feature available at the RDP-II database [143]. Multiple sequence alignments were performed using the program Muscle, provided in the software SeaView 4.0 [144]. MEGA 5.0 was used to construct phylogenetic trees, using neighbour-joining method together with Jukes-Cantor model and pairwise deletion of gaps to calculate the evolutionary distance [145]. A total of 1000 bootstrap replications were executed to test for branch robustness.
The identified phylotypes were grouped into 4 phyla and 10 families: 29 gammaproteobacteria (18 Enterobactereaceae, 8 Pseudomonadaceae, 1 Moraxellaceae and 1 Xanthomonadaceae), 13 Alphaproteobacteria (8 Rhizobiaceae, 4 Bradyrhizobiaceae and 1 Acetobactereaceae), 3 Betaproteobacteria (2 Burkholderiaceae and 1 Oxalobactereaceae) and 4 Bacteroidetes/Chlorobi (CFB), all belonging to Flavobacteraceae (Fig. 5.2). No Gram-positive bacteria sequence was detected within the mushroom samples, using SSCP

fingerprint.

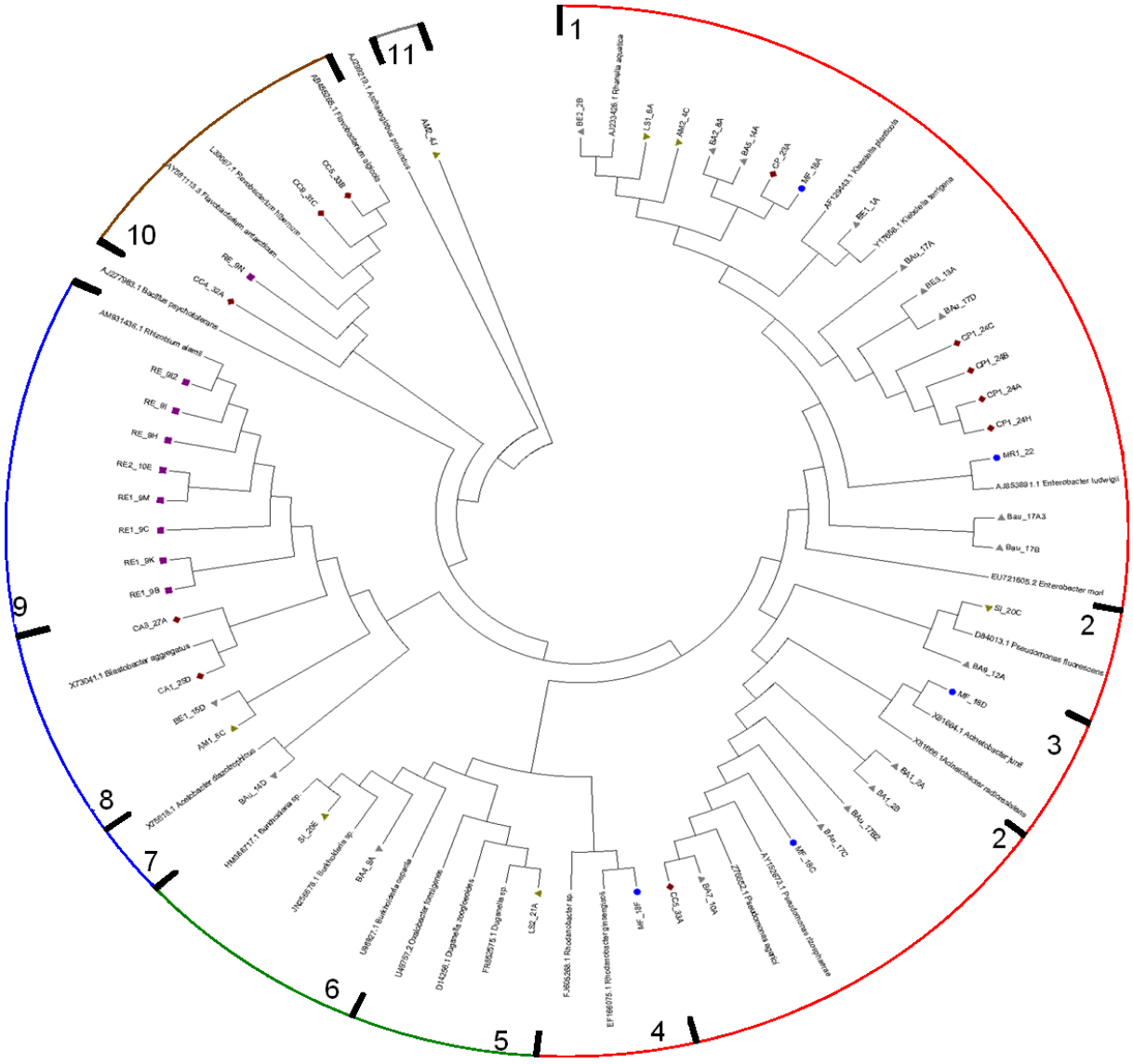

Figure 5.2: Neighbour joining tree of the 16S rRNA fragments sequences, obtained from SSCP fingerprint analysis from 31 mushrooms samples together with reference sequences. Evolutionary distances were computed using the Jukes-Cantor model. The red section of the circle represents the phyla gammaproteobacteria; the green represents the betaproteobacteria; the blue represents the alphaproteobacteria; the brown represents the Bacteroidetes / Chlorobi (CFB) and the grey sector represent a sequence with *incertae sedis*. The numbers represent bacterial families: 1. Enterobactereaceae; 2. Pseudomonadaceae; 3. Moraxellaceae; 4. Xanthomonadaceae; 5. Oxalobactereaceae; 6. Burkholdereaceae; 7. Acetobactereaceae; 8. Bradyrhizobiaceae; 9. Rhizobiaceae; 10. Flavobacteraceae; 11. Incertae sedis. The sequence of *Archaeoglobus* served as outgroup.

The software PRIMER (v.6.1.6, PRIMER-E, Plymouth Marine Laboratory, UK) was used to perform non-parametric multivariate statistical analysis [143, 144]. A binary matrix

(presence/ absence) was generated and subjected to a modified Bray-Curtis similarity measure, in order to compare the presence/absence of each of the 9 bacterial phylotypes distributed over all the 31 mushroom samples [146].

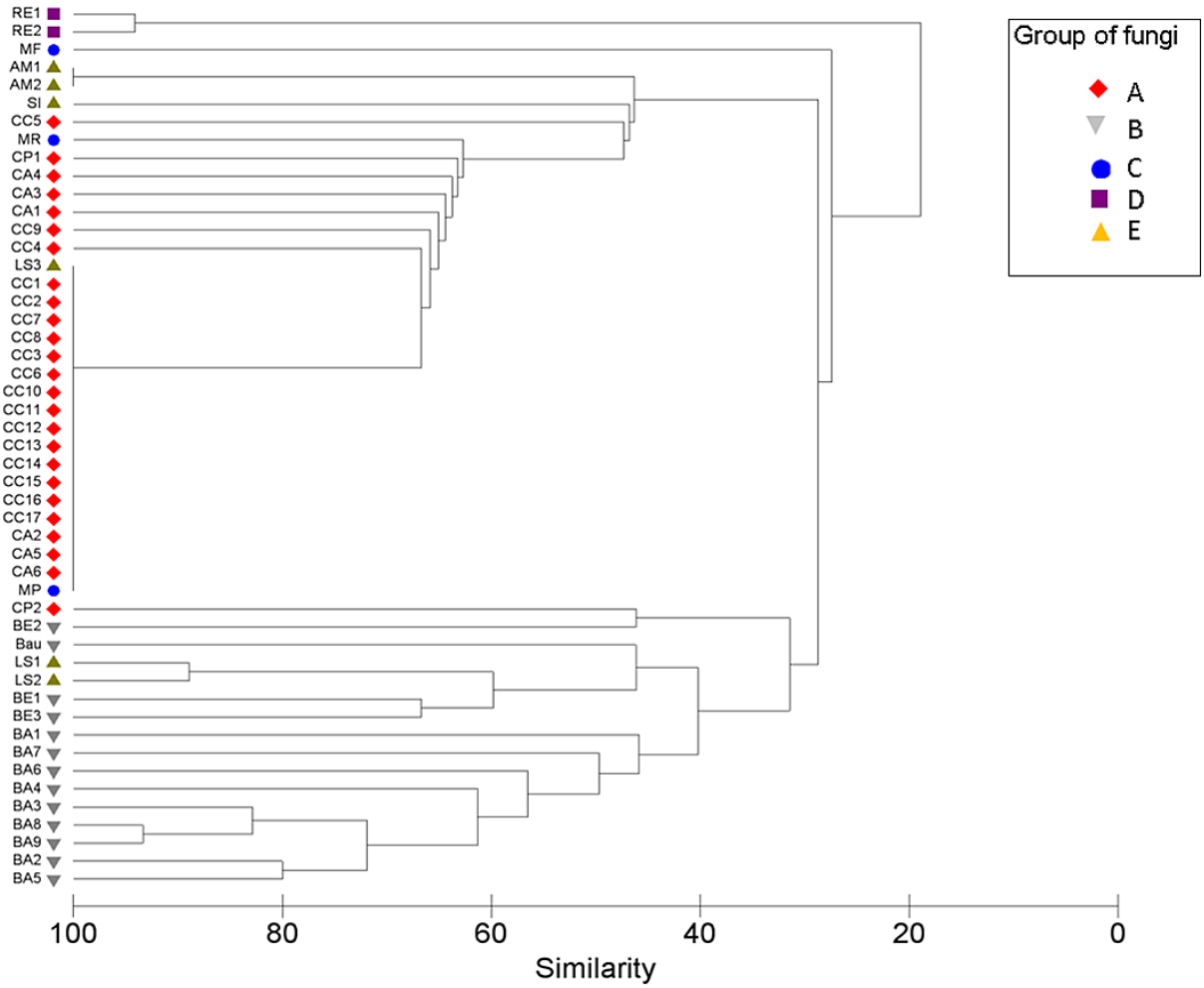

Figure 5.3: Dendrogram based on modified Bray Curtis similarity analysis. The dendrogram shows the differences among bacterial communities of 31 mushrooms samples. Samples were divided in 5 groups, in the following way: A) *Coprinus comatus* and *Coprinopsis* spp., B) *Boletus* spp., C) *Macrolepiota* spp., D) *Russula emetica*, E) mixed genera. The codes on the left side indicate the abbreviations to each fungal species. Those abbreviations are summarized in table 5.2.

Two main clusters can be distinguished according to the obtained dendrogram. The first one (upper section), is characterized by the presence of group A (24 from 25 samples), all samples comprising group C and D and group E (4 from 6 samples). Group D exhibited a very peculiar bacterial community, while samples belonging to group C where randomly distributed among the cluster. Also, two individuals belonging to group E (*Amanita* sp.) shared 100% of similarity (Fig. 5.3). The second dendrogram cluster (lower section) encloses all the samples belonging to group B. This cluster also included two samples of group E (*L. sulphureus*) and one belonging to group A (*C. picacea*). To provide more

details about the bacterial communities associated with mushrooms, sequences belonging to each established group (A - E), were subjected to phylogenetic analysis. Group A - in this group, 17 specimens of *Coprinus comatus*, 6 of *Coprinopis atramentaria* and 2 of *Coprinopsis picacea* were analysed. Among the collected *C. comatus*, bacterial phylotypes were detected only in 3 individuals. CC4 and CC5 were collected both in 2011 and in the same location (Bürgerpark, BS) and CC9, in 2012 at the HZI (BS). Bacterial phylotypes belonging to the Flavobacteraceae family were present in all of the 3 specimens, while a phylotype similar to *Pseudomonas agarici* was detected only on the hat of CC5. Moreover, no more than 2 bacterial phylotypes were identified on the surface of this fungal species. Additionally, the bacterial communities of 6 specimens of *Coprinopsis atramentaria*, all collected at HZI (BS), in 2012, were evaluated. Here, the samples CA1and CA3 showed the presence of 1 phylotype, sharing similarity with *Blastobacter aggregatus* and *Rhizobium alamii*, respectively. Furthermore, bacterial communities associated with 2 individuals of *C. picacea* (CP1 and CP2) were also assessed. On the hats of CP1 four phylotypes were detected, while on CP2 only 1 phylotype was observed. All of the bacterial phylotypes associated with *C. picacea* belong to the Enterobactereaceae family (Fig. 5.4).

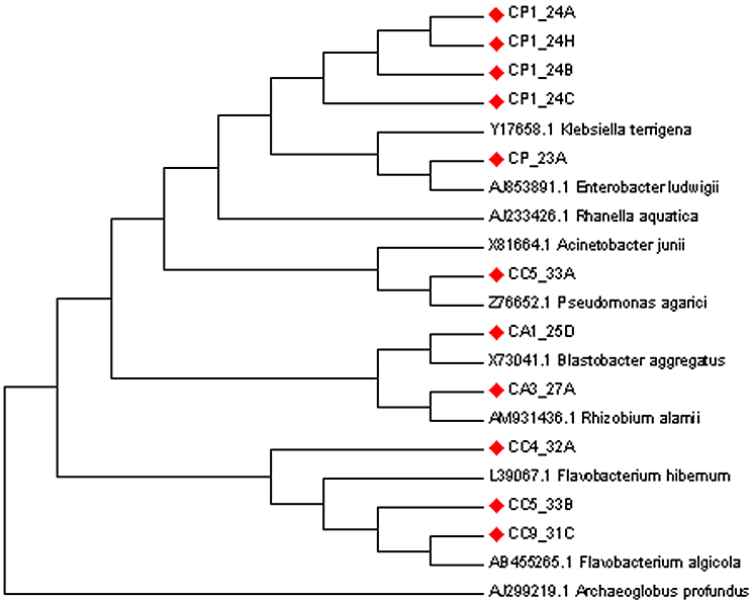

Figure 5.4: Neighbour joining tree of the 16S rRNA fragments sequences obtained from the hats of *Coprinus comatus* and *Coprinopsis* spp. individuals analysed using SSCP fingerprint analysis, together with reference sequences. Evolutionary distances were computed using the Jukes-Cantor model. The sequence of *Archaeoglobus* served as outgroup.

Group B - comprises thirteen specimens belonging to the genus *Boletus* spp. (9 specimens of *B. aestivalis*, 3 of *B. edulis* and 1 of *B. aureus*). This group demonstrated the highest bacterial richness among the 5 analysed mushrooms groups, harboring 2 to 9 of the detected phylotypes. The obtained 16S rRNA sequences were grouped in 4 families: Enterobactereaceae, Pseudomonadaceae, Burkholderiaceae and Acetobactereaceae. Among these families, only phylotypes related to Enterobactereaceae were found in all of the 3 *Boletus* spp. investigated. Between the nine specimens of *B. aestivalis* collected during 2009 - 2011, the sample BA1 showed 9 bacterial phylotypes associated. SSCP fin-

gerprint profiling demonstrated the presence of Enterobactereaceae, Pseudomonadaceae and Burkholdereaceae associated with this fungal species. Additionally, 3 *B. edulis* (BE) individuals used in this study showed the presence of Enterobactereaceae and Acetobactereaceae. Only 1 specimen of *B. aureus* (BAu) was evaluated according to its bacterial community analysed. From the obtained sequence the phylotypes associated with this mushroom shared similarity with *Acetobacter diazotrophicus* (Fig. 5.5).

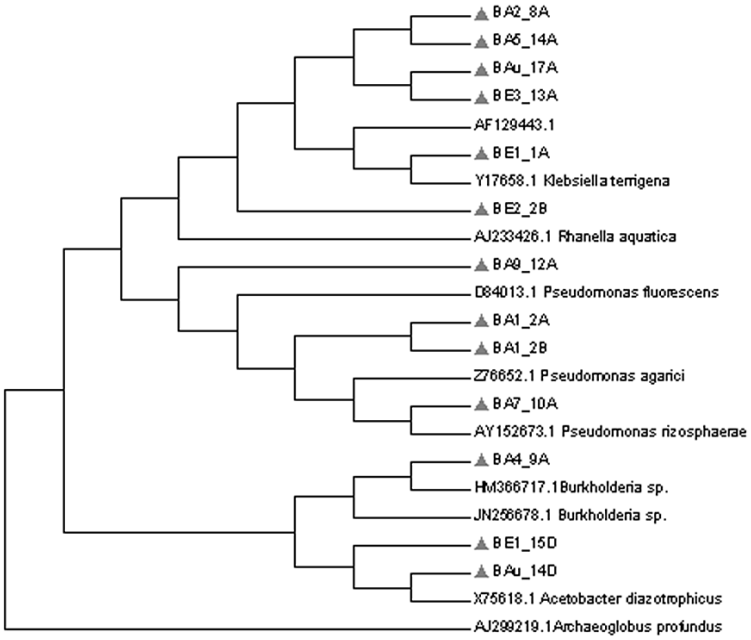

Figure 5.5: Neighbour joining tree of the 16S rRNA fragments sequences obtained from the hats of *Boletus* spp. individuals analysed using SSCP fingerprint analysis, together with reference sequences. Evolutionary distances were computed using the Jukes-Cantor model. The sequence of *Archaeoglobus* served as outgroup.

Group C - includes 3 *Macrolepiota* spp. specimens. On the hat of a specimen of *M. fuliginosa*, 4 phylotypes were detected, 3 belonging to the genera *Pseudomonas*, *Acinetobacter* and *Rhodanobacter* and 1 to the family Enterobactereaceae. A phylotype, occurring on the hat of *M. rhacodes* shares similarity with *Enterobacter ludwigii* (Fig. 5.6). Bacterial phylotypes could not be detected on *M.procera* hat.

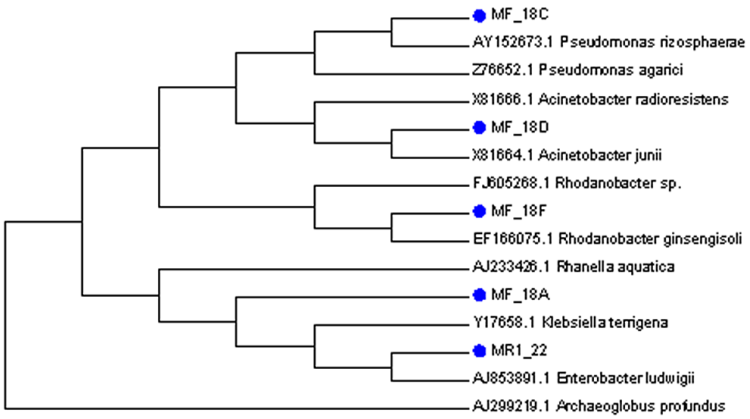

Figure 5.6: Neighbour joining tree of the 16 rRNA fragments sequences obtained from the hats of *Macrolepiota* spp. individuals analysed using SSCP fingerprint analysis, together with reference sequences. Evolutionary distances were computed using the Jukes-Cantor model. *Archeaoglobus* profundus was the outgroup used in the calculation.

Group D - encloses two individuals of *Russula emetica*. SSCP fingerprint analysis of those two specimens detected 8 phylotypes on RE1 and 7 phylotypes on RE2. Phylogenetic analysis of the obtained sequences showed that most of the phylotypes belongs to the Rhizobiaceae family. Only one sequence showed similarity with *Flavobacterium hibernum* (Fig. 5.7).

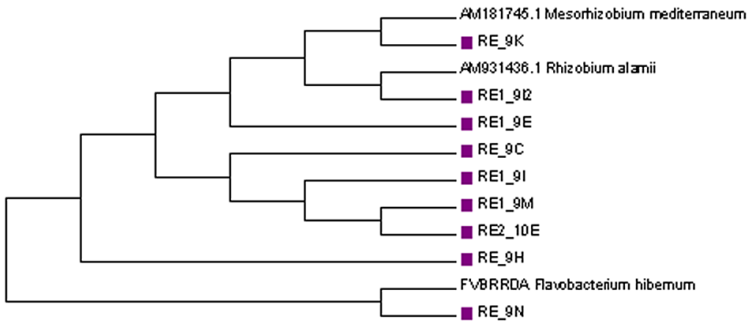

Figure 5.7: Neighbour joining tree of the 16S rRNA fragments sequences obtained from the hats of *Russula* emetica. Individuals analysed using SSCP fingerprint analysis, together with reference sequences. Evolutionary distances were computed using the Jukes-Cantor model.

Group E - comprises a mixture between fungal genera. Here, a *Burkholderia* sp. and a *Pseudomonas fluorescens* phylotypes were detected associated with *Stropharia* sp. On the fruiting bodies of *Laetiporus sulphureus* (LS1 and LS2) the Enterobactereaceae *Duganella* sp. and *Rhanella* sp. were identified. On the two *Amanita* sp. samples, *Acetobacter diazotrophicus* and an Enterobactreaceae phylotype were found. Moreover, an *incertae sedis* sequence was also detected (Fig. 5.8).

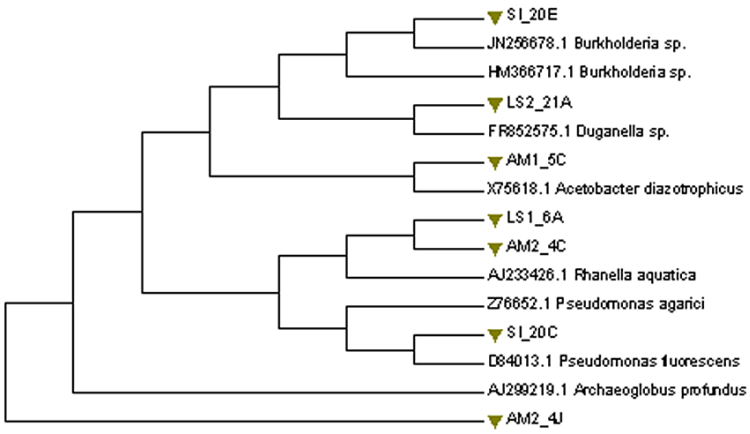

Figure 5.8: Neighbour joining tree of the 16S rRNA fragments sequences obtained from the hats of fungi belonging to group E, analysed using SSCP fingerprint analysis, together with reference sequences. Evolutionary distances were computed using the Jukes-Cantor model. The sequence of *Archaeoglobus* served as outgroup.

5.3 Screening

In order to determine appropriate conditions for the production of secondary metabolites with biological activity in liquid media, mycelia of the eleven isolated fungal species were grown on Petri dishes (90 x 90 mm), containing different solid culture media (BAF, MNM, PDA and YEM), with pH adjusted to 5.0, 7.0 and 9.0. Growth estimate (in days) was assessed by fungal colonies measurements, which were recorded during 30 days (table 5.3). The isolates which showed the ability to grow under the given incubation conditions, faster than 20 days were preferred for the screening experiments.

Table 5.3: Period of incubation (days) required by the fungal colony to reach the periphery of a 90 x 90 mm Petri dish. Eleven species were grown using different culture media.

Isolate	**BAF pH 5.0, pH 7.0, pH 9.0**	**MNM pH 5.0, pH 7.0, pH 9.0**	**PDA pH 5.0, pH 7.0, pH 9.0**	**YEM pH 5.0, pH 7.0, pH 9.0**
Coprinus comatus	13, 13, 15	25, 25, 27	13, 13, 15	13, 13, 15
Calcarisporium arbuscula	10, 10, 10	15, 15, 15	10, 10, 10	10, 10, 10
Boletus edulis	30*	30*	No growth	No growth
Boletus aestivalis	30*	30*	No growth	No growth
Boletus luridus	30*	30*	No growth	No growth
Laetiporus sulphureus	15, 15, 30*	28, 28, 30*	15, 15, 19	15, 15, 19
Macrolepiota fuliginosa	15, 15, 15	26, 26, 26	15, 15, 15	15, 15, 15
Macrolepiota procera	14, 14, 15	24, 24, 24	14, 14, 15	14, 14, 15
Macrolepiota rhacodes	30*	30*	30*	30*
Pholiota lenta	15, 15, 15	24, 24, 24	14, 14, 14	15, 15, 15
Hybeloma incarnatulum	30*	30*	30*	30*

After determining fungal growth, conditions used on the screening could be set as follows: a) media: BAF, PD and YEMB broth, with pH adjusted to 5.0, 7.0 and 9.0; b) temper-

ature: 20°C and 25°C; c) incubation period: 14, 21, 28, 35 and 42 days. None of isolated species showed satisfactory growth on MNM, therefore this medium was excluded from the screening strategy.
C. comatus, M. fuliginosa, M. procera and *P. lenta* were grown according to the conditions mentioned above, leading to 90 aqueous extracts each. From *L. sulphureus*, 80 extracts were obtained, since it showed a low growth rate when incubated in BAF broth adjusted to pH 9.0. Due to its high growth rate, *C. arbuscula* was incubated for 14, 21 and 28 days, generating 54 extracts. Each aqueous extract was obtained from a 110 mL filtrated culture. After concentration using lyophilisation, the extracts were resuspended in Milli-Q®water (1.1 mL), had their pH measured and were tested against *P. aeruginosa*, *S. aureus* and *S. mutans*, in liquid media for antibacterial and anti-biofilm activity. All of the 494 obtained extracts had pH defined between 5.0 and 5.5. 160 aqueous extracts were able to inhibit bacterial growth or biofilm formation from at least one of the microorganisms tested. Autoclaved media followed by lyophilisation and diluted similarly as the extracts were used as control. The respective fungal species and incubation conditions in which biological activities were detected are summarized on table 5.4.

Table 5.4: Fungal species and incubation conditions used for production of biological active secondary metabolites.

		C. comatus	*C. arbuscula*	*L. sulphureus*	*M. fuliginosa*	*M. procera*	*P. lenta*
				BAF media			
pH 5.0	20°C	**A** - 35 and 42 d	**A.G+** 14, 21 and 28 d	-	**A.G+** 28 d, 35 and 42 d	**A.G+** 28 d, 35 and 42 d	-
	25°C	**A** - 35 and 42 d	**A.G+** 14, 21 and 28 d	-	**A.G+** 28 d, 35 and 42 d	**A.G+** 28 d, 35 and 42 d	-
pH 7.0	20°C	**A** - 35 and 42 d	**A.G+** 14, 21 and 28 d	-	**A.G+** 28 d, 35 and 42 d	**A.G+** 28 d, 35 and 42 d	-
	25°C	**A** - 35 and 42 d	**A.G+** 14, 21 and 28 d	-	**A.G+** 28 d, 35 and 42 d	**A.G+** 28 d, 35 and 42 d	-
pH 9.0	20°C	**A** - 35 and 42 d	**A.G+** 14, 21 and 28 d	Not grown	**A.G+** 28 d, 35 and 42 d	**A.G+** 28 d, 35 and 42 d	-
	25°C	**A** - 35 and 42 d	**A.G+** 14, 21 and 28 d	Not grown	**A.G+** 28 d, 35 and 42 d	**A.G+** 28 d, 35 and 42 d	-

		C. comatus	*C. arbuscula*	*L. sulphureus*	*M. fuliginosa*	*M. procera*	*P. lenta*
				PDB media			
pH 5.0	20°C	-	**A.G+** 14, 21 and 28 d	-	**A.G+** 28 d, 35 and 42 d	**A.G+** 28 d, 35 and 42 d	-
	25°C	-	**A.G+** 14, 21 and 28 d	-	**A.G+** 28 d, 35 and 42 d	**A.G+** 28 d, 35 and 42 d	-
pH 7.0	20°C	-	**A.G+** 14, 21 and 28 d	-	**A.G+** 28 d, 35 and 42 d	**A.G+** 28 d, 35 and 42 d	-
	25°C	-	**A.G+** 14, 21 and 28 d	-	**A.G+** 28 d, 35 and 42 d	**A.G+** 28 d, 35 and 42 d	-
pH 9.0	20°C	-	**A.G+** 14, 21 and 28 d	-	**A.G+** 28 d, 35 and 42 d	**A.G+** 28 d, 35 and 42 d	-
	25°C	-	**A.G+** 14, 21 and 28 d	-	**A.G+** 28 d, 35 and 42 d	**A.G+** 28 d, 35 and 42 d	-
				YEM media			
pH 5.0	20°C	**A** - 35 and 42 d	**A.G+** 14, 21 and 28 d	**B SA** 21 d	-	-	-
	25°C	**A** - 35 and 42 d	**A.G+** 14, 21 and 28 d	**B SA** 21 d	-	-	-
pH 7.0	20°C	**A** - 35 and 42 d	**A.G+** 14, 21 and 28 d	**B SA** 21 d	-	-	**A.G+** 21 d **A** - 42 d
	25°C	**A** - 35 and 42 d	**A.G+** 14, 21 and 28 d	**B SA** 21 d	-	-	**A.G+** 21 d **A** - 42 d
pH 9.0	20°C	**A** - 35 and 42 d	**A.G+** 14, 21 and 28 d	-	-	-	**A.G+** 21 d **A** - 42 d

	C. comatus	*C. arbuscula*	*L. sulphureus*	*M. fuliginosa*	*M. procera*	*P. lenta*
25°C	**A** - 35 and 42 d	**A.G+** 14, 21 and 28 d	-	-	-	**A.G+** 21 d **A** - 42 d

A - antibacterial activity against all of three bacteria tested.
A.G+ - antibacterial activity against the tested Gram-positive bacteria.
B SA - *S. aureus* biofilm inhibition.

Aqueous extracts showing identical biological activity were submitted to liquid-liquid extraction using ethyl acetate followed by 2-butanol and analysed using RP-HPLC-MS. Chromatograms analyses showed high similarity between the extracts obtained from the same fungal species, in different media. Therefore, ethyl acetate or 2-butanol extracts obtained from the same fungal species were combined to proceed with the biological tests.

5.3.1 Biological activity of organic extracts

Extracts combination yielded 24 samples. Antibacterial activity and inhibition of biofilm formation were detected only when ethyl acetate extracts were used. 2-Butanol extracts did not show any of the investigated biological activities.
The antimicrobial spectra of the 12 ethyl acetate extracts were accessed using the disk diffusion method. Crude extracts were diluted with MeOH to 5 mg mL^{-1} and 25 μL of these solutions were used per paper disk. *C. comatus* and *P. lenta* (incubated during 42 days) extracts inhibited the growth of all bacteria tested. *C. arbuscula* and *P. lenta* (incubated during 21 days) showed inhibition of growth of Gram-positive bacteria. *C. arbuscula* was the only isolate which showed activity against yeasts. Within this method, *M. fuliginosa* and *M. procera* extracts did not show any activity. None of the sporocarps and mycelia extracts showed activity. The obtained inhibition zones are shown on table 5.5. Extracts are named according to the media and producer fungi. For *P. lenta*, incubation period is also given.

Table 5.5: Inhibition zone (mm) of the tested ethyl acetate extracts.

Extract	*S. aureus*	*E. coli*	*P. aeruginosa*	*C. albicans*
C. arbuscula BAF	35	-	-	23
C. arbuscula PD	36	-	-	25
C. arbuscula YEM	33	-	-	22
C. comatus BAF	16	12	13	-
C. comatus YEM	15	10	13	-
L. sulphureus YEM	-	-	-	-
M. fuliginosa BAF	-	-	-	-
M. fuliginosa PD	-	-	-	-
M. procera BAF	-	-	-	-
M. procera PD	-	-	-	-
P. lenta YEM 21d	14	-	-	-
P. lenta YEM 42 d	16	14	12	-

MICs against *P. aeruginosa*, *S. aureus* and *C. albicans* were also determined, using the micro dilution method. MBICs were assessed against *P. aeruginosa* and *S. aureus*. In this case, 100 μL of an initial solution (10 mg mL^{-1}) was serial diluted in liquid media. Herein, the observed activities were comparable to the ones observed for the aqueous extracts. MICs and MBICs values are found in table 5.6.

Table 5.6: MICs and MBICs (μg mL $^{-1}$) of the crude ethyl acetate extracts obtained from fungi.

Extract	*S. aureus* (MIC)	*S. aureus* (MIBC)	*P. aeruginosa* (MIC)	*P. aeruginosa* (MBIC)	*C. albicans* (MIC)
C. arbuscula BAF	62.5	-	-	-	23
C. arbuscula PD	62.5	-	-	-	25
C. arbuscula YEM	62.5	-	-	-	22
C. comatus BAF	250	-	500	-	-
C. comatus YEM	250	-	500	-	-
L. sulphureus YEM	-	125	-	-	-
M. fuliginosa BAF	500	125	-	-	-
M. fuliginosa PD	500	125	-	-	-
M. procera BAF	500	125	-	-	-
M. procera PD	500	125	-	-	-
P. lenta YEM 21d	500	-	-	-	-
P. lenta YEM 42 d	500	31.2	500	-	-

5.3.2 RP-HPLC Fractionation

Active extracts were submitted to RP-HPLC fractionation. Here, fractions were collected each 0.15 s in 96 - well microtiter plates. After complete dryness of solvent under N_2 stream, the microtiter plates were inoculated with *S. aureus*, *P. aeruginosa* or *C. albicans*, according to the crude extracts verified activities. Peak retention times (RT) were correlated with the activity observed in the microtiter plate.
Crude extracts obtained from *C. arbuscula* showed activity against *C. albicans* and *S. aureus*. Fractionation was performed using a C18 column (125 x 20 mm). The fraction

containing the peaks with the RT ranging between 7.0 and 7.14 min and the peak with the retention time at 12.31 min inhibited the growth of *S. aureus*. The fraction collected between 10.46 and 11 min showed activity against *C. albicans* (Fig. 5.9).

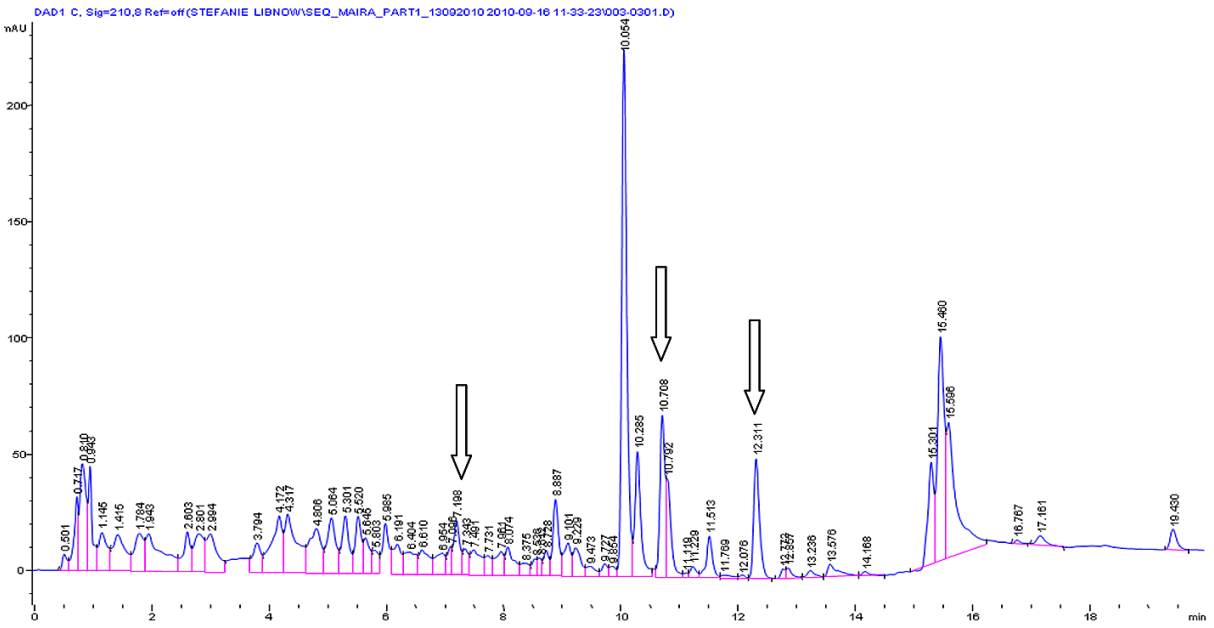

Figure 5.9: Chromatogram obtained from *C. arbuscula* ethyl acetate extract. Arrows indicate fractions with biological activity.

Fractionation of *C. comatus* extract was performed using a C18 column with the dimensions of 250 x 20 mm. The fraction collected between 9.0 and 9.15 min showed activity against *S. aureus* and *P. aeruginosa*. Within this fraction, only one peak could be observed in the chromatogram, which led to the correlation of the antibacterial activity with the peak with RT at 9.127 min (Fig. 5.10).

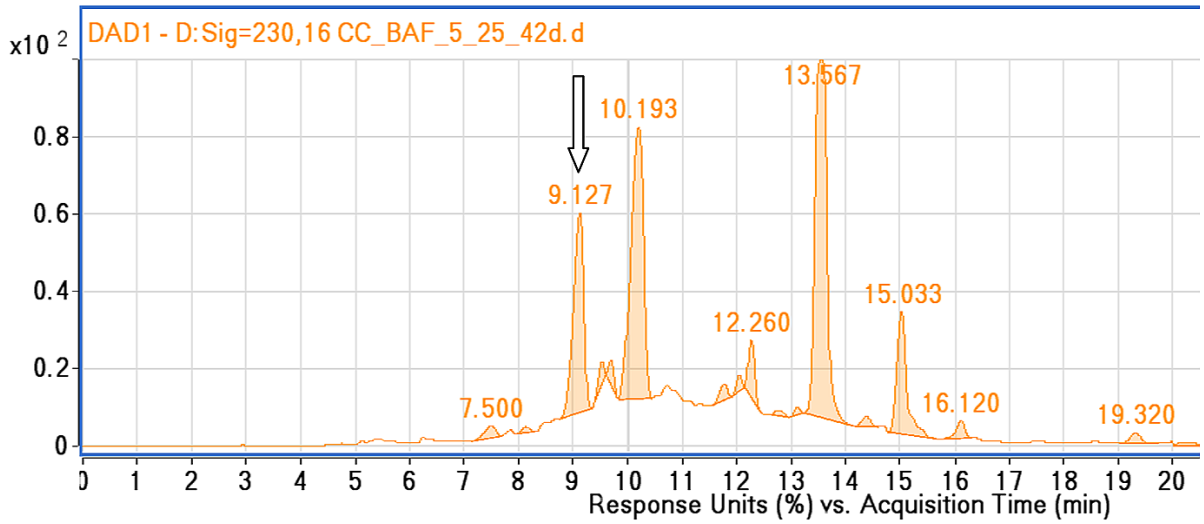

Figure 5.10: Chromatogram obtained from *C. comatus* extract fractionation. Arrow indicates the peak which was correlated with antibacterial activity.

L. sulphureus crude extracts inhibited *S. aureus* biofilm formation. A C18 250 x 20 mm column was used to fractionate this sample. Activity was correlated with the fraction obtained at 12 and 12.5 min of elution (Fig. 5.11). No antibiotic activity was observed.

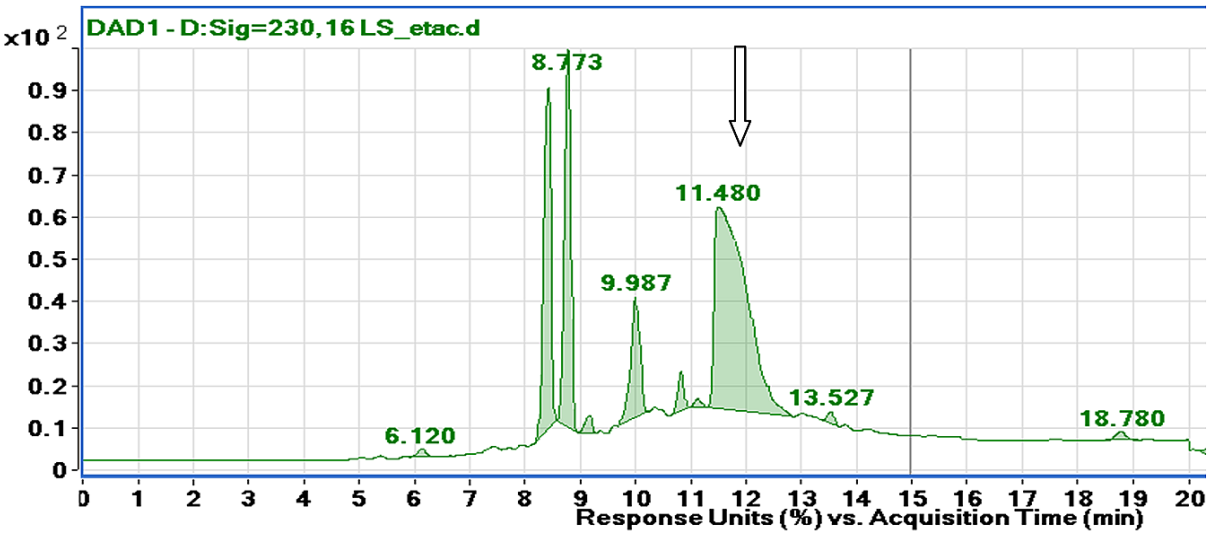

Figure 5.11: Chromatogram obtained from *L. sulphureus* extract fractionation. Arrow indicates the fraction with activity against *S. aureus* biofilm formation.

Organic extracts obtained from *M. fuliginosa, M. procera* and *P. lenta* did not show activities after HPLC fractionation.
All 6 fungal species were incubated in 5 L media, according to the following conditions: a) *C. arbuscula* was incubated in YEM broth pH 9.0, during 14 days, at 20°C; b) *C.*

comatus was incubated in BAF broth pH 9.0, during 42 days, at 25°C; c) *L. sulphureus* was incubated in YEM broth pH 5.0, during 21 days, at 20°C; d) *M. fuliginosa and M. procera* were incubated in PDB pH 7.0, during 28 days, at 20°C and e)*P. lenta* was incubated in YEM broth pH 9.0, during 42 days, at 20°C. Ethyl acetate was used to extract the compounds from the media in all of the cases.

5.3.3 Crude extracts fractionation and purification

5.3.3.1 *C. arbuscula*

Approximately 1.7 g of dark orange oil was obtained from *C. arbuscula* cultivation. The fractionation was performed using a 300 x 30 mm glass chromatographic column, packed with 450 g of Sephadex LH-20 resin. Column was eluted using methanol. 15 fractions were obtained and tested against *S. aureus* and *C. albicans*, using the disk diffusion method. Fractions number 3 and 4 were active against both microorganisms tested, showing inhibition zones of 35 mm for *S. aureus* and 13 mm for *C. albicans*. Fractions 11 and 12 showed an inhibition zone of 13 mm against *S. aureus*.
HPLC chromatograms were obtained for all four active fractions. Fractions number 3 and 4 were combined, generating a fraction named CA_A1; fractions 11 and 12 generated the fraction named CA_B1.
All 7 compounds present in the fraction CA_A1 were purified using a semi-preparative RP-HPLC, method A, described in the section 4.4.6.2. Compound numbers, retention times and purified amounts are described in table 5.7. Compounds **1** - **4** and **7** were purified yielding a white powder. Compounds **5** and **6** were purified as yellow oil.

Table 5.7: Compounds purified from the fraction CA_A1, obtained from the cultivation of C. arbuscula. Retention time (min) and compounds quantity (mg) are given.

Compound	Retention time (min)	Quantity (mg)
1	13.5	3
2	13.6	1.5
3	15	0.8
4	12.9	12
5	14.19	0.6
6	13.1	8
7	15.4	1.2

Fraction CA_B1 was purified using normal phase TLC followed by semi-preparative RP - HPLC. Dichloromethane: methanol (98 : 2) was used to develop the TLC plates. All bands, visualized under UV light 264 nm, were scraped and tested against *S. aureus*. The band with the retardation factor (Rf) value of 0.135 showed activity against the mentioned bacteria. The active TLC band was further purified using semi-preparative RP-HPLC, using the method B, described in section 4.4.6.2. The peak with RT of 7.3 min was collected, leading to the isolation of 1.5 mg of compound **8**, as yellow oil.
All of the purified compounds were analysed using RP-HPLC/MS and handed over to NMR measurements.

5.3.3.2 *Coprinus comatus*

From *C. comatus* 5 L cultivation, around 150 mg of crude extract was obtained. The crude extract was applied on SPE C18 cartridges and eluted with a mixture of MeOH and H_2O, generating 4 fractions. Fraction 1, obtained from an 80: 20 (H_2O : MeOH) mixture inhibited the growth of *S. aureus* and *P. aeruginosa*. This fraction was purified using a semi preparative RP - HPLC, with the method B, described on section 4.4.6.2. The peak with the RT 9.7 min was collected, leading to the isolation of 7 mg of compound **9**.
The purified compound was analysed using RP-HPLC-MS and NMR measurements.

5.3.3.3 *Laetiporus sulphureus*

About 110 mg were obtained from *L. sulphureus* cultivation in 5 L medium. C18 cartridges were used to fractionate the extract, again with a MeOH / H_2O mixture. The fraction obtained from a mixture MeOH / H_2O (50 : 50) was active against *S. aureus* biofilm formation. The fraction was submitted to further fractionation using a semi-preparative HPLC, method B described in the section 4.4.6.2, but no activity was detected.

5.3.3.4 *Macrolepiota fuliginosa* **and** *Macrolepiota procera*

From the cultivation *M. fuliginosa* and *M. procera*, about 150 mg and 195 mg of crude extract were obtained, respectively. SPE SiOH cartridges were used to fractionate both samples. Cartridges were elutes with hexane, followed by ethyl acetate and mixtures of ethyl acetate and MeOH (80 : 20, 50 : 50, 20 : 80). The fraction obtained after elution using the mixture 50 : 50 ethyl acetate: MeOH was active against growth (300 μg mL $^{-1}$) and biofilm formation (75 μg mL $^{-1}$) of *S. aureus*, for both fungi. A TLC using hexane / ethyl acetate was performed. Bands with the Rf 0.73 showed activity against *S. aureus* growth. From *M. fuliginosa* 0.4 mg and from *M. procera* 0.6 mg of yellow oil was obtained. The samples were directed to NMR measurements.

5.3.3.5 *Pholiota lenta*

About 2 g oil was obtained after *P. lenta* cultivation in 5 L media. The extract was fractionated using Sephadex LH-20, packed in a 600 x 30 mm glass chromatographic column, generating 65 fractions. Fractions 8 to 22 showed activity against *S. aureus* growth. Activity against *P. aeruginosa* was not detected after this fractionation procedure.
Fractions 8 to 22 were analysed using HPLC-MS, but a broad peak, eluted from 6 to 14 min of run was observed in all chromatograms. Several solvent systems were tested for TLC, but none of the used techniques was successful in isolating the active compound.
Regarding all the extracts, eight compounds were obtained from *C. arbuscula* (compound **1** - **8**) cultivation and *C. comatus* cultivation led to the isolation of one active compound (compound **9**). In order to identify the compounds, they were submitted to RP-HPLC-MS analysis, using a C18 column with the dimensions of 125 x 20 mm, and the method described in section 4.4.4, followed by NMR measurements.

5.4 RP-HPLC/MS analysis of the purified compounds

5.4.1 Compounds isolated from *Calcarisporium arbuscula*

Fraction CA_A1, obtained from *C. arbuscula* 5 L cultivation, yielded 7 compounds (Fig. 5.12). All these compounds were purified using semi preparative HPLC.
Compound **1** was eluted at 13.5 min and showed UV maximum absorbance at 260 nm. Three ions were detected using mass spectrometry analysis, operated in the positive mode: m/z 361.2, m/z 515.2 and m/z 1029.5. The m/z of compound **1** was calculated to 514.2 (Fig. 5.12, 1). Likewise compound **1**, compound **2** m/z was calculated to 514.2. Compound **2** was obtained at 13.6 min, with UV maximum absorbance also at 260 nm. Three ions, m/z 361.2, m/z 537.2 and m/z 1029.5, were identified. The ion at m/z 537.2 acquired a sodium ion (m/z 23) from the ionization process, corresponding to $[M + Na]^+$. The ion of m/z 1029.5 corresponded to $[2M + H]^+$ (Fig. 5.12, 2).
Compound **3** was recovered at 15.05 min, showing an UV maximal absorbance at 260 nm. The mass spectrum was analysed in the positive mode, revealing two peaks, of m/z 513.2 and m/z 1047.4. An m/z of 512 was calculated for compound 3 (Fig. 5.12, 3).
Compound **4** was obtained at 12.91 min, presenting UV maximum absorbance at 260 nm. Mass spectrometry analysis on the positive mode showed the presence of three ions, one at m/z 229.2, the second at m/z 529.2 and the third at m/z 1057.5. The m/z of compound 4 was calculated to 528, the first ion peak corresponding to $[M + H]^+$ and the second to $[2M + H]^+$ (Fig. 5.12, 4).
Compound **5** showed an RT of 14.19 min, also with the UV maximum absorbance at 260 nm. Mass spectrum, analysed in the positive mode revealed several peaks: m/z 229.1, m/z 285.2, m/z 511.2, m/z 571.2, m/z 837.4, m/z 1051.4 and m/z 1163.4. The m/z of compound 5 was calculated to 570 (Fig. 5.12, 5).
Compound **6** was eluted at 13.1 min and showed UV maximum absorbance at 260 nm. The mass spectrum in the positive mode showed the presence of two ions, one at m/z 529.2 and the second one at m/z 1079.5. The m/z of compound 6 was again calculated to be 528, the first ion corresponding to $[M + H]^+$ and the second corresponding to $[2 M + Na]^+$ (Fig. 5.12, 6).
Compound **7** was obtained at 15.4 min and showed an UV maximum absorbance at 220 nm. The mass spectrum was obtained from the negative-ion mode and two peaks were observed: m/z 515.3 and m/z 1031.7. The m/z of compound 7 was calculated to 516, corresponding to $[M-H]^-$ (Fig. 5.12, 7).

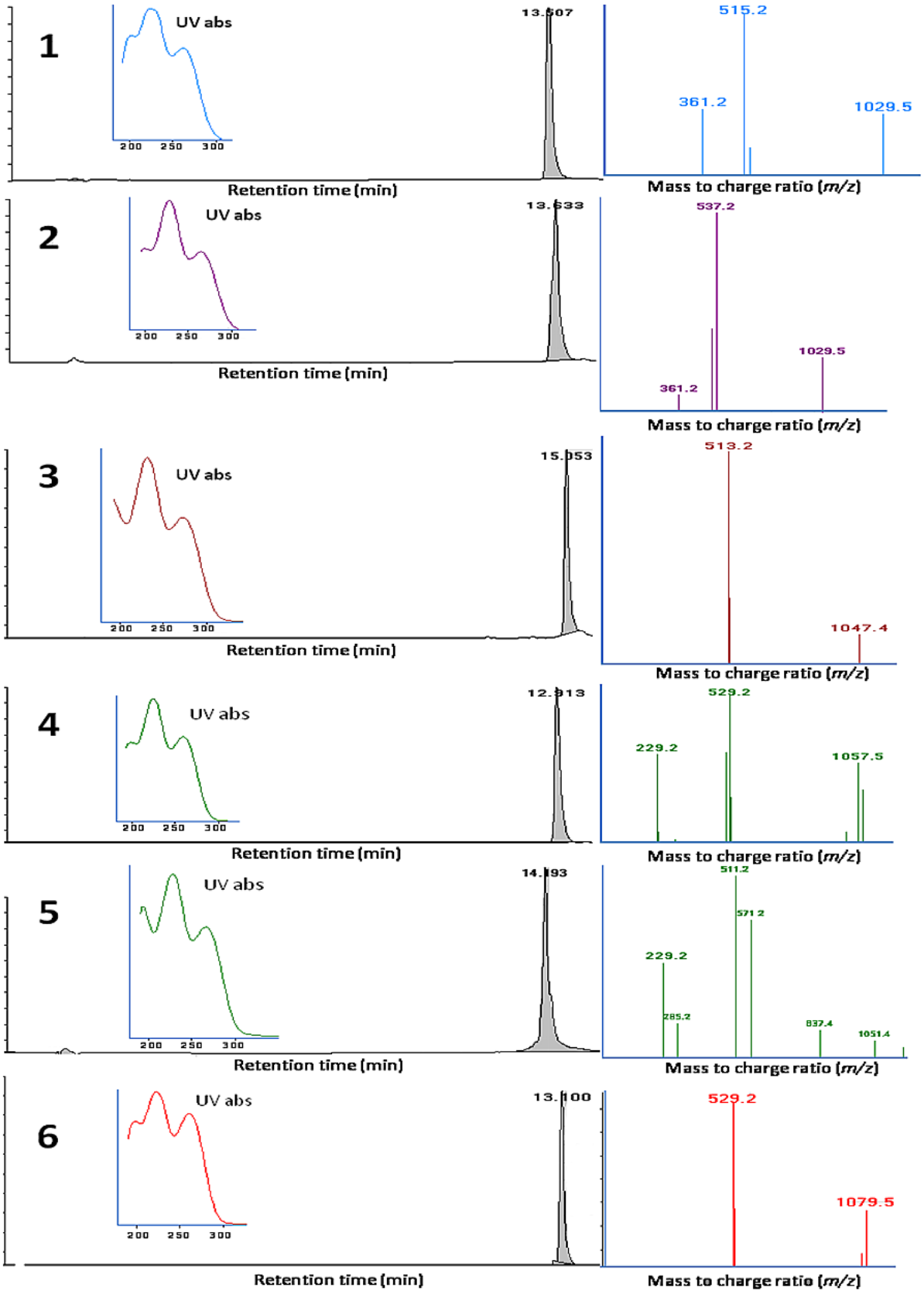
1
UV abs
200 250 300
13.507
Retention time (min)
515.2
361.2
1029.5
Mass to charge ratio (m/z)
2
UV abs
200 250 300
13.533
Retention time (min)
537.2
1029.5
361.2
Mass to charge ratio (m/z)
3
UV abs
200 250 300
15.053
Retention time (min)
513.2
1047.4
Mass to charge ratio (m/z)
4
UV abs
200 250 300
12.913
Retention time (min)
529.2
229.2
1057.5
Mass to charge ratio (m/z)
5
UV abs
200 250 300
14.193
Retention time (min)
511.2
571.2
229.2
285.2
837.4
1051.4
Mass to charge ratio (m/z)
6
UV abs
200 250 300
13.100
Retention time (min)
529.2
1079.5
Mass to charge ratio (m/z)

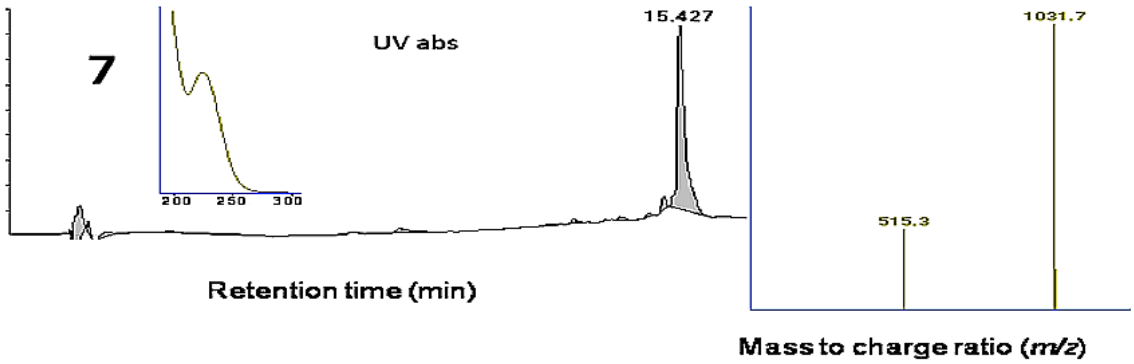

Figure 5.12: Retention times, UV absorbance and counts mass to charge ratio (m/z) of the compounds isolated from the fraction CA_A1.

Compound 7 was subjected to HRMS analysis, in the negative mode, yielding a peak at m/z 515.2999 (Fig. 5.13).

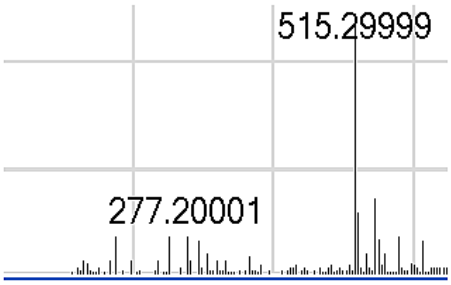

Figure 5.13: Counts mass to charge ratio (m/z) of compound **7**, using a HRMS.

Fraction CA_B1, obtained from *C. arbuscula* cultivation in 5 L of YEMB, yielded compound **8**. This compound was purified using TLC combined with semi preparative HPLC. HPLC-MS analysis revealed a peak at the RT of 7.72 min, with UV maximum absorbance at 260 nm. Mass spectrum, analysed in the positive ion mode showed 2 peaks, one at m/z 181 and the second one at m/z 383. Compound **8** m/z was calculated to 180. The peak at m/z 383 corresponded to $[2M + Na]^+$ (Fig. 5.14, 8).

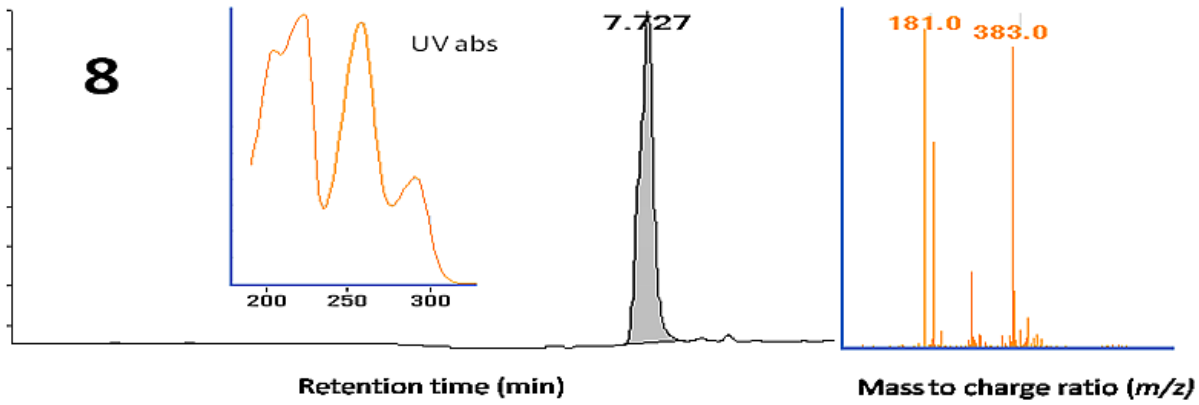

Figure 5.14: Retention time, UV absorbance and ion peaks obtained from RP-HPLC-MS analysis of compound **8**.

5.4.2 Compound isolated from *Coprinus comatus*

Compound **9** was purified from a *C. comatus* culture, after growth during 42 days in BAF medium, with pH adjusted to 9.0. HPLC-MS analysis showed a peak eluted at 9.1 min, with UV maximum absorbance at 210 nm. Mass spectrum, analysed in the positive mode, showed a peak at m/z 129. Compound **9** m/z was calculated to 128 (Fig. 5.15).

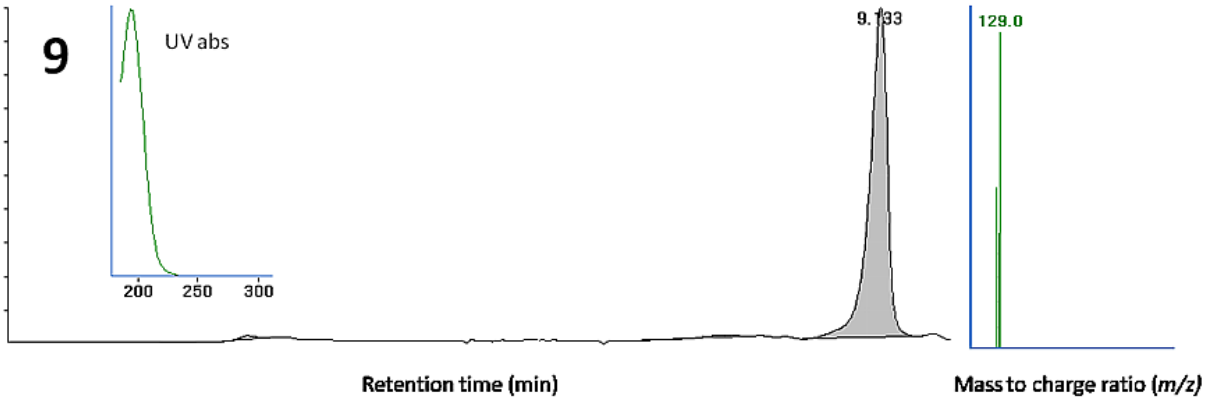

Figure 5.15: Retention time, UV absorbance and ion peaks obtained from RP-HPLC-MS analysis of compound **9**.

5.5 Structure elucidation

5.5.1 Compounds isolated from the fraction CA_A1, obtained from *Calcarisporium arbuscula* cultivation

5.5.1.1 Roridins

^{1}H NMR spectra from compound **1** showed four methyl groups at δ_H 0.79 (s), 1.14 (d), 1.71 (s(br)), and 2.26 (s(br)) and an epoxy-methylene with doubletts at 3.14 and 2.82 coupling with J=4.1 Hz, pointing together with protons of a 1,4-disubstituted diene moiety with δ_H-resonances at 7.53, 6.60, 5.89 and 5.82 to a macrocyclic mero-sesquiterpene (Fig. 5.16). Careful analysis of the NMR spectra led to the conclusion that **1** was one of the four epimeric roridins E. Comparison with published ^{1}H- and ^{13}C-NMR [147, 148, 149] data of all four roridins in question showed that in **1** 4-H, 11-H, 15A-H, 6'-H, and especially 13'-H were deshielded, but 15b-H and 2'-H were shielded compared to roridin E and epiroridin E. All NMR data fitted well to those reported for epiisororidin E and **1** was identified being this compound (Fig. 5.7, 1). The minor compound **2** also belonged to one of the epimeric roridins E as judged by its ^{1}H- and ^{13}C-NMR data, very similar to those of **1** (Fig. 5.17 and Fig. 5.18). Again a comparison with the ^{1}H- NMR data of all four roridins E isomers revealed that in **2** compared to roridin E and epiroridin E 4-, 11-, and 15A-H were deshielded and 2'- and 7'H were shielded. 13'-H was deshielded against roridin E but shielded against epiroridin E. Compared to the ^{1}H-NMR data of epiisororidin E (Fig. 5.16) 2'-, 6'-, 7'-, and especially 13'-H were shielded in compound **2**. All NMR data fitted well to those reported for isororidin E leading to the identification of **2** as this compound (Fig. 5.7, 2).

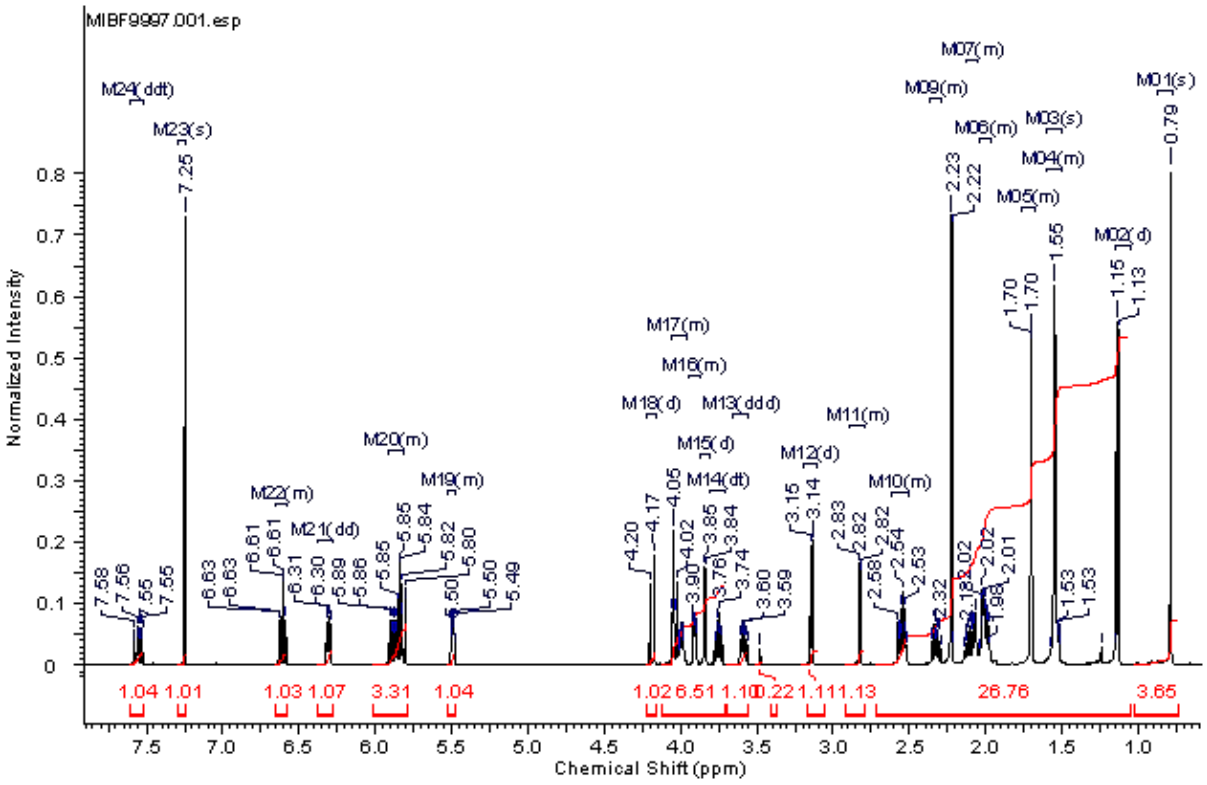

Figure 5.16: 700 MHz ^{1}H NMR spectrum from compound **1**, in $CDCl_3$. This compound was identified as epiisororidin E.

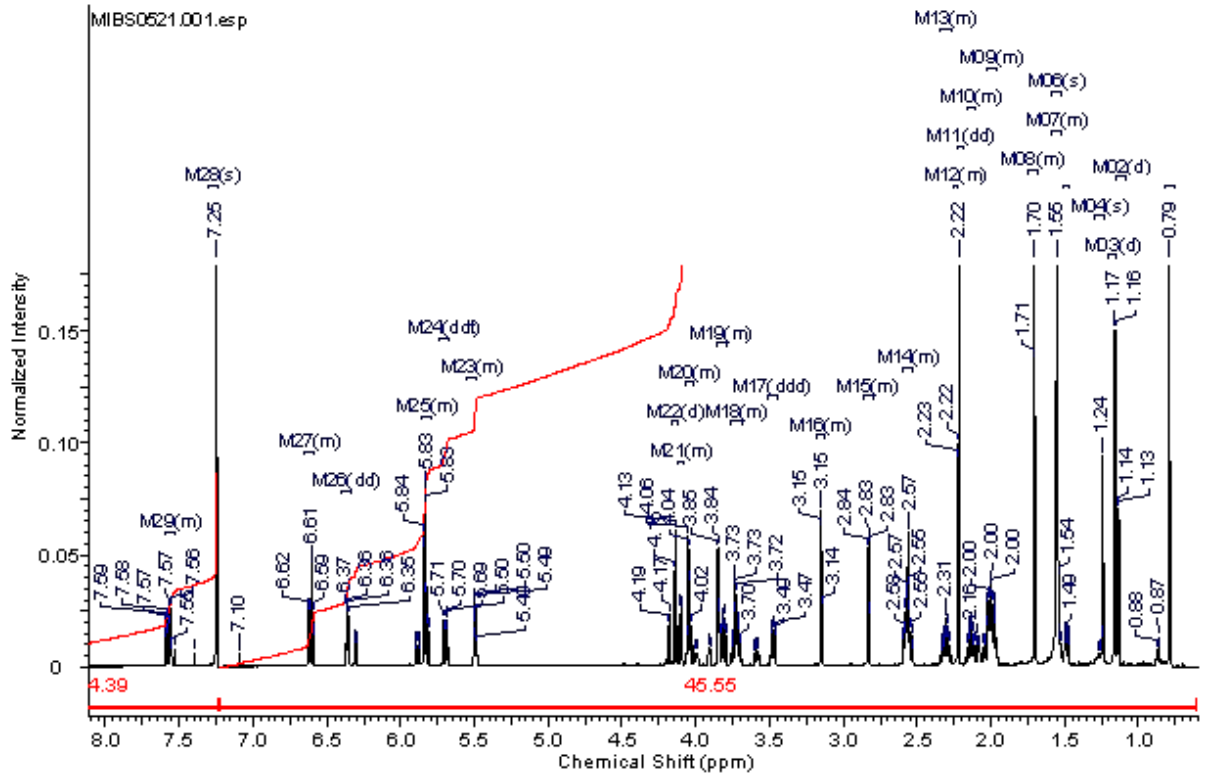

Figure 5.17: 700 MHz ^{1}H NMR spectrum from compound **2**, in $CDCl_3$. This compound was identified as isororidin E.

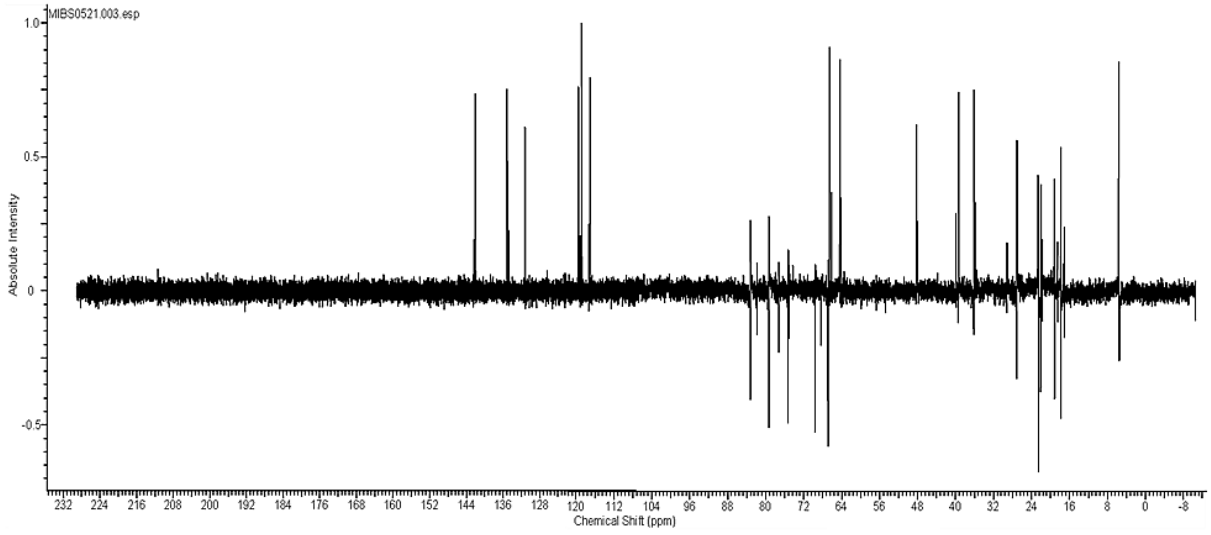

Figure 5.18: Isororidin E **2** ^{13}C-NMR spectrum.

The ^{1}H NMR of compound **3** was similar to the ones seen for the roridin E isomers (Fig. 5.19). However, resonances of the 5'-protons were replaced by a fourfold doublet at δ_H

5.53. This and the downfield-shift of the 14'-methyl group to δ_H 1.33 fitted mostly to the data reported for roridin H by Traxler and Tamm [150].
After assigning all the resonances of all protons, compound **3** was identified as roridin H (Fig. 5.7, 3). However, the relative configuration at C-6' and C-13' has not been solved by these authors. A comparison of the ^{1}H NMR data of the closely related 1,3-dioxolanes of erythro- and threo-10,11-dihydroxy-trans-12-nornerolidol revealed a deshielding of the 13-methyl group to δH = 1.25 ppm in the threo-compound compared to δH = 1.15 ppm in the erythro-compound and a shielding of 11-H to δH = 3.72 ppm in the threo-compound (instead of δH = 4.21 ppm in the erythro-compound) [151]. These chemical shifts of the threo-compound fitted well with the one observed in roridin H, revealing that the stereochemistry of roridin H is that of isororidin E with 6'S,13'S-configuration. This stereochemistry was also confirmed by single crystal X-ray crystallography for 8α-acetoxy-roridin H [152]. Compound **4** was therefore identified as 8α-hydroxy-roridin H, a compound recently reported from a halotolerant *Myrothecium* species (Fig. 5.7) [153].^{1}H NMR chemical shifts for all roridin E isomares are summarized in the table 5.8. ^{1}H NMR chemical shifts for epiisororidin E **1** and isororidin E **2**, together with the corresponding literature, are outlined in the table 5.9.
The fourth roridin, compound **4**, bore one additional oxygen compared to roridin H. The diene moiety of the macrocyclic diester at δH 5.80 (H-10'), δH 6.55 (H-9'), δH 7.70 (H-8') and δH 5.93 (H-7') showed couplings to a broad double duplet at δH 4.06 (H-6') which coupled with a dq at δH 1.32 (H-14') (Fig. 5.20). The resonance of H-13' was considerable deshielded compared to those of the roridin E isomers. Resonances of H-14' at such positions however are known for macrocyclic trichothecanes carrying acetals between C-5' and C-6'. This hypothesis was confirmed by the presence of a resonance at δH 5.52 (H-5') indicating the presence of two oxygen substituents. The H-5' coupled to two allylic protons at δH 2.61 and 2.26 which coupled allylicly to an olefinic proton at δH 5.69 (H-2') and a methyl group at δH 2.26 (H-12'). The diester of the macrocyclic ring system coupled on the one hand to the proton at δH 5.93 (H-4) which coupled to a methylene group with resonances at δH 2.48 and 2.17 (H-3). Both H-3 coupled to δH 3.82 (H-2). On the other hand stood H-15 of the oxymethylene group forming an ABq at δH 4.39. The olefinic proton H-10 of the sesquiterpene moiety at δH 5.55 showed couplings to δH 3.75 (H-11) and allylic couplings to the C-16-methyl group at δH 1.85 and δH 4.11 (H-8). H-8 finally coupled to a methylene group at δH 2.17 and 2.06. The presence of the epoxy-group found in all roridins so far was revealed by resonances at δH 3.10 and 2.82. The deshielding of H-8 together with the deshielding of H-16 and H-10 pointed to a C-8-hydroxylation of compound **4**. Both 8α- and 8β-hydroxylations are known from natural products with trichothecane skeleton. While 8α-hydroxylations have been reported from fungi, 8β-hydroxylations are only known from plants [154]. The shielding of H-15 and the deshielding of H-16 and H-10 in compound **4** compared to roridin H required the 8α-configuration of the hydroxyl-group. An 8β-configuration would have caused almost no change in the H-15 resonances but a stronger upfield shift of H-16 [155]. 8α-Hydroxy-roridin H has been reported from *Myrothecium* sp. GS-17 [153] and from *C. arbuscula* [156].
The fifth roridin isolated from this fungus has very similar ^{1}H NMR spectra (Fig. 5.21) to 8α-hydroxy-roridin H 4 and was identified as its acetate, 8α-acetoxy-roridin H (cal-

carisporin B1) **5** (Fig. 5.7, 5). This compound has already been reported from two *Myrothecium* species [152] but also from *C. arbuscula* [156]. ^{1}H NMR chemical shifts for 8α-hydroxy-roridin H **4**, 8α-acetoxy-roridin H and roridin H **3**, compared with the corresponding literature, are outlined in table 5.10 and 5.11.

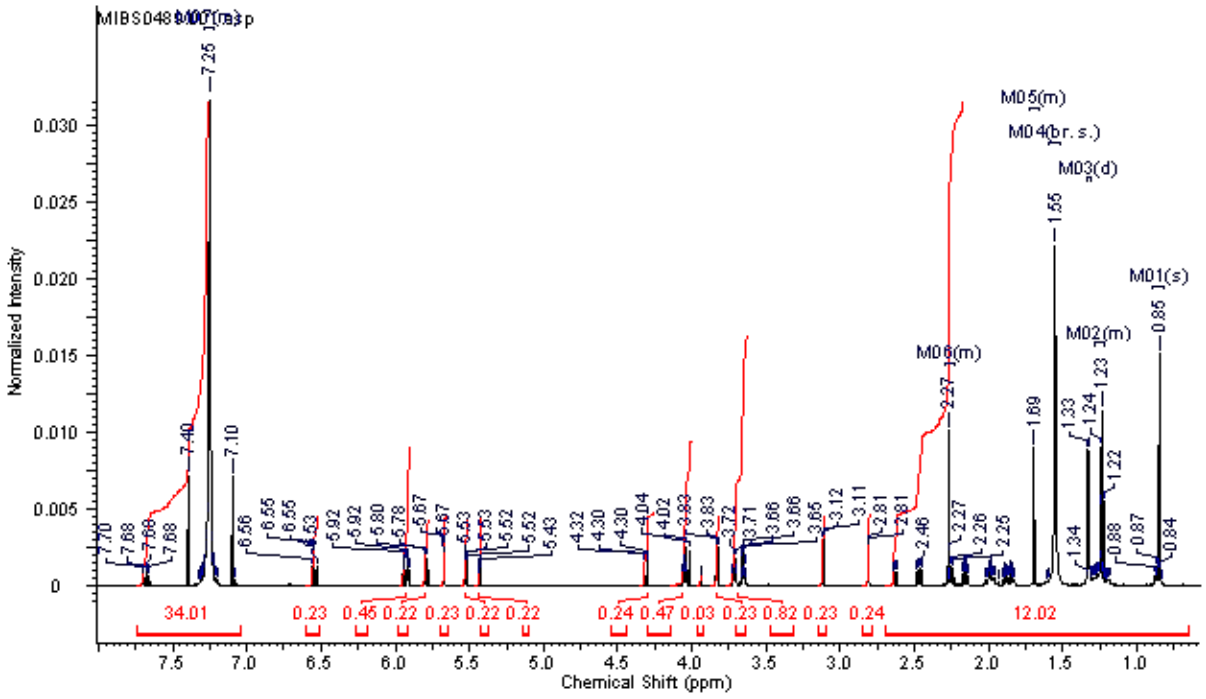

Figure 5.19: 700 MHz ^{1}H NMR spectrum from compound **3**, in $CDCl_3$. This compound was identified as roridin H.

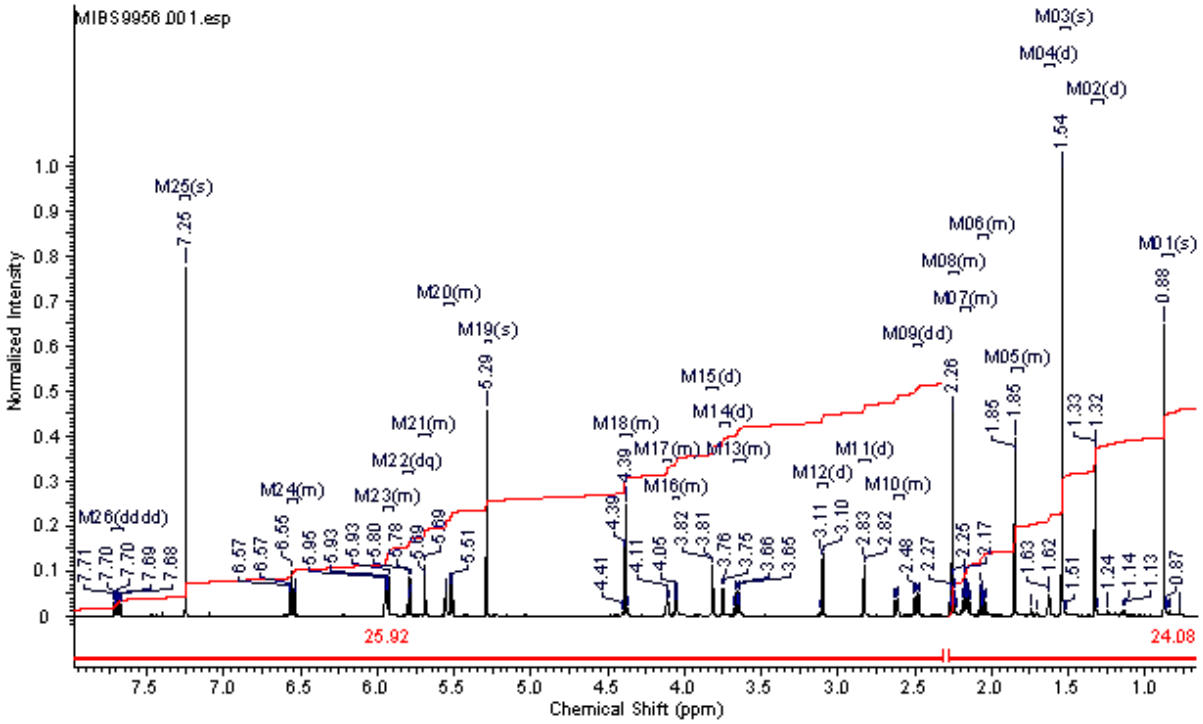

Figure 5.20: 700 MHz ^{1}H NMR spectrum from compound **4**, in $CDCl_3$. This compound was identified as 8α-hydroxy-roridin H.

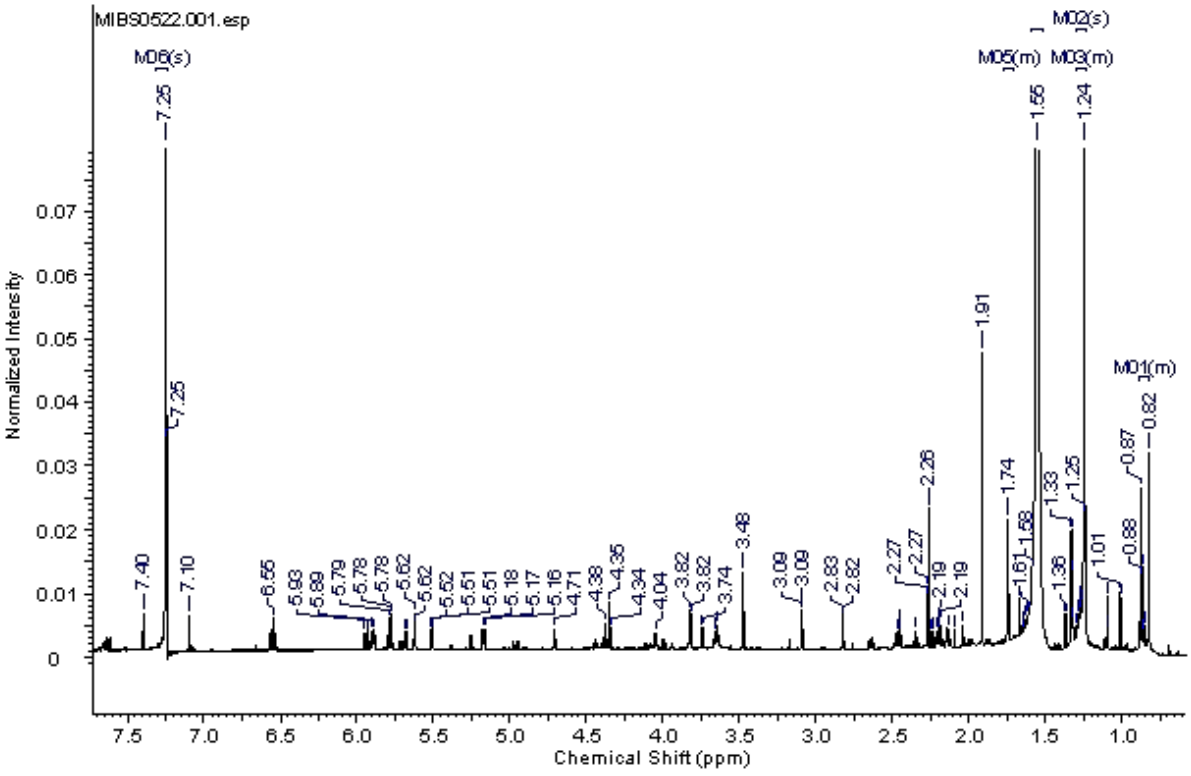

Figure 5.21: 700 MHz ^{1}H NMR spectrum from compound **5**, in $CDCl_3$. This compound was identified as 8α-acetoxy-roridin H.

Finally, a sixth roridin, compound **6**, was found. The resonances seen in the ^{1}H-NMR spectra are again very similar to those of roridin H **3**, significant shifts could only be seen in the lactone ring (Fig. 5.22). Here the 5'-H shifted to lower fields at δH 5.75 and a slight shift was only seen for 14'-H which moved to δH 1.36. 5'-H was deshielded and showed a doublet at δH 5.24 with J=6.9 Hz. Of the two 4'-H one is missing and the other one moved to δH 3.82 and became a double doublet with J=6.9 and 0.5 Hz indicating a hydroxy group at this site. 4'-Hydroxy roridin H **6** is known as roridin J (Fig. 5.7, 6) and has been reported from *Myrothecium verrucaria* [157] and from *C. arbuscula* [156]. The large coupling constant between 4'-H and 5'-H requires a dihedral angle of close to 180° between these two protons. Model inspections showed that this is only possible if the 4'-hydroxy group is in β-position. Its stereochemistry at 4'-H has not yet been determined and is reported here for the first time being 4'R. ^{1}H NMR chemical shifts for roridin J **6**, together with the corresponding literature, are summarized intable 5.10 and 5.11.

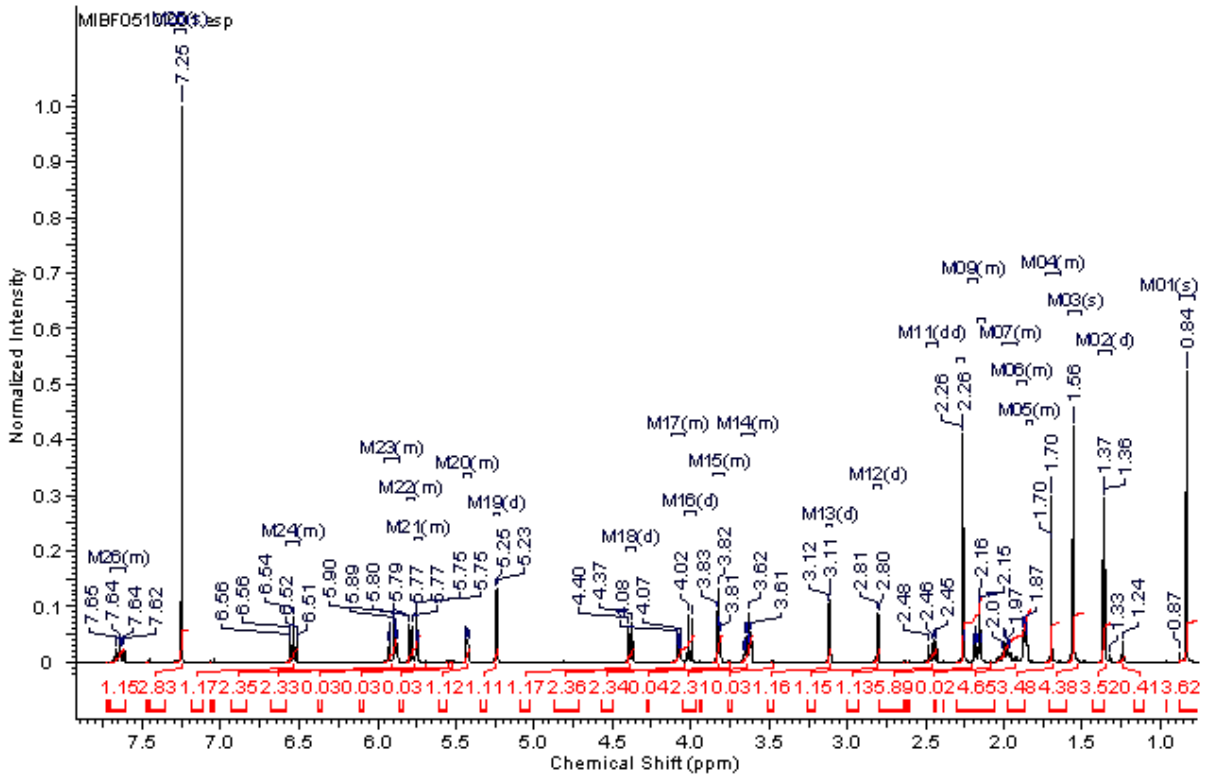

Figure 5.22: 700 MHz ^{1}H NMR spectrum from compound **6**, in $CDCl_3$. This compound was identified as roridin J.

Table 5.8: ^{1}H NMR chemical shifts reported in the literature for roridin E, epiroridin E, epiisororidin E and isororidin E.

Reference	[147, 148]	[147]	[147]	[149]
H	**roridin E**	**epi roridin E**	**epiiso roridin E**	**iso roridin E**
2-H	3.84 (1H, d, J=4.9 Hz)	3.87 (1H, d, J=5.0 Hz)	3.83 (1H, d, J=5.0 Hz)	3.84 (1H, d)
3A-H	2.05 (1H, m)			2.03 (1H, ddd)
3B-H	2.53 (1H, m)			2.55 (1H, dd)

Reference	[147, 148]	[147]	[147]	[149]
4-H	6.20 (1H, dd, J=8.2, 4.0 Hz)	6.15 (1H, dd, J=8.0, 4.0 Hz)	6.29 (1H, dd, J=8.0, 4.1 Hz)	6.30 (1H, dd)
7A-H	2.00 (1H, m)			
7B-H	1.66 (1H, m)			
8A-H	2.02 (1H, m)			
8B-H	2.02 (1H, m)			
10-H	5.47 (1H, d br, J=4.3 Hz)	5.44 (1H, d, J=5.0 Hz)	5.47 (1H, d, J=5.5 Hz)	5.50 (1H, dm)
11-H	3.89 (1H, d, J=4.3 Hz)	3.91 (1H, d, J=5.0 Hz)	4.03 (1H, d, J=5.5 Hz)	4.09 (1H, d)
13A-H	3.13 (1H, d, J=4.1 Hz)	3.15 (1H, d, J=4.0 Hz)	3.13 (1H, d, J=4.0 Hz)	3.15 (1H, d)
13B-H	2.81 (1H, d, J=4.1 Hz)	2.83 (1H, d, J=4.0 Hz)	2.81 (1H, d, J=4.0 Hz)	2.83 (1H, d)
14-H	0.78 (3H, s)	0.76 (3H, s)	0.77 (3H, s)	0.80 (3H, s)
15A-H	3.93 (1H, d, J=12.0 Hz)	3.89 (1H, d, J=12.0 Hz)	4.01 (1H, d, J=12.5 Hz)	4.06 (1H, d)
15B-H	4.30 (1H, d, J=12.0 Hz)	4.31 (1H, d, J=12.0 Hz)	4.17 (1H, d, J=12.5 Hz)	4.16 (1H, d)
16-H	1.70 (3H, s br)	1.67 (3H, s)	1.68 (3H, s)	1.71 (3H, s br)
18-H				
2'-H	5.95 (1H, s br)	5.98 (1H, s)	5.82 (1H, d, J=1.2 Hz)	5.83 (1H, q)
4'A-H	2.50 (1H, m)			

Reference	[147, 148]	[147]	[147]	[149]
4'B-H	2.50 (1H, m)		2.29 (1H, m)	
5'A-H	3.56 (1H, m)	3.50 (1H, dt, J=15.0, 6.0 Hz)	3.56 (1H, ddd, J=10.1, 7.4, 5.0 Hz)	
5'B-H	3.56 (1H, m)	3.69 (1H, dt, J=15.0, 6.0 Hz)	3.73 (1H, ddd, J=10.1, 7.5, 7.4 Hz)	
6'-H	3.69 (1H, m)		3.89 (1H, m)	3.74 (1H, m)
7'-H	5.90 (1H, dd, J=15.4, 3.2 Hz)	5.86 (1H, dd, J=15.0, 3.0 Hz)	5.87 (1H, dd, J=15.6, 6.1 Hz)	5.71 (1H, dd)
8'-H	7.51 (1H, dd, J=15.4, 11.4 Hz)	7.45 (1H, dd, J=15.0, 11.0 Hz)	7.54 (1H, dd, J=15.6, 11.0 Hz)	7.55 (1H, dd)
9'-H	6.56 (1H, dd, J=11.4, 11.4 Hz)	6.54 (1H, dd, J=11.0, 11.0 Hz)	6.60 (1H, dd, J=11.0, 11.0 Hz)	6.60 (1H, dd)
10'-H	5.74 (1H, d, J=11.4 Hz)	5.70 (1H, d, J=11.0 Hz)	5.80 (1H, d, J=11.0 Hz)	5.82 (1H, d)
12'-H	2.26 (3H, d, J=1.4 Hz)	2.24 (3H, s)	2.21 (3H, d, J=1.2 Hz)	2.22 (3H, d)
13'-H	3.63 (1H, m)		3.98 (1H, qd, J=6.5, 3.0 Hz)	3.70 (1H, m)
14'-H			1.12 (3H, d, J=6.5 Hz)	1.17 (3H, d)

Table 5.9: ^{1}H NMR chemical shifts for epiisororidin E **1** and isororidin E **2**, together with their respective reference.

Reference	**1**	[147]	**2**	[149]
H	**epi isororidin E**	**epi isororidin E**	**iso roridin E**	**iso roridin E**
2-H	3.83	3.83 (1H, d, J=5.0 Hz)	3.84	3.84 (1H, d)
3A-H	2.01		1.99	2.03 (1H, ddd)
3B-H	2.56		2.58	2.55 (1H, dd)
4-H	6.32	6.29 (1H, dd, J=8.0, 4.1 Hz)	6.37	6.30 (1H, dd)
7A-H	1.51		1.49	
7B-H	2.11		2.1	
8A-H	2.0		2.0	
8B-H	2.0		2.0	
10-H	5.50	5.47 (1H, d, J=5.5 Hz)	5.50	5.50 (1H, dm)
11-H	4.08	4.03 (1H, d, J=5.5 Hz)	4.08	4.09 (1H, d)
13A-H	3.14	3.13 (1H, d, J=4.0 Hz)	3.15	3.15 (1H, d)
13B-H	2.82	2.81 (1H, d, J=4.0 Hz)	2.83	2.83 (1H, d)
14-H	0.79	0.77 (3H, s)	0.79	0.80 (3H, s)

Reference	**1**	[147]	**2**	[149]
15A-H	4.04	4.01 (1H, d, J=12.5 Hz)	4.06	4.06 (1H, d)
15B-H	4.17	4.17 (1H, d, J=12.5 Hz)	4.16	4.16 (1H, d)
16-H	1.71	1.68 (3H, s)	1.71	1.71 (3H, s br)
18-H				
2'-H	5.84	5.82 (1H, d, J=1.2 Hz)	5.83	5.83 (1H, q)
4'A-H	2.57		2.55	
4'B-H	2.33	2.29 (1H, m)	2.32	
5'A-H	3.59	3.56 (1H, ddd, J=10.1, 7.4, 5.0 Hz)	3.48	
5'B-H	3.75	3.73 (1H, ddd, J=10.1, 7.5, 7.4 Hz)	3.81	
6'-H	3.91	3.89 (1H, m)	3.73	3.74 (1H, m)
7'-H	5.89	5.87 (1H, dd, J=15.6, 6.1 Hz)	5.70	5.71 (1H, dd)
8'-H	7.53	7.54 (1H, dd, J=15.6, 11.0 Hz)	7.54	7.55 (1H, dd)
9'-H	6.60	6.60 (1H, dd, J=11.0, 11.0 Hz)	6.60	6.60 (1H, dd)
10'-H	5.82	5.80 (1H, d, J=11.0 Hz)	5.82	5.82 (1H, d)

Reference	**1**	[147]	**2**	[149]
12'-H	2.21	2.21 (3H, d, J=1.2 Hz)	2.21	2.22 (3H, d)
13'-H	3.99	3.98 (1H, qd, J=6.5, 3.0 Hz)	3.71	3.70 (1H, m)
14'-H				

Table 5.10: ^{1}H NMR chemical shifts reported in the literature for 8α-OH-roridin H , 8α-acetoxy-roridin H and roridin J.

	[153]	[152]	[150]	[157]
	8α-OH-roridin H	**8α-acetoxy-roridin H**	**roridin H**	**roridin J**
H	3.82 (1H, d, J=5.0 Hz)	3.84 (1H, d, J=5.0 Hz)	3.8 (1H, d, J=5 Hz)	3.85d
2-H	2.49 (1H, dd, J=15.2, 8.2 Hz)	2.19 (1H, m)		2.1 m
3A-H	2.17 (1H, m)	2.48 (1H, dd, J= 8.5, 15.5 Hz)		2.48dd
3B-H	5.94 (1H, dd, J=8.2, 4.1 Hz)	5.90(1H, dd, J= 4.5, 8.5 Hz)	5.9 (1H, m)	6.0dd
4-H	2.18 (1H, m)	2.11 (1H, m)		2.0 m
7A-H	2.07 (1H, m)	2.24 (1H, m)		
7B-H	4.12 (1H, d(br), J=4.8 Hz)	5.19 (1H, d, J= 4.5 Hz)		2.0 m

	[153]	[152]	[150]	[157]
8A-H	-		-	
8B-H	5.56 (1H, d(br), J=5.8 Hz)	5.70 (1H, dt, J= 0.5, 5.5 Hz)	5.42 (1H, d, J=4 Hz)	5.44d
10-H	3.75 (1H, d, J= 5.8 Hz)	3.76 (1H, d, J= 5.5 Hz)	3.64 (1H, m)	3.63d
11-H	3.10 (1H, d, J=4.1 Hz)	2.84 (1H, d, J= 4.0 Hz)	2.96 (1H, ABq, J=4 Hz)	2.97
13A-H	2.83 (1H, d, J=4.1 Hz)	3.11 (1H, d, J= 4.0 Hz)	2.96 (1H, ABq, J=4 Hz)	
13B-H	0.88 (3H, s)	0.84 (3H, s)	0.85 (3H, s)	0,87
14-H	4.39 (1H, s(br))	4.36 (1H,d, J= 12.5 Hz)	4.15 (1H, ABq, J=12 Hz)	4.21
15A-H	4.39 (1H, s(br))	4.41 (1H, d, J= 12.5 Hz)	4.15 (1H, ABq, J=12 Hz)	
15B-H	1.86 (3H, m)	1.76 (3H, s)	1.69 (3H, s)	1.74
16-H		1.93 (3H, s)		
18-H	5.69 (1H, s(br))	5.64 (1H, s)	5.67 (1H, s)	5.84 d
2'-H	2.63 (1H, m)	2.24 (1H, m)	2.64 (1H, d, J=11 Hz)	3.85 d
4'A-H	2.26 (1H, m)	2.66 (1H, dd, J= 3.5, 12.0 Hz)		

	[153]	[152]	[150]	[157]
4'B-H	5.52 (1H, dd, J= 8.3, 3.2 Hz)	5.53 (1H, dd, J= 3.5,8.5 Hz)	5.58 (1H, dd, J=8, 3.5 Hz)	5.24 d
5'A-H	-		-	
5'B-H	4.06 (1H, d, J=8.5 Hz)	4.07 (1H,dt, J= 2.5, 8.5 Hz)	4.03 (1H, m)	3.87
6'-H	5.95 (1H, dd, J=15.3, 15.3 Hz)	5.96 (1H, dd, J= 2.5 Hz)	5.9 (1H, m)	5.80 d
7'-H	7.70 (1H, dd, J=15.3, 11.4 Hz)	7.65 (1H, ddt, J= 1.0, 11.5, 15.5 Hz)	7.68 (1H, dd, J= 15.5, 11 Hz)	7.70 dd
8'-H	6.56 (1H, t, J=11.4 Hz)	6.57 (1H, dd, J= 11.5 Hz)	6.55 (1H, t, J=11 Hz)	6.54 t
9'-H	5.80 (1H, d, J=11.4 Hz)	5.80 (1H, dd, J= 1.0, 11.5 Hz)	5.79 (1H, d, J=11 Hz)	5.9 d
10'-H	2.27 (3H, s)	2.28 (3H, d, J= 1.0 Hz)	2.27 (3H, d, J=1.5 Hz)	2.28 d
12'-H	3.66 (1H, dq, J=8.5, 6.0 Hz)	3.67 (1H, dq, J= 6.0,8.5 Hz)	3.65 (1H, m)	3.70 q
13'-H	1.32 (3H, d, J=6.0 Hz)	1.35 (3H, d, J= 6.0 Hz)	1.32 (3H, d, J=6 Hz)	1.36 d
14'-H				

Table 5.11: ^{1}H NMR chemical shifts for 8α-OH-roridin H **4** , 8α-acetoxy-roridin H **5** and roridin J **6** 1H NMR chemical shifts for 8α-OH-roridin H , together with their respective reference.

	[150]	**3**	[153]	**4**	**5**	[152]	**6**	[157]
	roridin H	**roridin H**	**8α-OH-roridin H**	**8α-OH-roridin H**	**8α-acetoxy-roridin H**	**8α-acetoxy-roridin H**	**roridin J**	**roridin J**
H	3.8 (1H, d, J=5 Hz)	3.83 (1H, d, J=5.3 Hz)	3.82 (1H, d, J=5.0 Hz)	3.82 (1H, d, J=5.2 Hz)	3.82 (1H, d, J=5.1 Hz)	3.84 (1H, d, J=5.0 Hz)	3.85 (1H, d, J=5 Hz)	3.85d
2-H		2.46 (1H, dd, J=15.3, 8.4 Hz)	2.49 (1H, dd, J=15.2, 8.2 Hz)	2.49 (1H, dd, J=15.4, 8.3 Hz)	2.46 (1H, dd, J=15.3, 8.4 Hz)	2.19 (1H, m)	2.48 (1H, dd, J=15, 8 Hz)	2.1 m
3A-H			2.17 (1H, m)	2.17 (1H, m)	2.17 (1H, ddd, J=15.4, 5.2, 4.6 Hz)	2.48 (1H, dd, J= 8.5, 15.5 Hz)	2.1 (1H, m)	2.48dd
3B-H	5.9 (1H, m)	5.92	5.94 (1H, dd, J=8.2, 4.1 Hz)	5.93 (1H, m)	5.89 (1H, dd, J=8.2, 4.5 Hz)	5.90(1H, dd, J= 4.5, 8.5 Hz)	6.00 (1H, dd, J=8, 4 Hz)	6.0dd
4-H			2.18 (1H, m)	2.17 (1H, m)		2.11 (1H, m)	2 (1H, m)	2.0 m
7A-H			2.07 (1H, m)	2.06 (1H, dd, J=15, 14 Hz)		2.24 (1H, m)	2 (1H, m)	

	[150]	**3**	[153]	**4**	**5**	[152]	**6**	[157]
7B-H			4.12 (1H, d(br), J=4.8 Hz)	4.11 (1H, m)		5.19 (1H, d, J= 4.5 Hz)	2 (1H, m)	2.0 m
8A-H	-		-	-			2 (1H, m)	
8B-H	5.42 (1H, d, J=4 Hz)	5.43	5.56 (1H, d(br), J=5.8 Hz)	5.55 (1H, d J=6 Hz)	5.43 (1H, ddq, J=4.8, 1.9, 1.1 Hz)	5.70 (1H, dt, J= 0.5, 5.5 Hz)	5.44 (1H, d, J=5 Hz)	5.44d
10-H	3.64 (1H, m)		3.75 (1H, d, J= 5.8 Hz)	3.75 (1H, d, J=5.7 Hz)	3.62 (1H, d(br), J=5.8 Hz)	3.76 (1H, d, J= 5.5 Hz)	3.63 (1H, d, J=5 Hz)	3.63d
11-H	2.96 (1H, ABq, J=4 Hz)	3.11 (1H, d, J=4.0, 1.0Hz)	3.10 (1H, d, J=4.1 Hz)	3.10 (1H, d, J=4.1 Hz)	3.12 (1H, d, J=4.0 Hz)	2.84 (1H, d, J= 4.0 Hz)	2.97 (1H, AB)	2.97
13A-H	2.96 (1H, ABq, J=4 Hz)	2.81 (1H, d, J=4.2 Hz)	2.83 (1H, d, J=4.1 Hz)	2.83 (1H, d, J=4.1 Hz)	2.81 (1H, d, J=4.0 Hz)	3.11 (1H, d, J= 4.0 Hz)	2.97 (1H, AB)	
13B-H	0.85 (3H, s)	0.85 (3H, s)	0.88 (3H, s)	0.88 (3H, s)	0.84 (3H, s)	0.84 (3H, s)	0.87 (3H, s)	0,87
14-H	4.15 (1H, ABq, J=12 Hz)	4.31 (1H, d, J=12.6 Hz)	4.39 (1H, s(br))	4.39 (1H, m)	4.38 (1H, d, J=12.4 Hz)	4.36 (1H,d, J= 12.5 Hz)	4.21 (1H, AB)	4.21

	[150]	**3**	[153]	**4**	**5**	[152]	**6**	[157]
15A-H	4.15 (1H, ABq, J=12 Hz)	4.03 (1H, d, J=12.6 Hz)	4.39 (1H, s(br))	4.39 (1H, m)	4.01 (1H, d, J=12.4 Hz)	4.41 (1H, d, J= 12.5 Hz)	4.21 (1H, AB)	
15B-H	1.69 (3H, s)	1.69	1.86 (3H, m)	1.85 (3H, s(br))	1.70 (3H, dd, J=1.1, 1.1 Hz)	1.76 (3H, s)	1.74 (3H, s)	1.74
16-H					5.75 (1H, qd, J=1.4, 0.7 Hz)	1.93 (3H, s)	5.84 (1H, q, J=1.2 Hz)	
18-H	5.67 (1H, s)	5.67	5.69 (1H, s(br))	5.69 (1H, s(br))	3.82 (1H, ddq, J=6.9, 0.5, 0.2 Hz)	5.64 (1H, s)	3.85 (1H, d, J=7 Hz)	5.84 d
2'-H	2.64 (1H, d, J=11 Hz)	2.63 (1H, d(br), J=12.5 Hz)	2.63 (1H, m)	2.61 (1H, d, J=11 Hz)		2.24 (1H, m)		3.85 d
4'A-H		2.26 (1H, dd J=12.5, 8.5Hz)	2.26 (1H, m)	2.26 (1H, d(br), J=14 Hz)	5.24 (1H, d, J=6.9 Hz)	2.66 (1H, dd, J= 3.5, 12.0 Hz)	5.24 (1H, d, J=7 Hz)	

	[150]	**3**	[153]	**4**	**5**	[152]	**6**	[157]
4'B-H	5.58 (1H, dd, J=8, 3.5 Hz)	5.53 (1H, dddd, J=8.5, 3.4, 0.7, 0.2 Hz)	5.52 (1H, dd, J= 8.3, 3.2 Hz)	5.52 (1H, J=8, 4 Hz)		5.53 (1H, dd, J= 3.5,8.5 Hz)		5.24 d
5'A-H	-		-	-	4.08 (1H, dddd, J=8.6, 2.7, 2.7, 0.7 Hz)		3.87 (1H, m)	
5'B-H	4.03 (1H, m)	4.05 (1H, d, J=8.5, 2.7 Hz)	4.06 (1H, d, J=8.5 Hz)	4.06 (1H, d(br), J=8 Hz)	5.91 (1H, dddd, J= 15.2, 2.6, 0.8, 0.8 Hz)	4.07 (1H,dt, J= 2.5, 8.5 Hz)	5.8 (1H, d, J= 15.5 Hz)	3.87
6'-H	5.9 (1H, m)	5.93	5.95 (1H, dd, J=15.3, 15.3 Hz)	5.93 (1H, m)	7.64 (1H, dddd, J=15.2, 11.6, 2.2, 1.1 Hz)	5.96 (1H, dd, J= 2.5 Hz)	7.70 (1H, dd, J=15.5, 11.5 Hz)	5.80 d
7'-H	7.68 (1H, dd, J= 15.5, 11 Hz)	7.68 (1H, dddd, J=15.3, 11.6, 2.2, 1.0 Hz)	7.70 (1H, dd, J=15.3, 11.4 Hz)	7.70 (1H, dddd, J=15.2, 11.7, 2.2, 1.1 Hz)	6.54 (1H, dddd, J=11.3, 11.3, 0.7, 0.7 Hz)	7.65 (1H, ddt, J= 1.0, 11.5, 15.5 Hz)	6.54 (1H, dd, J=11.5, 11.5 Hz)	7.70 dd

	[150]	**3**	[153]	**4**	**5**	[152]	**6**	[157]
8'-H	6.55 (1H, t, J=11 Hz)	6.55 (1H, dddd, J=11.4, 11.4, 0.4, 0.4 Hz)	6.56 (1H, t, J=11.4 Hz)	6.55 (1H, dd, J=11.7, 11.1 Hz)	5.78 (1H, dddd, J=11.1, 1.1, 0.9, 0.9 Hz)	6.57 (1H, dd, J= 11.5 Hz)	5.9 (1H, d, J=11.5 Hz)	6.54 t
9'-H	5.79 (1H, d, J=11 Hz)	5.79 (1H, dd, J=11.1, 0.9 Hz)	5.80 (1H, d, J=11.4 Hz)	5.79 (1H, dd, J=11.1, 0.9 Hz)	2.26 (3H, d, J=1.5 Hz)	5.80 (1H, dd, J= 1.0, 11.5 Hz)	2.28 (3H, d, J=1.2 Hz)	5.9 d
10'-H	2.27 (3H, d, J=1.5 Hz)	2.27 (3H, s(br))	2.27 (3H, s)	2.26 (3H, s(br))	3.64 (1H, dq, J=8.8, 6.0 Hz)	2.28 (3H, d, J= 1.0 Hz)	3.70 (1H, q, J=6 Hz)	2.28 d
12'-H	3.65 (1H, m)	3.66 (1H, m)	3.66 (1H, dq, J=8.5, 6.0 Hz)	3.65 (1H, dq, J=9, 6.0 Hz)	1.36 (3H, d, J=6.0 Hz)	3.67 (1H, dq, J= 6.0,8.5 Hz)	1.36 (3H, d, J=6 Hz)	3.70 q
13'-H	1.32 (3H, d, J=6 Hz)	1.33 (3H, d, J=6.1 Hz)	1.32 (3H, d, J=6.0 Hz)	1.33 (3H, d, J=6.0 Hz)	3.82 (1H, d, J=5.1 Hz)	1.35 (3H, d, J= 6.0 Hz)	3.85 (1H, d, J=5 Hz)	1.36 d
14'-H					2.46 (1H, dd, J=15.3, 8.4 Hz)		2.48 (1H, dd, J=15, 8 Hz)	

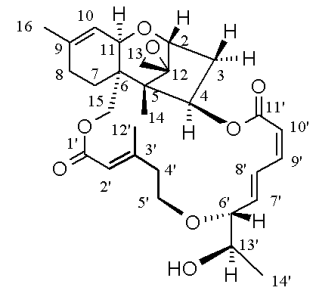

Roridin E (6'R, 13'R)

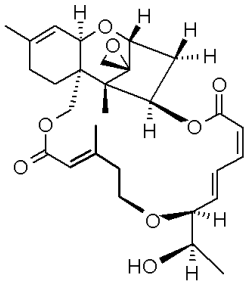

1 Epiisororidin E (6'S, 13'R)

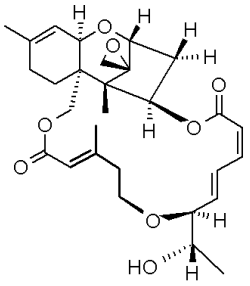

2 Isororidin E (6'S, 13'S)

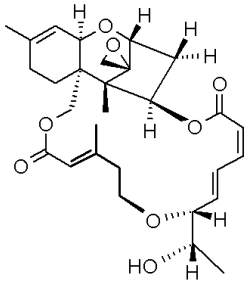

Epiroridin E (6'R, 13'S)

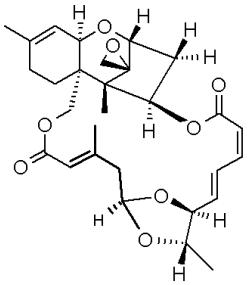

3 Roridin H (6'S, 13'S)

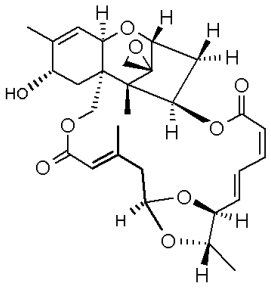

4 8α-Hydroxy-roridin H (8S,6'S, 13'S)

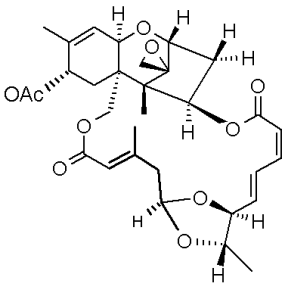

5 8α-Acetoxy-roridin H (8S,6'S, 13'S)

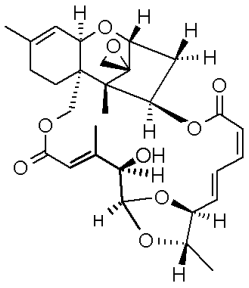

6 Roridin J (4'S,6'S, 13'S)

Figure 5.23: Chemical structures from the *Calcarisporium arbuscula* isolated roridins (**1** – **6**).

5.5.1.2 Fusidic acid

The mass spectra obtained from compound **7** in the negative mode showed an ion at m/z 515.2999 $[M\text{-}H]^-$, pointing to a molecular ion of $C_{31}H_{48}O_6$. The ^{13}C NMR of this compound confirmed the molecular formula derived by mass spectra by showing 31 resonances and revealed that the eight double bound equivalents required for such a molecular formula were formed by two double bonds with resonances at δC 151.20, 132.73, 129.34, and 123.04 and two carbonyl with ^{13}C resonances at δC 173.15 and 170.70 (Fig. 5.24). Four double bond equivalents remained demanding a tetracyclic compound. Careful inspection of the ^1H and ^{13}C NMR spectra (Fig. 5.24 and Fig. 5.25) led to the conclusion that we

were dealing with a rearranged sterol skeleton bearing six methyl groups. The six oxygen atoms were located in the acetate unit revealed by its characteristic resonance at δH 1.96, a free carboxyl group (δC at 173.15) and two hydroxyl groups with the adjacent carbons at δC 71.42 and 68.33. The α-protons of the hydroxyl groups could be found at δH 3.75 and 4.34. Analysis of the 2D-NMR spectra (COSY-45 and HETERO-COSY) (Fig. 5.26 and Fig.5.27) and comparison with data from the literature [158] led to the identification of the compound as fusidic acid **7** (Fig. 5.28). Fusidic acid **7** ^{1}H NMR and ^{13}C chemical shifts are found in table 5.12.

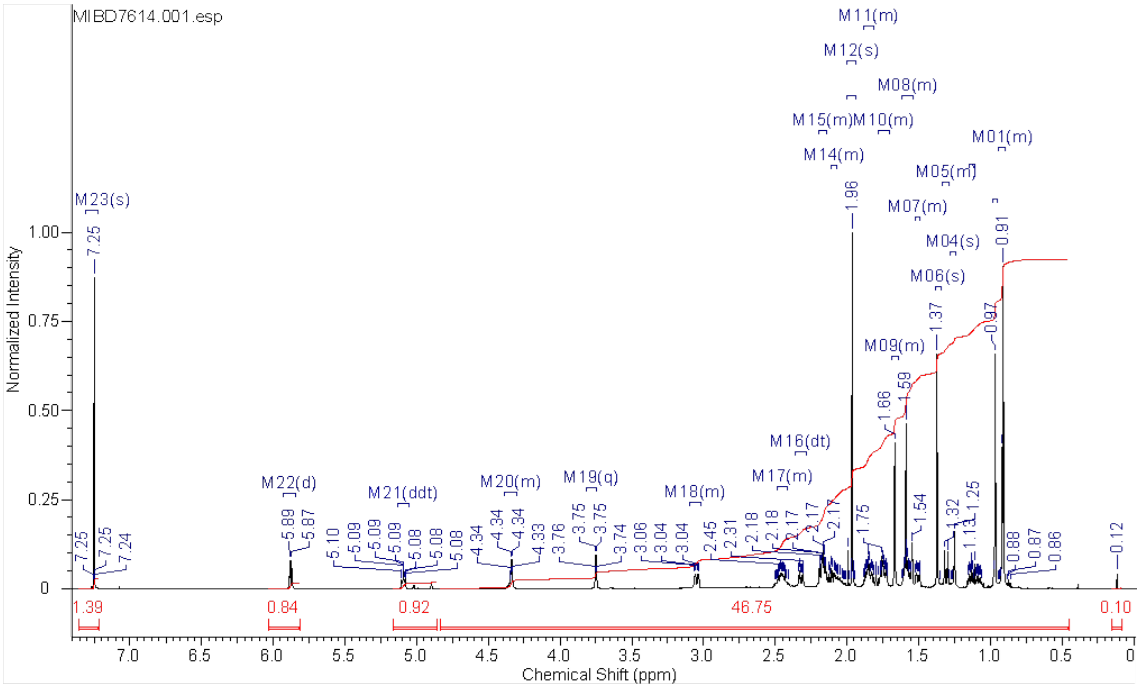

Figure 5.24: 600 MHz ^{1}H NMR spectrum from compound **7**, in $CDCl_3$. This compound was identified as fusidic acid.

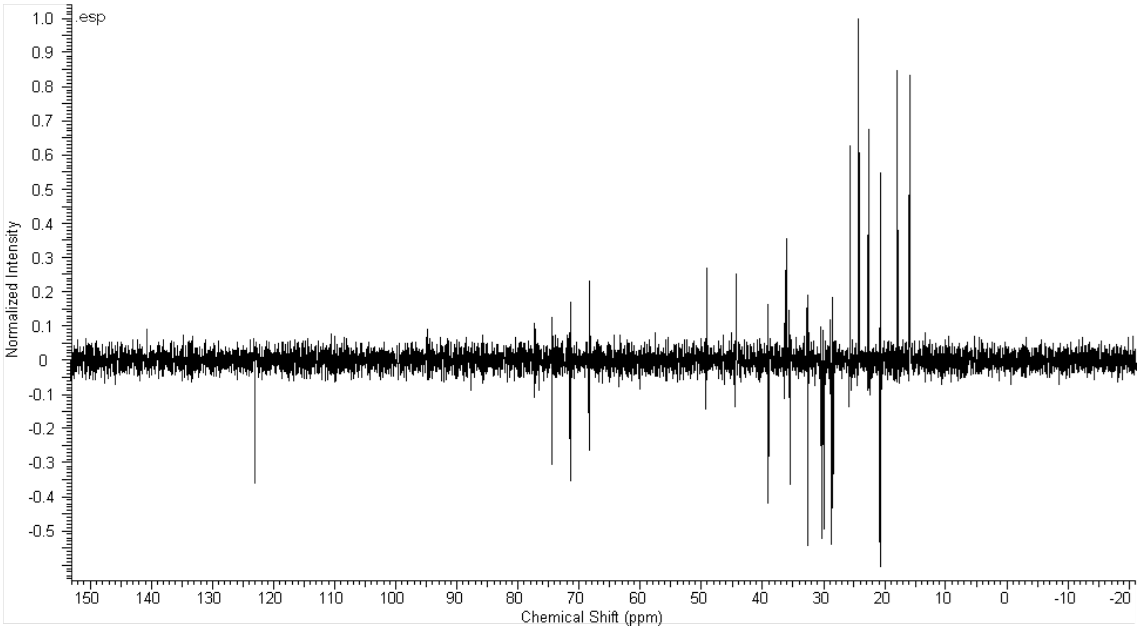

Figure 5.25: Fusidic acid **7** ^{13}C-NMR spectrum.

Table 5.12: ^{1}H NMR and ^{13}C chemical shifts for fusidic acid **7**, together with the data obtained from the literature.

	Fusidic acid **7**			[158]	
No	13C	1H	J	13C	1H
C-1	t 30,37	m 2,16	30,17	2,17	
		d 1,51			1,51
C-2	t 30,01	m 1,85		29,84	1,86
	m 1,73			1,75	
C-3	d 71,42	q 3,75	2	71,53	3,76
C-4	d 36,17	m 1,58		36,38	1,58
C-5	d 36,32	m 2,10		36,01	2,11
C-6	t 20,75	m 1,59		20,87	1,59
	m 1,08			1,13	
C-7	t 32,58	m 1,75		32,14	1,74
	m 1,12			1,12	
C-8	s 39,49			39,48	
C-9	d 49,22	m 1,54		49,32	1,57
C-10	s 37,16			36,95	
C-11	d 68,33	q 4,34	2	68,24	4,35

C-12	t 35,59	dt 2,32	12,5; 3	35,58	2,33
	m 1,83			1,85	
C-13	d 44,38	d br 3,05		44,29	3,06
C-14	s 48,8			48,72	
C-15	t 39,03	m 2,16		38,96	2,19
	d 1,31	13,5		1,3	
C-16	d 74,45	d 5,88	8	74,47	5,88
C-17	s 151,2			150,75	
C-18	q 17,83	s 0,90		17,78	0,91
C-19	q 22,69	s 0,97		22,99	0,98
C-20	s 129,34			129,64	
C-21	s 173,15			174,37	
C-22	t 28,83	m 2,45		28,77	2,46
C-23	t 28,45	m 2,15		28,46	2,17
	m 2,04			2,07	
C-24	d 123,04	tq 5,09	7; 2	123,1	5,1
C-25	s 132,73			132,58	
C-26	q 18,02	s 1,59		17,84	1,6
C-27	q 25,75	s 1,66		25,71	1,67
C-28	q 15,96	d 0,91		15,92	0,92
C-30	q 24,32	s 1,37		23,94	1,38
Ac-CO	s 170,55			170,7	
Ac	q 20,69	s 1,96		20,7	1,96

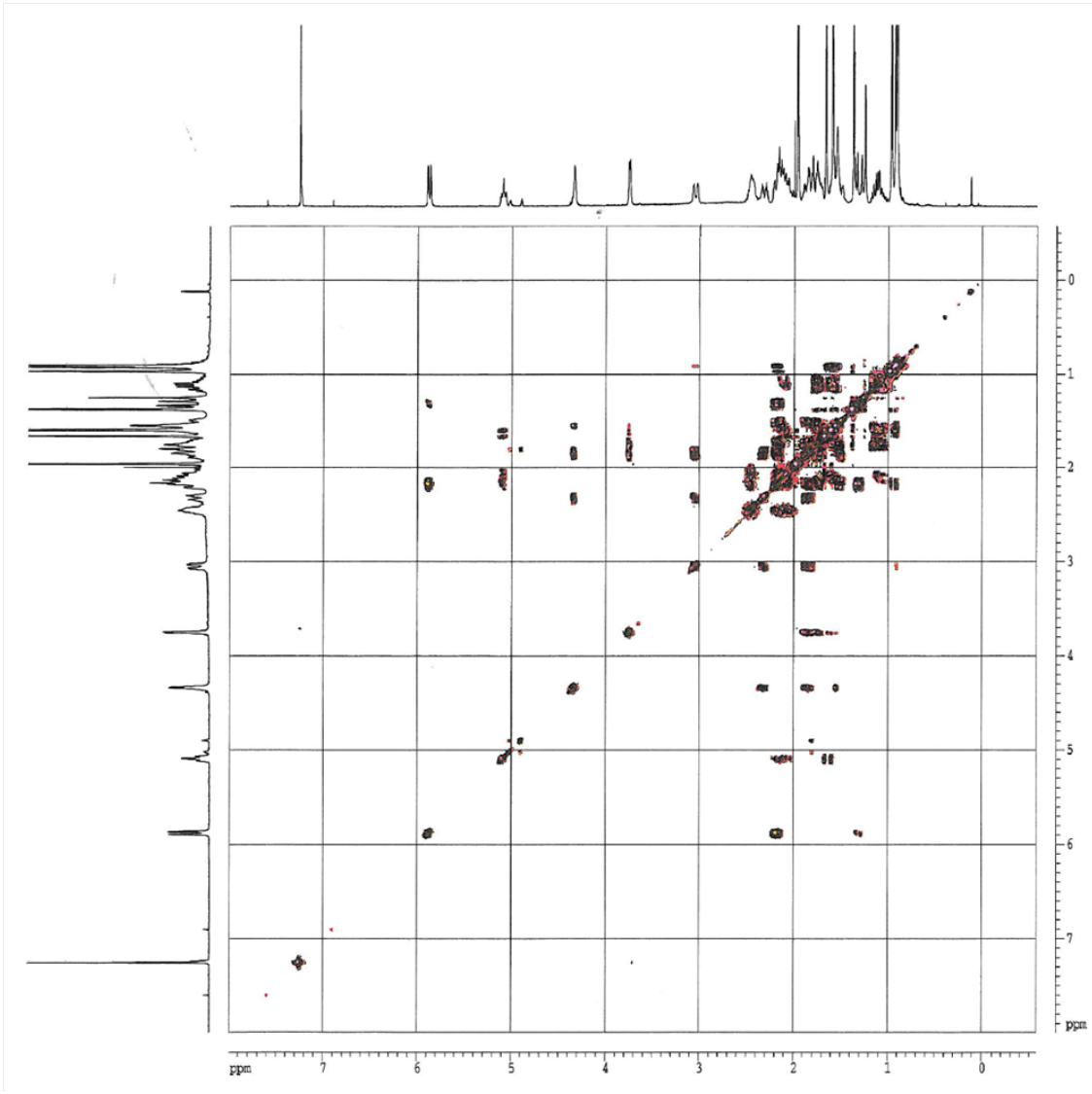

Figure 5.26: 2D NMR correlation spectroscopy (COSY) of fusidic acid **7**.

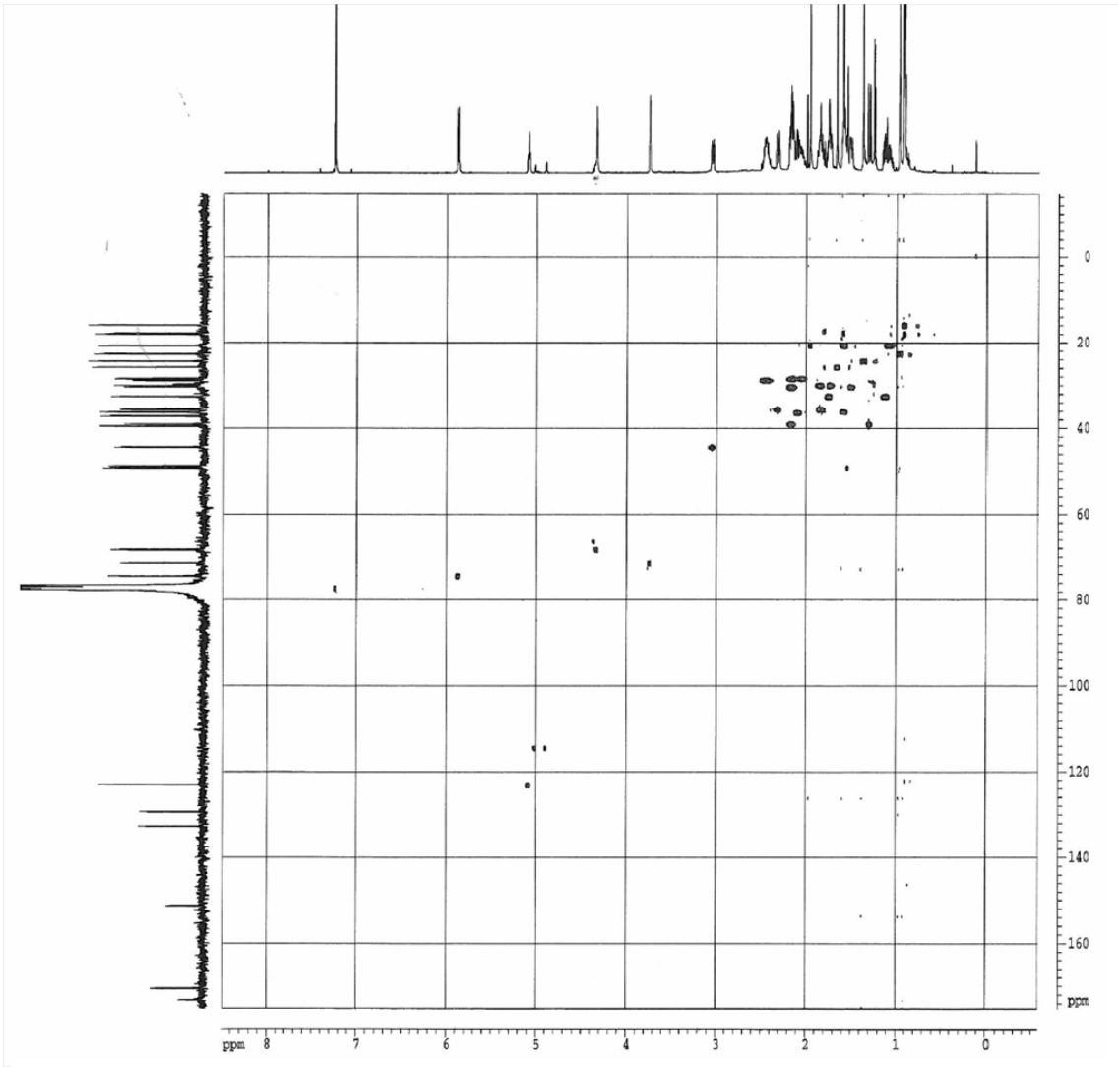

Figure 5.27: HMBC (Heteronuclear Multiple Bond Correlation) spectrum from fusidic acid **7**, produced by *Calcarisporium arbuscula*.

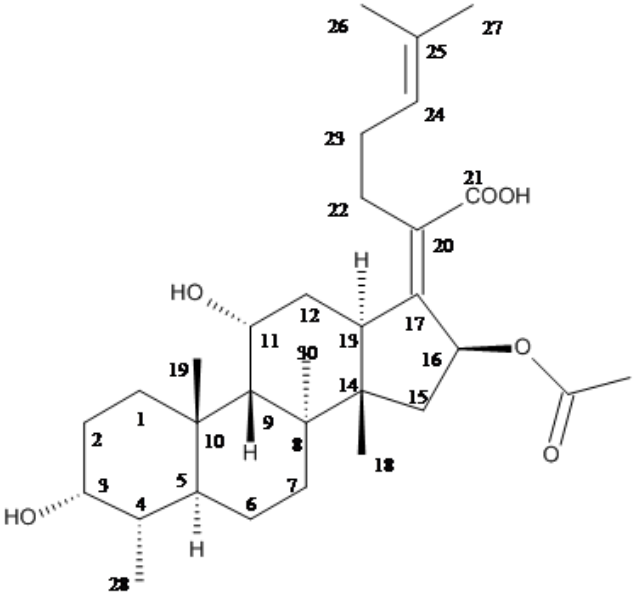

Figure 5.28: Fusidic acid **7** chemical structure.

5.5.2 Compound isolated from the fraction CA_B1 of *C. arbuscula* cultivation.

C. arbuscula cultivation in 5L of medium yielded 1.5 mg of compound **8**. The *m/z* of was calculated to 180. ^{1}H NMR spectra analysis pointed to a mixture, instead of a pure compound. Further purification led to the isolation of 0.4 mg of compound **8**. This sample was again subjected to ^{1}H NMR (Fig. 5.29), however, compound insufficient amount restrained additional NMR measurements. Therefore, structure of compound **8** remained unsolved.

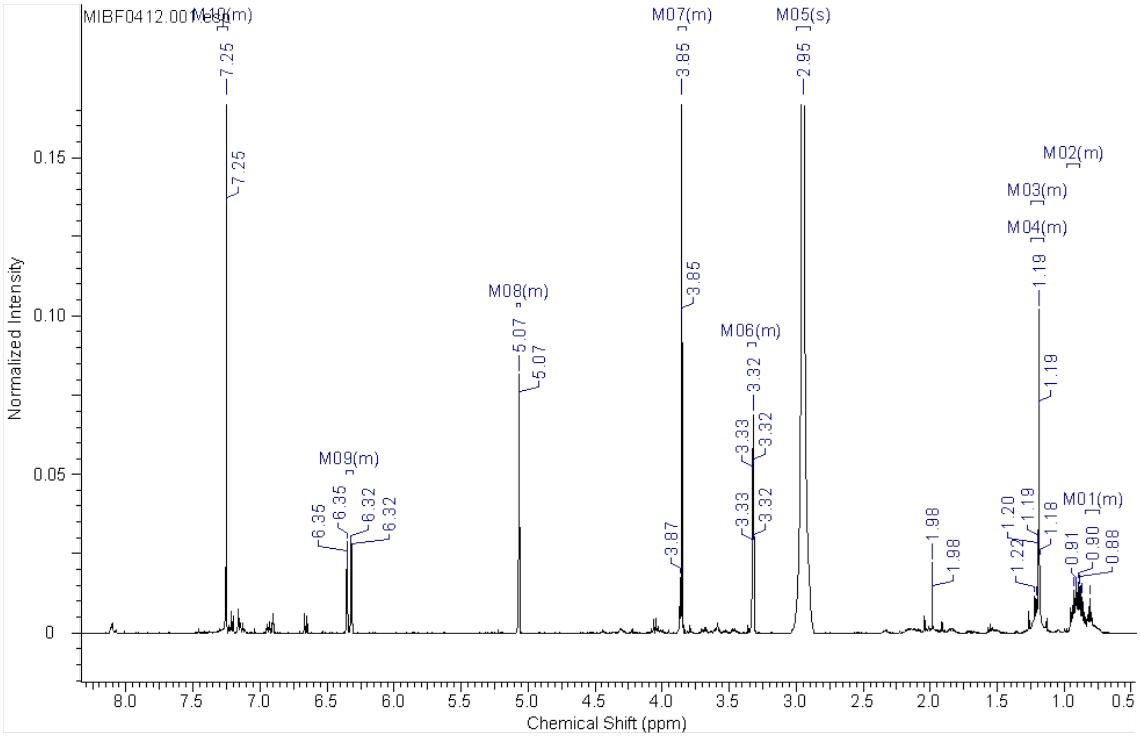

Figure 5.29: 700 MHz ^{1}H NMR spectrum from compound **8**, in $CDCl_3$. Structure of this compound remained unsolved.

5.5.3 Compounds isolated from *Coprinus comatus*.

Compound **9** had a molecular mass of 128 with the composition $C_6H_8O_3$. ^{1}H NMR showed an exo-methylene moiety at δH 6.34 and 5.98, a doublet of a methyl group at δH 1.44 and two protons at δH 4.45 and 4.34 (Fig. 5.30). Using ^{1}H-^{13}C-correlated NMR (Fig. 5.32) spectra structure elucidation led to the identification of **9** as 2-methylene-3,4-dihydroxypentanoic acid 1,4-lactone. Trans-configuration of the compound was deduced from the resonances of the methyl group at δH 1.44 instead of 1.40 and the 4-H at δH 4.34 instead of 4.7-5.0 reported for the cis-isomer (table 5.13) [159]. Absolute configuration was deduced from the negative sign of the optical rotation to be 3R, 4S as reported for this compound prepared by asymmetric synthesis [160]. Compound **9** was therefore identified as (3R,4S)-2-methylene-3,4-dihydroxypentanoic acid 1,4-lactone and named comatuslactone **9** (Fig. 5.34). This molecule was hitherto only known from synthesis but not reported as natural product.

Table 5.13: ^{1}H NMR and ^{13}C chemical shifts for comatuslactone **9**, together with the data obtained from the literature.

	2-methylene-3,4-dihydroxypentanoic acid 1,4-lactone [159, 160]		Cis-2-methylene-3,4-di hydroxy-pentanoic acid 1,4-lactone [159]	Compound **9** (comatuslactone)			
13C	1H	1H	1H	13C	1H	COSY	CH-long range
169.22				170.79			6.34, 5.98, (4.34)
138.43			s 141.11			6.34	
125.84	6.42 (1H, d, J=2 Hz)	6.36 (1H, d, J=2 Hz)	6.36 (1H, d, J=2 Hz)	t 125.41	6.34 (1H, d, J=2.4 Hz)	5.98, 4.46	-
	5.98 (1H, d, J=2 Hz)	6.00 (1H, d, J=1.8 Hz)	6.00 (1H, d, J=1.8 Hz)		5.98 (1H, d, J=2.2 Hz)	6.34, 4.46	
74.17	4.45 (1H, s)	4.3-4.6	4.7-5.0	d 75.32	4.45 (1H, dt, J=4.6, 2.3 Hz)	6.34, 5.98, 4.34, 1.44	6.34, 5.98, 4.34, 1.44
82.10	4.40 (1H, q, J=6.7 Hz)	4.3-4.6	4.7-5.0	d 83.37	4.34 (1H, dq, J=6.5, 4.6 Hz)	4.46, 1.44, 1.36	4.46, 1.44
19.02	1.3 (3H, d, J=6.7 Hz)	1.45 (3H, d, J=6.4 Hz)	1.40 (3H, d, J=6.0 Hz)	q 19.11	1.44 (3H, d, J=6.4 Hz)	4.48 o. 4.46, 4.34, 1.21	-

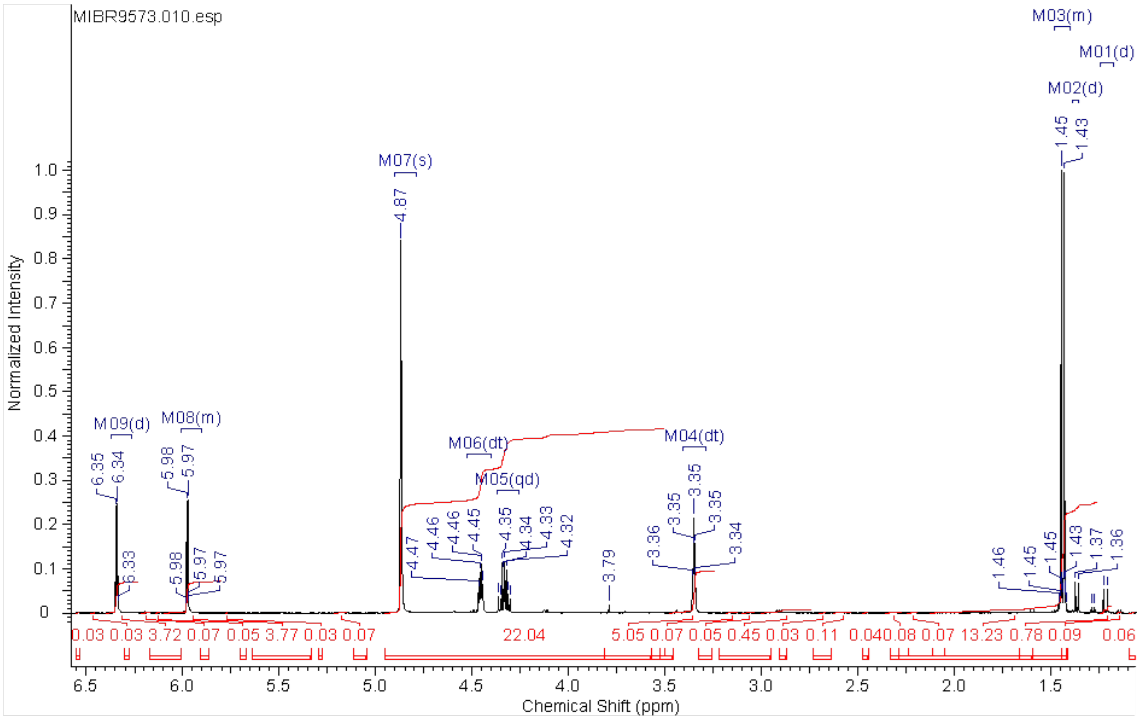

Figure 5.30: 400 MHz ^{1}H NMR spectrum from compound 9, in $MeOD_3$. This compound was identified as 2-methylene-3,4-dihydroxypentanoic acid 1,4-lactone (comatuslactone **9**).

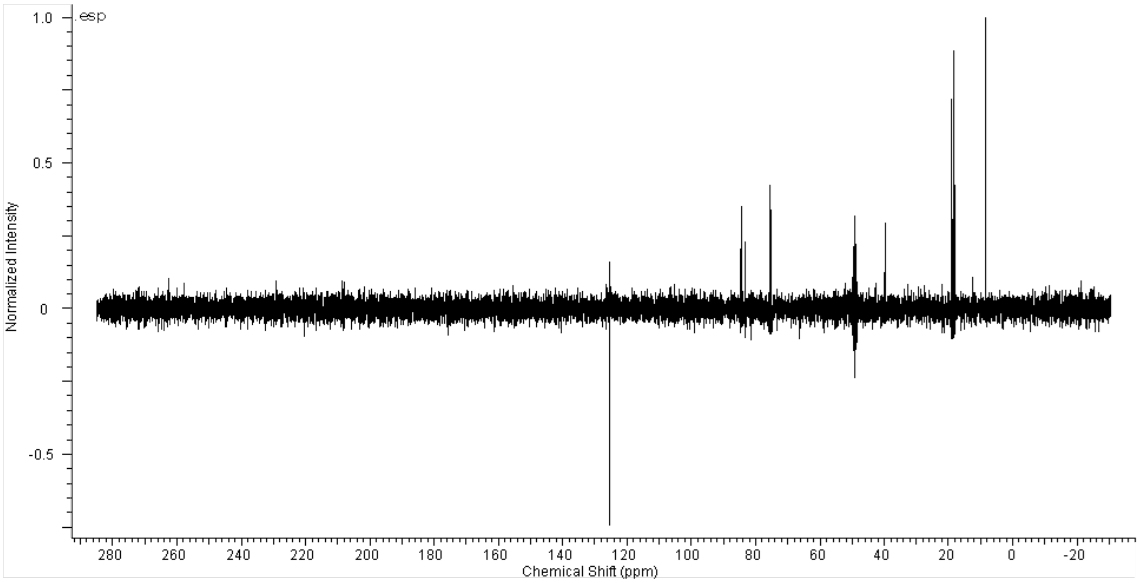

Figure 5.31: Comatuslactone **9** ^{13}C-NMR spectrum.

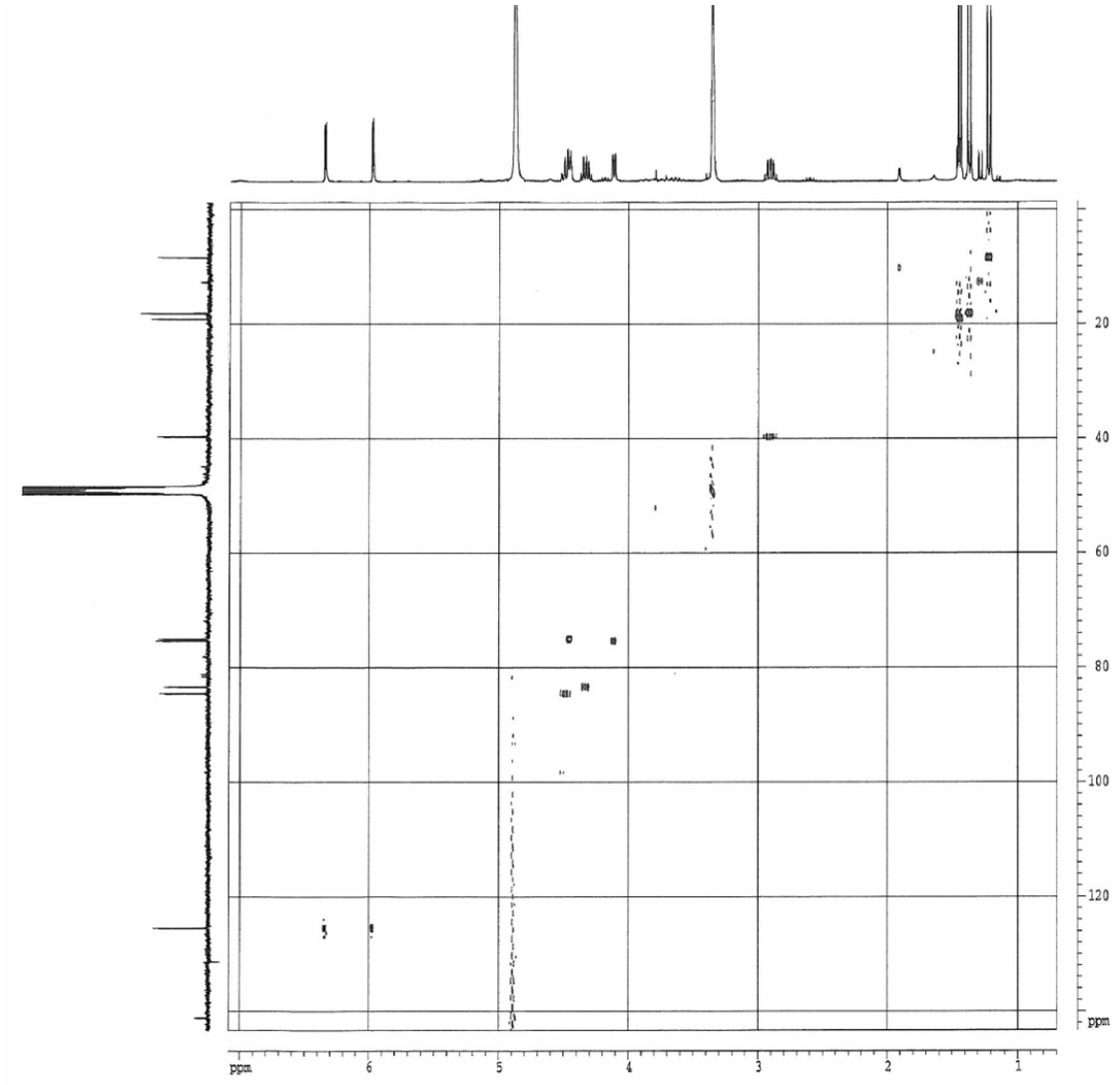

Figure 5.32: HMBC (Heteronuclear Multiple Bond Correlation) spectrum from comatuslactone **9**.

Together with **9** a second small molecule was isolated with the mass of 130 and the composition $C_6H_{10}O_3$. Because of its NMR (Fig. 5.33) spectra this metabolite, compound **10**, proved to be the dihydro-derivative of comatuslactone **9**. The relative configuration of the ring substituents were determined by comparison with NMR resonances of known compounds. Using NMR data of (2R,3R,4S)- and (2S,3R,4S)-2-methyl-3,4-dihydroxypentanoic acid 1,4-lactone [159], 5S, 3'R, 4'S, 5'S- and 5S, 3'S, 4'S, 5'S-hydroxyancepsenolide as well as (2S*,3R*,4S*)-2-n-hexadecyl-3,4-dihydroxypentanoic acid 1,4-lactone [161] it could be shown that a trans-configuration of the 3-OH to the 4-methyl group causes a shielding of about δH 0.3-07 ppm and a deshielding of about δC 5 ppm compared to a cis-arrangement. The ^{1}H NMR and optical rotation data data of both the (2R,3R,4S)-trans,trans- and (2S, 3R, 4S)-cis,trans-comatuslactone reported by Bernadi *et al.* [160] led to the identification of **10** as (2S, 3R, 4S)-2-methyl-3,4-dihydroxypentanoic acid 1,4-lactone. As for comatuslactone **9** its dihydro-derivative has not been reported as natural product.

Table 5.14: ^{1}H NMR and ^{13}C chemical shifts for compound **10** ((2S,3R ,4S)-2-methyl-3,4-dihydroxypentanoic acid 1,4-lactone), together with the data obtained from the literature.

(2S,3R ,4S)-2-methyl-3,4-dihydroxypentanoic acid 1,4-lactone [164, 165]		Compound **10**		
1H	13C	1H	COSY	CH-long range
181.06			4.46, 4.11, 2.89, 1.21	
4.5 (1H, dq, J=5.9, 1.3 Hz)	d 84.52	4.48 (1H, qd, J=6.8, 1.4 Hz)	4.11, 1.36	4.11, 1.36
4.15 (1H, dd, J=5.9, 1.3 Hz)	d 75.02	4.12 (1H, dd, J=5.7, 1.3 Hz)	4.48, 2.89, 1.21	4.48, 1.36, 1.21
2.75 (1H, dq, J=6, 5.9 Hz)	39.70	2.89 (1H, dq, J=7.3, 4.4 Hz)	4.11, 1.21	1.21
1.35 (3H, d, J=6 Hz)	q 18.14	1.37 (3H, d, J=6.8 Hz)	4.48, 4.46, (4.34), 1.21	4.11
1.25 (3H, d, J=6 Hz)	q 8.40	1.22 (3H, d, J=7.3 Hz)	4.11, 2.89, 1.44, 1.36	2.89

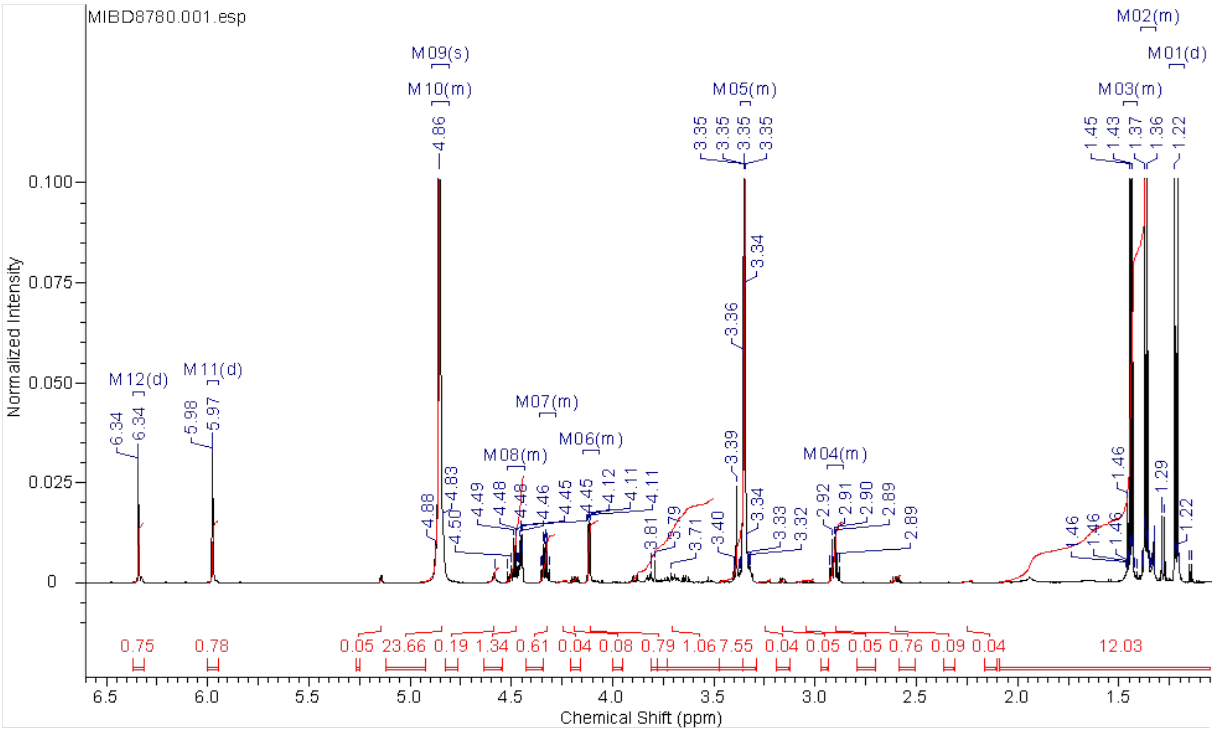

Figure 5.33: 400 MHz ^{1}H NMR spectrum from a mixture comprising 2-methylene-3,4-dihydroxypentanoic acid 1,4-lactone (comatuslactone **9**) together with (2S, 3R, 4S)-2-methyl-3,4-dihydroxypentanoic acid 1,4-lactone **10**, in CD_3OD.

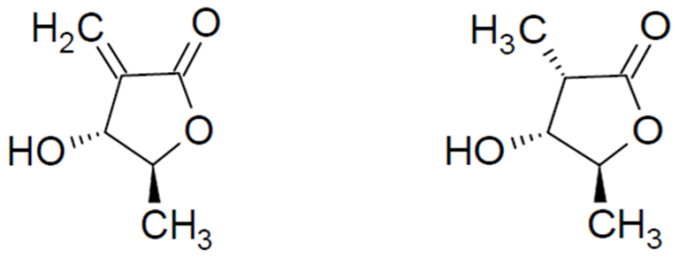

2-methylene-3,4-dihydroxypentanoic acid 1,4-lactone (comatuslactone **9**)

(2S,3R ,4S)-2-methyl-3,4-dihydroxypentanoic acid 1,4-lactone) **10**

Figure 5.34: Structures from comatuslactone **9** and its dihydro-derivative, (2S, 3R, 4S)-2-methyl-3,4-dihydroxypentanoic acid 1,4-lactone **10**.

5.6 Biological activity displayed by the isolated compounds

5.6.1 Planktonic cells

5.6.1.1 Minimal inhibitory concentration (MIC)

MIC values of six purified compounds (epiisororidin E **1**, isororidin E 2 **2**, roridin H **3**, 8α-hydroxyl roridin H **4**, roridin J **6** and comatuslactone **9**) were determined using bacterial and yeast strains listed on the sections 4.2.2 and 4.2.3. Compound **5** and compound **8** were not isolated as pure compounds (compound **5** was isolated as a mixture between a roridin (8α-acetoxy roridin H **5**) and a phenolic compound and compound **8** exhibited impurities); nevertheless, their MIC values were determined as well. The only exception here was fusidic acid **7**. This compound is already used in the clinics against infections caused by Gram-positive bacteria; therefore neither the antibacterial nor the antifungal activity was tested. Due to quantities constraints, compound 5 was tested only against *C. albicans*, *P. aeruginosa* and *S. aureus*.

All of the isolated roridins, inhibited the growth of *Y. lipolytica*. Interestingly, epiisororidin E **1** and isororidin E **2** showed a fungicide activity, while roridin H 3 and 8α-hydroxyl roridin H **4** worked as fungistatic compounds. Roridin H **3** showed the highest activity between the isolated roridins (table 5.16). None of the roridins showed activity against bacterial growth (table 5.15).

The mixture comprising compound **5** was active against *C. albicans* and *S. aureus* (table 5.15). Compound **8** showed antibiotic properties only against Gram-positive bacteria, although no effect was verified when *S. mutans* cultures were employed (table 5.15). Comatuslactone demonstrated a broad spectrum activity, inhibiting the growth of all of the investigated bacteria. When the treated bacteria were incubated on fresh media, the growth capacity was restored, revealing a bacteriostatic effect (table 5.15). A lack of activity on yeast cells was verified (table 5.16).

MIC values established against bacteria are presented on table 5.15, as also compounds showing bactericidal or bacteriostatic effects. On table 5.16, MIC values obtained against yeasts as also their fungicide/ fungistatic effects are summarized.

Table 5.15: Minimal inhibitory concentrations (μg mL $^{-1}$) and growth effects from the isolated compounds against bacterial strains.

	B. cereus	*E. coli*	*M. roseus*	*P. aeruginosa*	*S. aureus*	*S. epidermidis*	*S. mutans*
01	>250	>250	>250	>250	>250	>250	>250
02	>250	>250	>250	>250	>250	>250	>250
03	>250	>250	>250	>250	>250	>250	>250
04	>250	>250	>250	>250	>250	>250	>250
05	nt	nt	nt	>250	125[1]	nt	nt
06	>250	>250	>250	>250	>250	>250	>250
07	nt	nt	nt	nt	nt	nt	nt
08	250	>250	125[1]	>250	250[1]	125[1]	>250
09	125[2]	125[2]	37.25[2]	150[2]	125[2]	125[2]	62.5[2]

Effect on growth: [1] Bactericide, [2] Bacteriostatic
nt - not tested

Table 5.16: Minimal inhibitory concentrations (μg mL $^{-1}$) and growth effects from the isolated compounds against yeasts.

	C. albicans	*C.* guilliermondii	*C.* krusei	*C.* parapsilosis	*C.* tropicalis	*R.* glutinis	*Y.* lipolytica
01	62.5 [2]	62.5 [2]	62.5 [1]	125 [2]	62.5 [2]	62.5 [1]	62.5 [1]
02	62.5 [2]	62.5 [2]	3 [1]	>250	62.5 [1]	62.5 [2]	31.25 [1]
03	>250	>250	>250	>250	31.25 [2]	>250	31.25 [2]
04	>250	>250	>250	>250	>250	>250	31.25 [2]
05	125[2]	nt	nt	nt	nt	nt	nt
06	>250	>250	>250	>250	>250	>250	31.25 [2]
07	nt	nt	nt	nt	nt	nt	nt
08	>250	>250	>250	>250	>250	>250	>250
09	>250	>250	>250	>250	>250	>250	>250

Effect on growth: [1] Fungicide, [2] Fungistatic
nt - not tested

5.6.1.2 Effects of comatuslactone on bacterial cells

Since comatuslactone **9** showed bacteriostatic activity, transmission electron microscopy (TEM) was applied to verify its effects on cellular structures. *P. aeruginosa* and *S. aureus* were grown overnight and treated with the established MICs of comatuslactone **9**. After 20 h of incubation, the cells were washed and submitted to microscopy procedures. Controls were treated with identical MeOH concentration.

5.6.1.2.1 *Pseudomonas aeruginosa* Images from samples treated only with MeOH (control) show cells in the late log phase, and cells with normal dense cytoplasm exist to an amount of roughly 30%. Ghost cells can be visualized (Fig. 5.35A, arrow 1). When a higher magnification was used, cytoplasmic membranes revealed to be intact and the cytoplasm showed normal densities and an adequate fibrillar meshwork of the bacterial chromosome (Fig. 5.35B, arrows 1). Cells treated with comatuslactone **9** showed a high amount of intracellular electron dense bodies (Fig. 5.35C, arrows 1- 5; 1D, arrows 2 and 3), which in general appear in contact with the cytoplasmic membrane. These electron dense bodies are also present in the controls (Fig. 5.35B, arrows 2 and 3) but here they are far less observed in the ghost-like residuals. Leakage of intracellular content could be observed by the appearance of extracellular fibrillar matter, similar to that of the cytoplasmic chromosome area (Fig. 5.35D, arrow 1), which undoubtedly represents DNA.

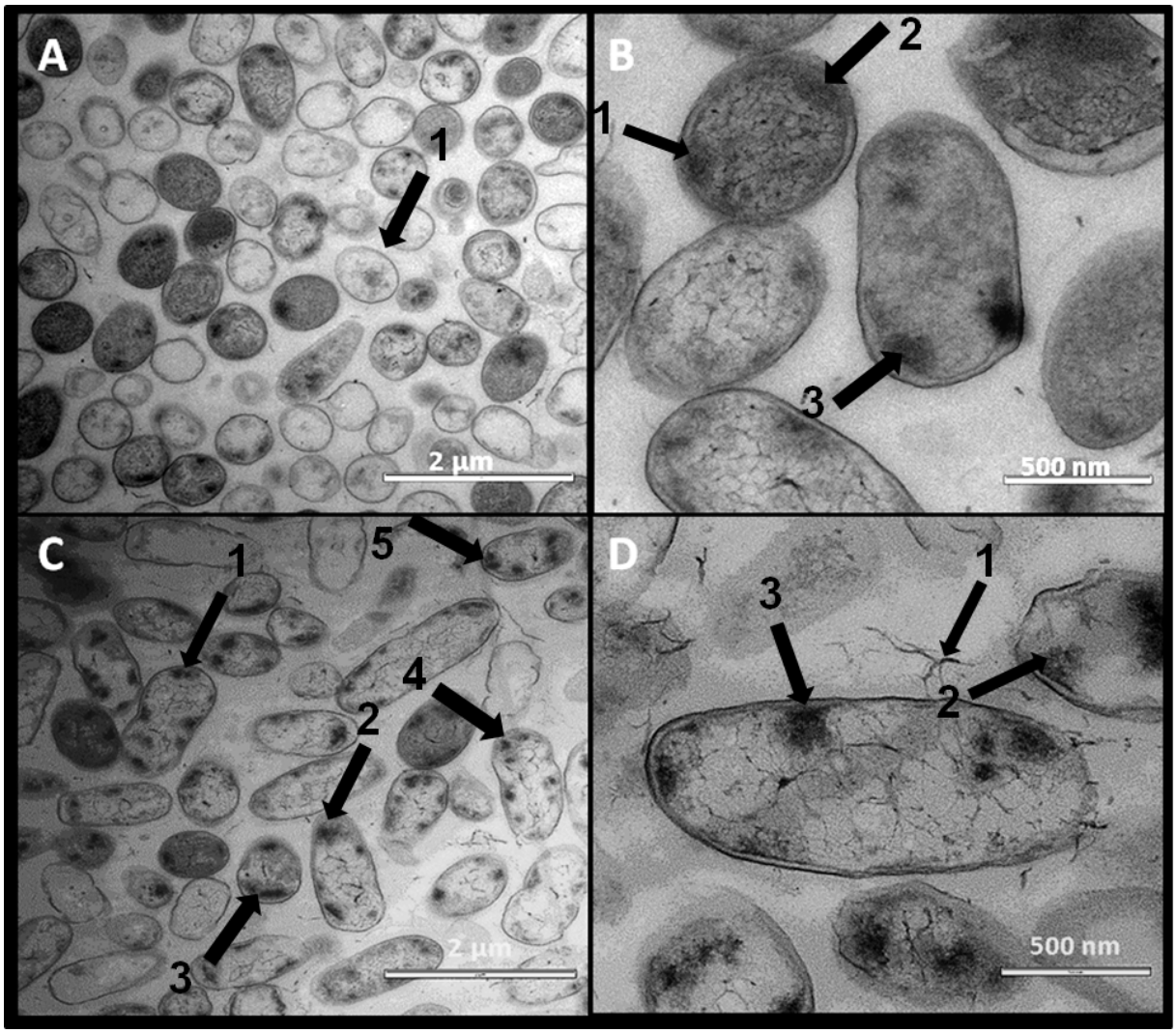

Figure 5.35: Effects caused by comatuslactone **9** on *P. aeruginosa* cells, visualized using transmission electron microscopy. Fig. 5.35A, arrow 1 indicates a ghost cell observed in the control samples (MeOH treated). Fig. 5.35B, arrow 1 shows the MeOH treated cells (control) using a higher magnification. Intact membranes and cytoplasmic organization can be observed. Fig. 5.35C and 5.35D demonstrate comatuslactone **9** treated cells. Fig. 5.35C arrows 1-5, point to electron dense bodies. Fig. 5.35D arrow 1 indicates extracellular fibrillar matter, caused by intracellular material leakage; arrows 2 and 3 indicate electron dense bodies. Photos: Dr. Heinrich Lünsdorf- HZI.

5.6.1.2.2 *Staphylococcus aureus* Micrographs obtained from late-log samples treated only with MeOH (control) show about 75% of the cells with normal dense cytoplasm. The overall cell size was obtained by the measurement of 10 cells and calculated to 0.8 $\pm$ 0.11 μm. Dividing and ghost cells can be both recognized Fig. 5.36A, arrows 1, 2 and 3). When the cells were visualized using a higher magnification, intact membranes and a normal cytoplasmic organization was noticed, with numerous cells in the state of division Fig. 5.36B, arrow 1). After treatment with comatuslactone **9**, a decrease of 31% of cell

diameter was observed Fig. 5.36C, arrow 1), clearly demonstrated by the comparison of Fig. 5.36A with 5.36C. Interestingly, only very few cells were observed in the division process Fig. 5.36C, arrow 2). Images obtained using a higher magnification show a myelin-like organization of the cytoplasmic membrane Fig. 5.36D, arrows 2 and 3), which can be taken as a characteristic feature of the lactone influence.

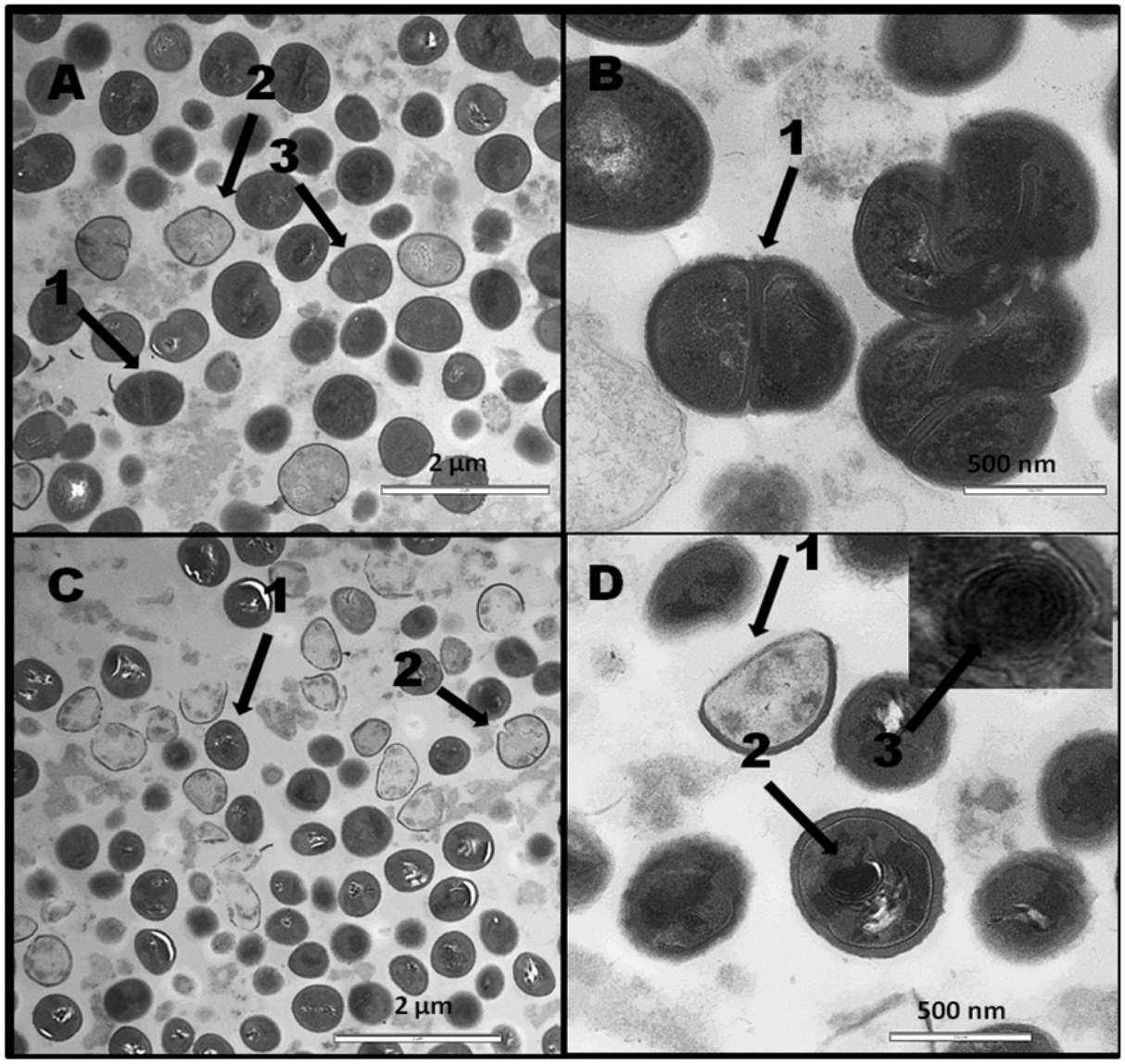

5

Figure 5.36: Electron micrographs of *S. aureus* cells, using transmission electron microscopy. A and B represent cells treated with MeOH (control). Fig. 5.36A, arrows 1 and 3 show cells with a normal dense cytoplasm, and in the state of cell division. Fig. 5.36B, arrow 1 shows the MeOH treated cells on a higher magnification, where intact membranes and a normal cytoplasmic matrix can be observed. Fig. 5.36C and 5.36D indicate cells treated with comatuslactone **9**. Fig. 5.36C, arrow 1 indicates a cell with dense cytoplasm, and a decreased diameter in comparison to the control. Fig. 5.36D, arrow 1 points to a ghost cell, and arrow 2 indicates the myeline-like structures. This myeline-like structure is shown in detail (arrow 3) in the inset. Photos: Dr. Heinrich Lünsdorf- HZI.

5.6.2 Biofilms

5.6.2.1 Minimal biofilm inhibitory concentration (MBIC)

MBIC was determined using *P. aeruginosa* and *S. aureus*. Biofilm formation was evaluated in polystyrene microtiter plates subsequently stained with crystal violet. Among the nine compounds tested, epiisororidin E **1**, roridin H **3** and compound **5** showed activity against biofilm formation of *S. aureus*. 100% of biofilm inhibition was observed, when the 250 μg mL^{-1} of epiisororidin E **1** was used and 50% of inhibition at the concentration of 125 μg mL^{-1}. Roridin H **3** inhibited 80% of biofilm formation at 250 μg mL^{-1}. Compound 5 inhibited *S. aureus* biofilms formation at the concentration of 62.5 μg mL^{-1}. When higher concentrations were used, this compound mixture also displayed antibiotic activity against *S. aureus*. None of the compounds could inhibit *P. aeruginosa* biofilm formation.

5.6.2.2 Activity on *in vitro* established biofilms

Considering comatuslactone **9** activity against *P. aeruginosa* and *S. aureus*, the purity and obtained quantity, the compound was selected for evaluation of its biofilm damaging properties. Therefore, bacteria were allowed to grow on 8-well chamber slides, in order to develop a biofilm. After the incubation time, medium was discharged and replaced by a medium containing serial dilutions of comatuslactone **9**, with concentrations ranging between 37.5 μg mL^{-1} and 300 μg mL^{-1} for *P. aeruginosa* biofilms and 37.5 μg mL^{-1} to 150 μg mL^{-1} for *S. aureus* biofilms. Isopropanol (50 μL) was used to treat the negative controls. Positive controls were treated with the same concentration of MeOH used in the experiments. Chambers were re-incubated for 20 h. Subsequently, biofilms were washed, fixed using a 2% paraformaldehyde aqueous solution and stained with a Live/Dead®staining kit. In this case, living cells were visualized as green entities and damaged cells as red. Slides were visualized under a confocal laser scanning microscope. Z-stacks of *P. aeruginosa* biofilms were performed and biofilm volume was calculated using the program Fiji. Percentage of remaining live or damaged cells was calculated using ImageJ. Treated samples were normalized to the control. For *S. aureus*, only the percent of live and damaged cells was calculated.

5.6.2.2.1 ***Staphylococcus aureus*** **biofilms** Treatments with 100 μg mL^{-1} of comatuslactone **9** were effective in damaging 90% ± 10% of the staphylococcal biofilms. When 50 μg mL^{-1} were used, 65% ± 15% of the cells were red stained, demonstrating that even in concentrations lower than the MIC, comatuslactone **9** can cause cellular disturbance (Fig. 5.37). Images representing the control and treated samples of *S. aureus* biofilms controls are shown in Fig. 5.38.

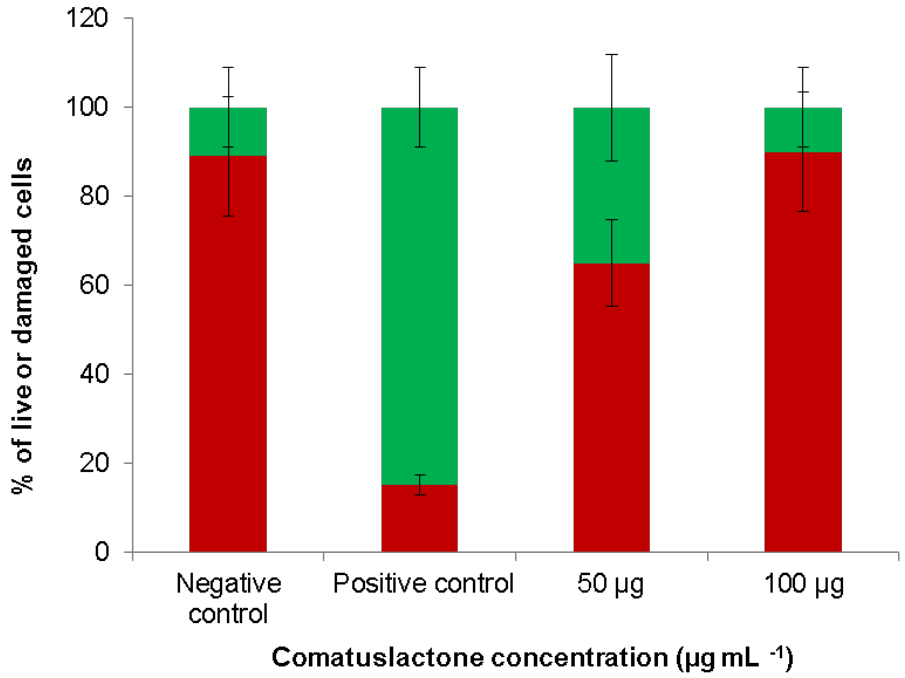

Figure 5.37: Effect of different concentrations (50 and 100 μg mL^{-1}) of comatuslactone **9** on *S. aureus* biofilms. Biofilms were stained using Live/Dead®staining kit. Areas covered by live (green) and damaged (red) cells were quantified using ImageJ.

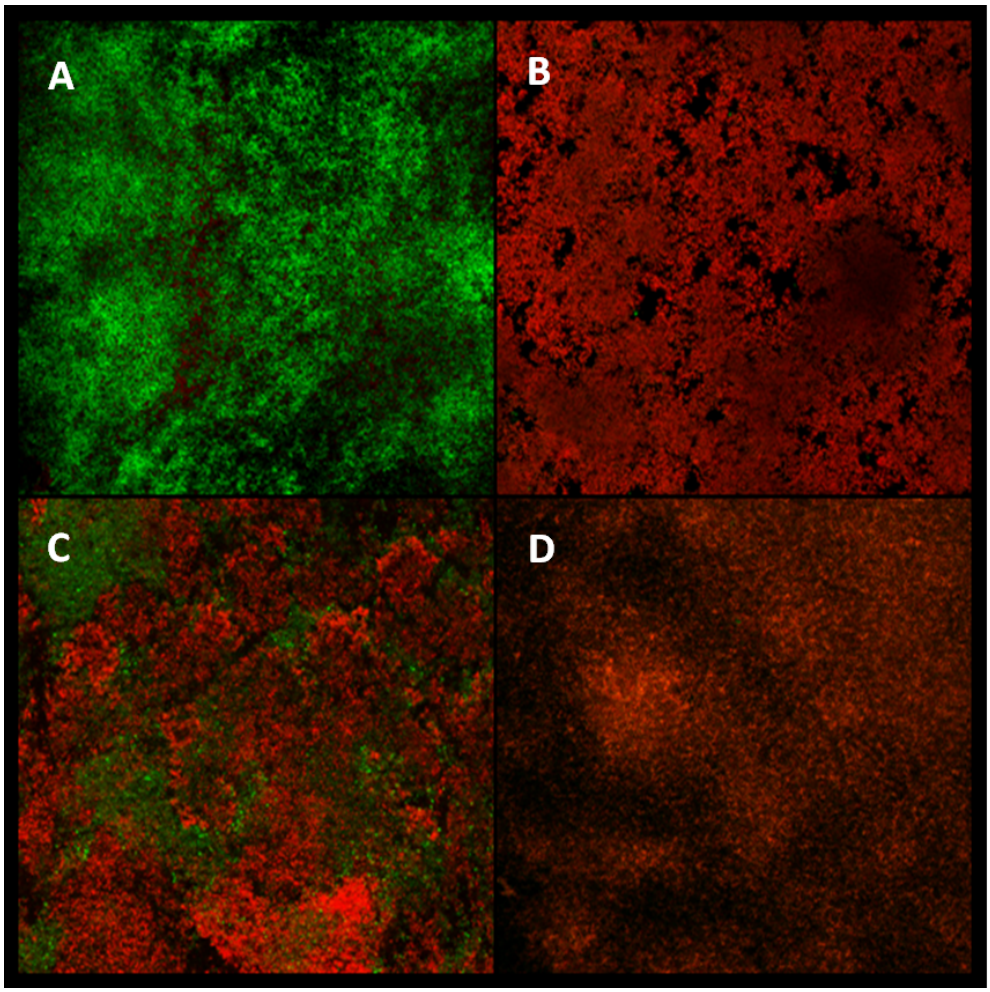

Figure 5.38: Effects of different concentrations of comatuslactone **9** on *S.aureus* biofilms. In vitro biofilms were stained using the Live/Dead®staining kit and visualized under a confocal laser scanning microscope. Areas covered by live (green) and damaged (red) cells were quantified using the software ImageJ. Fig 34A and 34B indicate the controls, positive and negative, respectively; Fig 34C and 34D exhibit the consequence of treatments with comatuslactone **9**, using the concentration of 50 μg mL^{-1} (Fig. 5.38C) and 100 μg mL^{-1} (Fig. 5.38D).

5.6.2.2.2 *Pseudomonas aeruginosa* Treatments with the established MIC (150 μg mL^{-1}) of comatuslactone **9** against *P. aeruginosa* were effective in damaging 99.9% ± 0.3% of the *in vitro* developed biofilms. According to the results obtained after biofilm volume quantification, only 1% ± 0.5% of the biofilm remained, in comparison to the control. When biofilms were treated with 0.5 of the MIC, a severe damage was visualized. In this case, a biofilm volume of 7.5 ± 1% was noticed, comprising less than 1% ± 0.6% of living bacterial cells. Moreover, a treatment using the concentration of 37.5 μg mL^{-1}, was also effective, showing the biofilm volume decreased to 15% ± 2%. Nevertheless, in this case 88% ± 5% of cells remained alive and 12% ± 7% were damaged (Fig. 5.39). 3D reconstructions of *P. aeruginosa* biofilms, including the positive control and samples treated with different concentrations of comatuslactone **9** (37.5 μg mL^{-1}, 75 μg mL^{-1} and

150 μg mL^{-1}) are represented in Fig. 5.40.

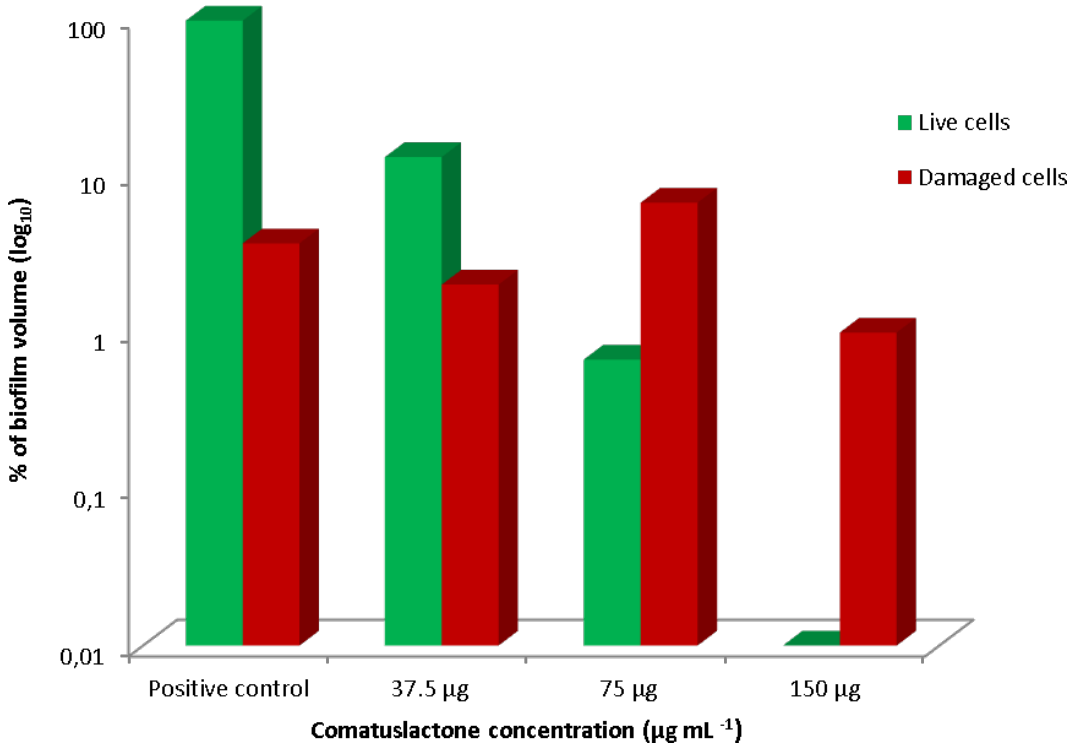

Figure 5.39: Effect of different concentrations of comatuslactone **9** on *P. aeruginosa* biofilms. Biofilm volume was quantified using the software Fiji, control volume corresponded to 100%. Areas covered by live (green) and damaged (red) cells were also quantified. Green columns correspond to living cells and red columns to damaged cells.

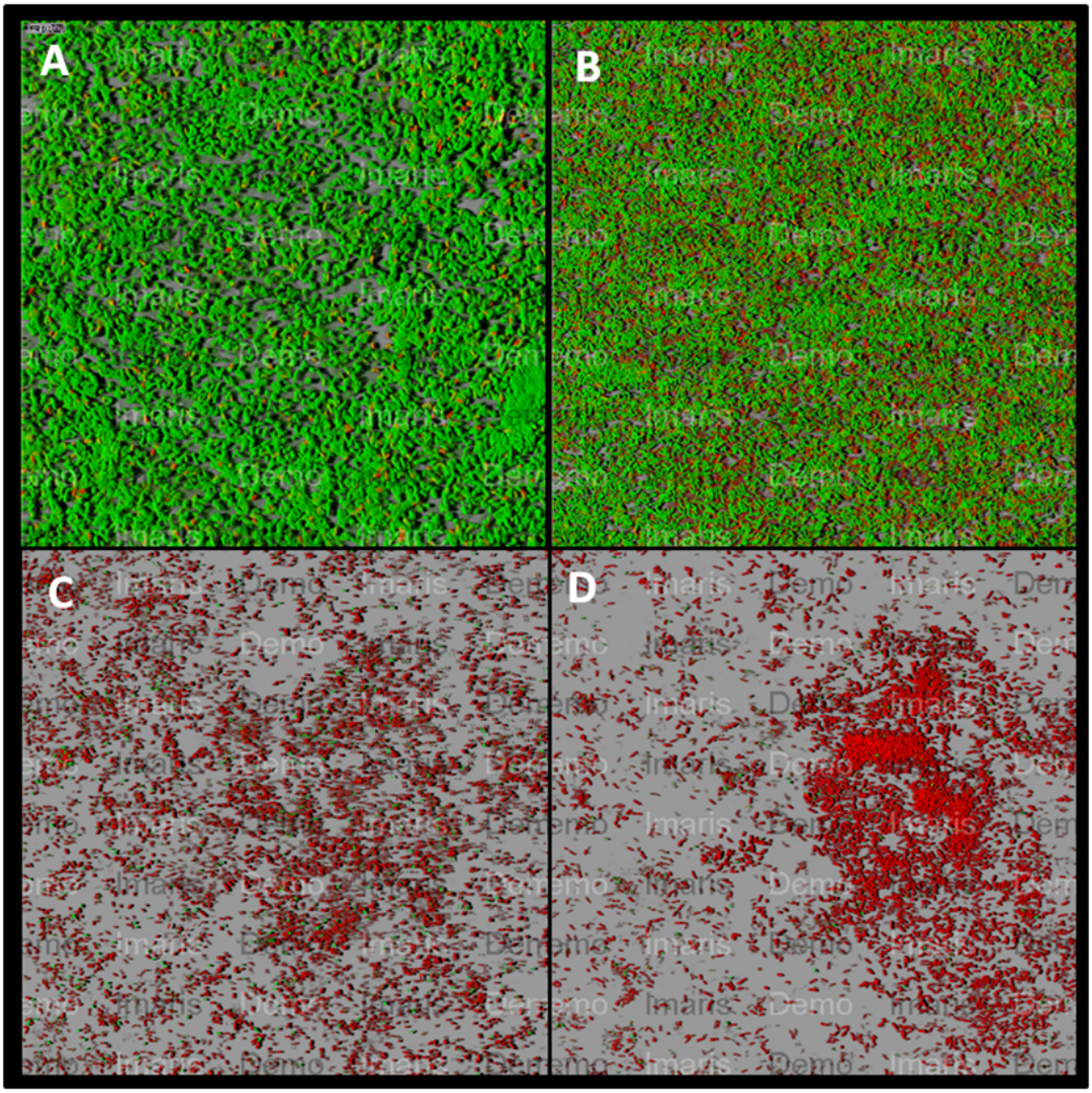

Figure 5.40: 3D reconstructions of *P. aeruginosa* biofilms z-stacks, using Imaris software. A-positive control, B-treatment with 37.5 μg mL^{-1} of comatuslactone **9**, C-treatment with 75 μg mL^{-1} and D-treatment with 150 μg mL^{-1} of comatuslactone **9**.

5.6.3 *Quorum sensing* inhibition

As comatuslactone **9** showed to be efficient in biofilm damaging and dispersal, its influence on *quorum sensing* systems was also tested. Therefore, two mutants were selected: (a) *Escherichia coli* MT102 (pSB403) - a reporter for genes *lux*, responding to short chain AHLs and (b) *Pseudomonas putida* F117 (pKR-C12) - based on the *las* QS-system of *P. aeruginosa*, responding to long chain AHLs. Both mutants were allowed to grow overnight; the media was diluted with a new media containing the respective AHL and pipetted into a 96-well black microtiter plate. Comatuslactone **9** was added on serial dilutions, with concentration ranging between 60 μg mL $^{-1}$ and 0.015 μg mL $^{-1}$. Controls were treated with MeOH and background controls were performed without AHL and comatuslactone addition. Bioluminescence (for short chain AHL) and fluorescence (for long chain AHL)

were quantified using a plate reader.
(a) *E. coli* MT102 (pSB403): bioluminescence quantification shows a complete abolishment of the QS response at the concentration 3.75 ± 0.25 μg mL $^{-1}$. At the concentration of 60 μg mL $^{-1}$, the compound displayed antibacterial activity against the mutant (Fig. 5.41).

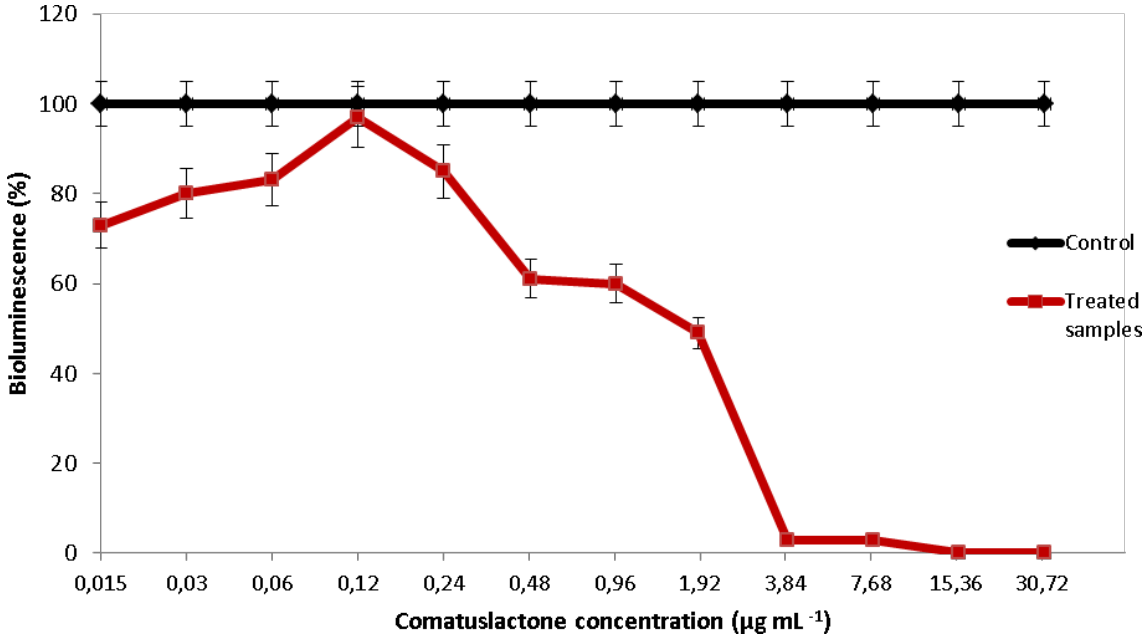

Figure 5.41: Influence of comatuslactone **9** on *E. coli* MT102 (pSB403) QS, a reporter for genes lux, responding to short chain AHLs. The black line corresponds to the control and red line to the treated samples.

(b) *P. putida* F117 (pKR-C12): fluorescence measurement demonstrated that comatuslactone **9** was able to decrease by 80% ± 5% the QS response at the concentration 30 μg mL $^{-1}$. Again, at the concentration of 60 μg mL $^{-1}$, antibacterial activity against the mutant was verified (Fig. 5.42).

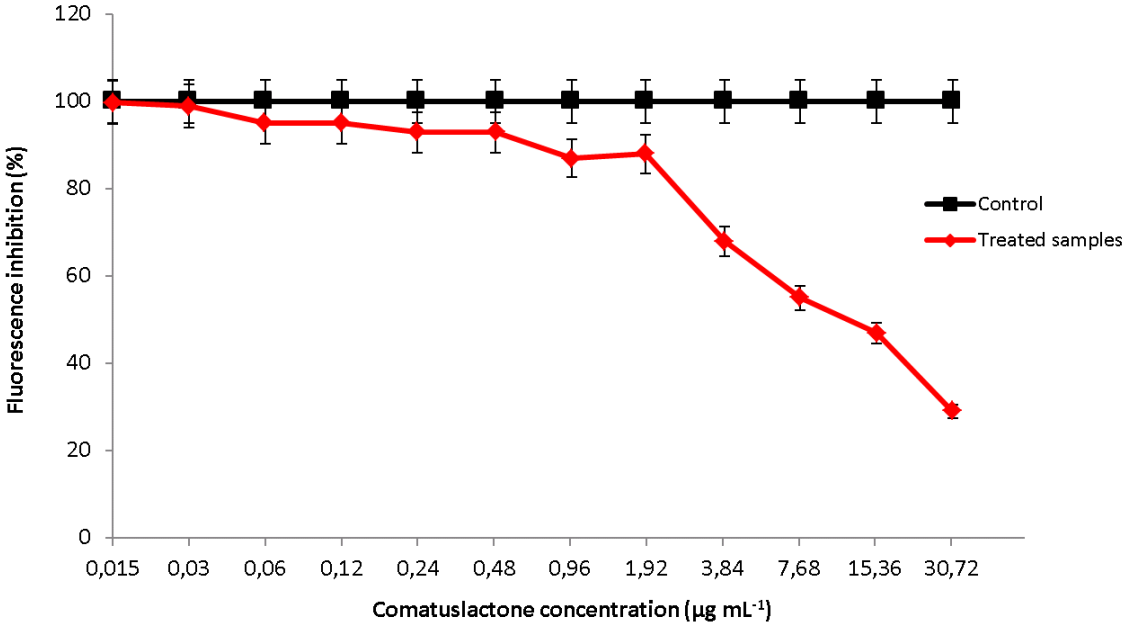

Figure 5.42: Influence of comatuslactone **9** on *P. putida* F117 (pKR-C12) QS,a mutant based on the las QS-system of *P. aeruginosa*, responding to long chain AHLs. The black line corresponds to control and red line to the treated samples.

5.6.3.1 Pyocyanin and rhamnolipid B inhibition

Pyocyanin and rhamnolipid B are synthesized via *P. aeruginosa* QS systems and are virulence factors. To verify the effect of comatuslactone **9** on these secondary metabolites production, *P. aeruginosa* was incubated and serial dilutions of comatuslactone **9** were added to 96-well microtiter plates. After 30 h of incubation, the cell-free supernatants were extracted using ethyl acetate. Pyocyanin and rhamnolipid B concentration was measured using tandem mass spectrometry analysis (HPLC-MS/MS). Here, the target parent ions m/z 211 $[M + H]^+$ for pyocyanin and m/z 652 $[M + H]^+$ for rhamnolipid B were fragmented. After fragmentation, the two most intense product ions were chosen to perform the analysis of both metabolites present in the samples. Therefore, each individual sample was always injected in triplicate and the product ions obtained from fragmentation of pyocyanin (m/z 168 and m/z 77) and rhamnolipid B (m/z 217 and m/z 70) were monitored using the multiple reaction monitoring (MRM) mode, in order to avoid any discrepancy originated from the equipment.
Pyocyanin concentrations were compared to a curve generated from a commercial standard (Fig. S3), using the MassHunter quantitative analysis software from Agilent Technologies. Rhamnolipid B quantities were normalized to the positive control and the relative concentrations calculated according to the area under the peaks.
Quantification of pyocyanin demonstrated that treatments using 75 μg mL^{-1} of comatuslactone **9** were able to reduce its production by 80%± 3% (Fig. 5.43), as well as 100% of rhamonolipid B (Fig. 5.44). When 37.5 μg mL^{-1} of the active compound was applied to the samples, 48% ± 5% of pyocyanin production was inhibited (Fig. 5.43). In the case of rhamnolipid B, when the same concentration was used, an inhibition of 97.4% ± 2%

was verified (Fig. 5.44). Surprisingly, treatments using 18.75 μg mL^{-1} of comatuslactone **9** allowed the production of only 44% ± 10% of rhamnolipid B (Fig. 5.44). On the other hand, pyocyanin production was restored to almost 80% when this concentration was used (Fig. 5.43).

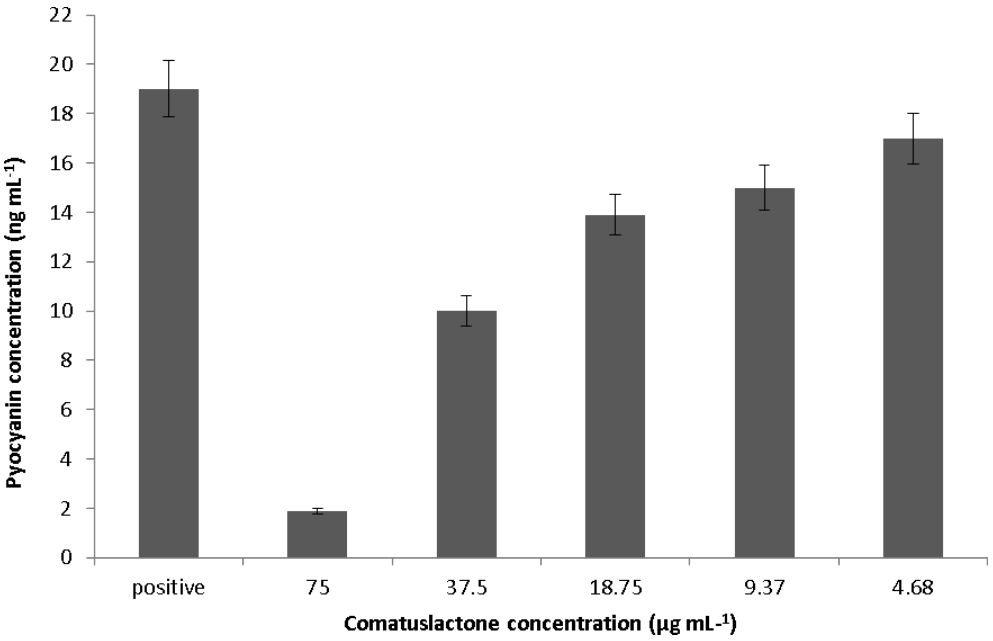

Figure 5.43: Impact of comatuslactone **9** on pyocyanin production. Samples were treated with serial dilutions of the active compound, using a concentration range of 4.68 μg mL^{-1} to 75 μg mL^{-1}. Pyocyanin concentration (ng mL^{-1}) was calculated according to the values obtained from a curve generated with a commercial standard and analysed using the MassHunter quantitative analysis software from Agilent Technologies.

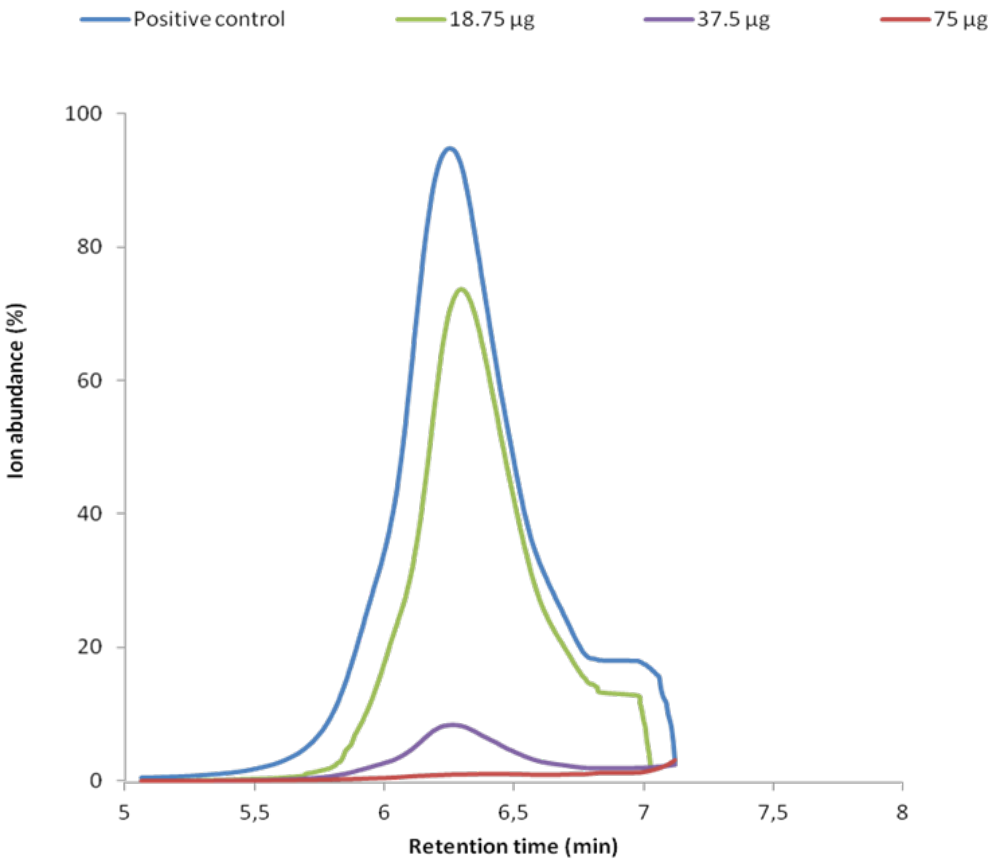

Figure 5.44: HPLC-MS/MS rhamnolipid B quantification (%), after treatment with serial dilutions of comatuslactone **9**. The results obtained using the concentrations of 75 μg mL^{-1}, 37.5 μg mL^{-1} and 18.75 μg mL^{-1} are shown. Calculations were performed according to the area under the peaks and normalized to the positive control.

5.6.4 Cytotoxicity

5.6.4.1 MTT assays

Comatuslactone **9**, epiisororidin E **1**, isororidin E **2**, 8α-hydroxyl roridin H **4** and roridin J **6** cytotoxicity was evaluated using the mouse fibroblast cell line L-929. Here the compounds were serial diluted in a 96-well microtiter plate, in medium containing 5 x 10^4 cells with a starting concentration of 30 μg mL^{-1}. 8α-hydroxyl roridin H **4** and roridin J **6** showed the highest cytotoxicity, with IC_{50} value calculated to 1.1 ng mL $^{-1}$ and 3.2 ng mL $^{-1}$, respectively. Both epiisororidin E **1** and isororidin E **2** exhibited an IC_{50} value of 50 ng mL $^{-1}$. On the other hand, MTT assays of cell cultures treated with comatuslactone **9**, show 10% of remaining cells, even when the highest concentrations were used.

5.6.4.2 Impedance measuraments

Cells treated with comatuslactone **9**, epiisororidin E **1** and isororidin E **2** were submitted to analysis on an xCELLigence™system, which measures time-dependent cell response profiling. These measurements provide information about cellular status, as morphology, cell number and viability. Therefore, cells were incubated in the presence of the

IC_{90} concentration of each compound (30 μg mL^{-1} in the case of comatuslactone 9), electrical-impedance was measured and obtained data were processed using the implemented workflow. After results processing, a heatmap was constructed, and hierarchical cluster analysis of the reference compounds together with the isolated compounds was performed. Co-clustering of an isolated compound with a reference compound with known mode of activity indicates the compounds mode of action. Here, cluster analysis shows both roridins in the same group, which was separated from all of the reference compounds. This result indicates that these metabolites display a different mechanism of action than the class label compounds used in the assay (Fig. 5.45, group 1). Comatuslactone **9** clustered together with the control (DMSO), suggesting no evidence of cytotoxic mechanisms (Fig. 5.45, group 2).

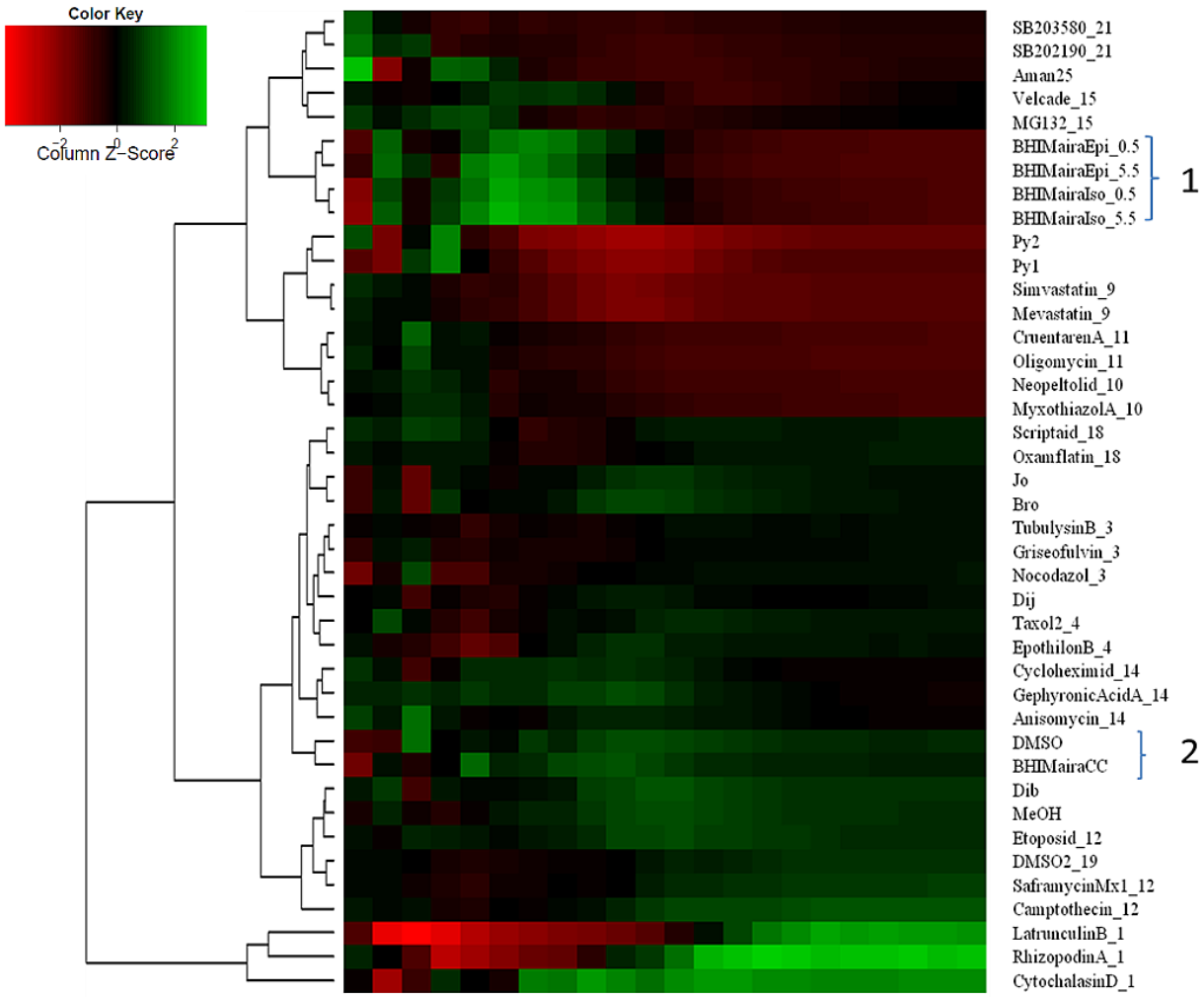

Figure 5.45: Hierarchical cluster analysis of data from impedance curves obtained using L-929 cells, incubated with epiisororidin E **1**, isororidin E **2** and *comatus*latone **9**. Group 1 indicates epiisororidin E **1** and isororidin E **2** cluster. Group 2 indicates comatuslactone **9** clustering together with the control (DMSO).

5.6.4.3 Eukaryotic cell morphology

In order to investigate morphological changes caused by comatuslactone **9**, L-929 mouse fibroblast cells were treated with the compound and subjected to immunofluorescence, using anti-α-tubulin. The nucleus was stained with DAPI. Fig. 5.46A shows cells treated with MeOH (as control) with a typical microtubular organization and nuclear appearance (Fig. 5.46A, arrow 1). However, in comatuslactone **9** treated cells (Fig. 5.46B) an increase of multinucleated cells (Fig. 5.46B, arrows 1 and 2) was visualized. Nevertheless, the majority of the cells still presented a normal microtubular distribution and nuclear morphology (Fig. 5.46B, arrow 3).

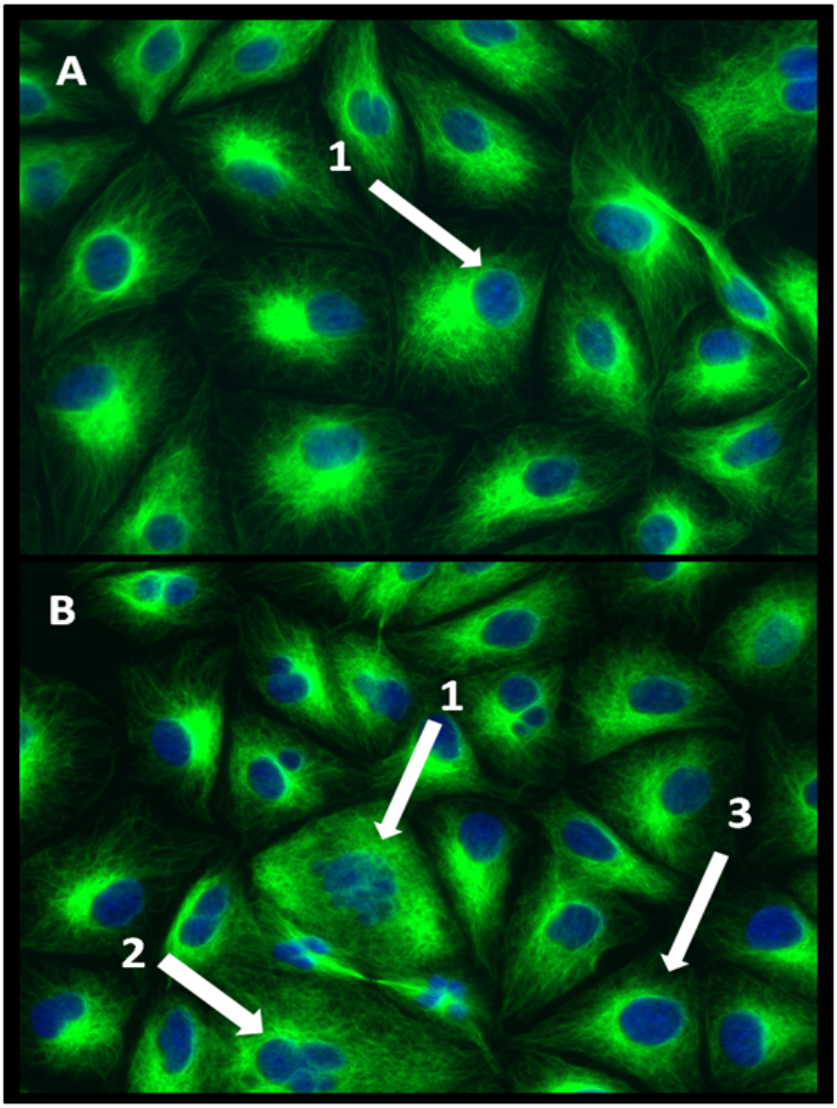

Figure 5.46: L-929 mouse fibroblast cells immunofluorescence images, stained with anti-α-tubulin and DAPI. A - cells treated with MeOH, representing the control. B - cells treated with comatuslactone **9**. Here multinucleated and normal cells can be visualized.

Chapter 6

Discussion

This study was focused on the exploitation of fungal secondary metabolites for their antibiofilm, antifungal and antimicrobial properties. Thus, it was assumed that fungi possess chemical self-defense mechanisms to prevent bacterial growth and/or biofilm formation on their fruiting bodies, warranting a successful life cycle. Due to a lack of reports in the literature about biofilm formation and bacterial composition associated with mushrooms fruiting bodies and to provide a solid explanation about the hypothesis of this work, bacterial communities of the surface of 49 mushrooms fruiting bodies were evaluated. Furthermore, 5 isolated fungi, *Calcarisporium arbuscula*, *Coprinus comatus*, *Macrolepiota fuliginosa*, *Macrolepiota procera* and *Pholiota lenta* were subjected to a screening performed using different incubation conditions aiming bioactive compounds production.
Although the 5 studied fungal species were able to produce bioactive metabolites, not all of the compounds could be successfully isolated. Occasionally, after a number of purification steps, the biological activities were no longer detected. These findings may indicate a synergistic effect between two or more compounds present in the crude extracts or even very labile compounds, which were degraded during the experiments.
Nevertheless, the screening strategy used in this work led to the isolation and identification of comatuslactone, a novel natural product from *C. comatus*, together with 6 roridins and fusidic acid from *C. arbuscula*. Their respective biological activities and importance will be discussed in the following sections.

6.1 Bacterial communities associated with basidiomycetes fruiting bodies

Fungi and bacteria coexist for billions of years, sharing frequently the same ecological niche and often depending on each other. In consequence, they have evolved complex interaction mechanisms, which vary from beneficial symbiosis to deleterious diseases [68, 158, 159]. A number of secondary metabolites produced by fungi have the same function as our immune system: protection of the producing organism. Thus, the goal of this work was to exploit compounds produced by fungi capable of modulating pathogenic bacterial biofilms. Fruiting bodies forming fungi are exposed to rain and moist climate, offering ideal substrata for bacterial colonization. Therefore, those organisms are extremely de-

pendent on their self-defense molecules to modulate their interaction with their friendly and unfriendly environmental counterparts [158, 159]. Some efforts have been made before to characterize bacterial communities associated with fungi, as well as their possible ecological role. Nevertheless, most studies concerning these associations are restricted to culturable bacteria, isolated from fruiting bodies of symbiotic and economic important species [159, 160, 161, 162]. Therefore, a combined investigation of their associated bacterial communities and the production of secondary metabolites with biofilm modulatory properties is an interesting approach. Hence, bacterial communities composition of 49 basidiomycetes, both saprophytic and ectomycorrhizal, belonging to 7 genera, were analysed using SSCP fingerprinting.

Herein, it was demonstrated that 18 fungi showed no bacteria associated with their surfaces. Among those fungi, 14 individuals were identified as *Coprinus comatus*, 3 as *Coprinopsis atramentaria*, 1 as *Macrolepiota procera* and 1 as *Laetiporus sulphureus*. Interestingly, only Gram-negative bacteria were detected at the remaining 31 samples. In 2013, Zagriadskaia *et al.* [163], investigated the bacterial communities associated with the hyphosphere soil and fruiting bodies surface and internal tissues of *Laccaria laccata*, *Lactarius aurantiacus, Gymnopus confluens, Lycoperdon perlatum, Coltricia perennis*, and *Clavariadelphus ligula*. In this case, Gram-negative bacteria showed prevalence among the surface samples. Dahm *et al.* 2005 [164], published similar data, where Gram-negative rods were the predominant bacteria isolated from the fruiting bodies of ectomycorrhyzal fungi. Moreover, Kataoka *et al.* 2008 [165] evaluated bacterial communities associated with root tips *Pinus thunbergii* mycorrhizae. A prevalence of Gram-negative microorganisms, specially *Burkholderia* sp. and *Bradyrhizobium* sp. was observed. Comparison of arbuscular mycorhizal fungi (AMF) associated bacteria, considering both attached and non-attached communities, showed that the Gram-negative ones are better hyphae colonizers [166]

In 2009, Warmink *et al.* [159] introduced the term fungiphile, to characterize bacteria which are detected frequently in association with fungi. Here, *Pseudomonas* spp. and *Rhanella* spp. were identified from several mycosphere samples using DGGE. In this work, SSCP fingerprint analysis detected 118 phylotypes, distributed among 31 fruiting bodies samples. Among those, 15 were identified as *Rhanella* spp., showing association with specimens belonging to *Boletus* spp. 20 phylotypes belonging to *Pseudomonas* spp. were detected, showing a broad distribution between the analysed fungal genera. Interestingly, the two specimens at *Russula emetica* showed a very close association with Rhizobiaceae. Regarding those individuals, 15 bacterial phylotypes were detected, 13 belonging to Rhizobiaceae and 2 identified as *Flavobacterium* sp. Additionally, communities associated with *Boletus* spp. showed a high prevalence of Enterobactereaceae. One *incertae sedis* sequence was obtained from *Amanita* sp. In this case, there is the possibility of fungal genomic fragment amplification, generating such sequence.

Warmink and van Elsas, 2008 [167], discussed the involvement of the type-III secretion system (TTSS) on the bacterial cells binding to *Laccaria proxima* hyphae. TTSS are virulence-associated systems, widespread among symbiotic and pathogenic Proteobacteria, being related to interactions between bacteria with their respective hosts [168]. They showed a selection of TTSS positive bacteria on those associations, particularly *Pseudomonas* spp. [167]. Within the data obtained in this work, only Gram-negative bacteria

were detected in association with fruiting bodies. Many of those bacteria are known to possess TTSS systems. Therefore, it can be hypothesized that these systems are required for the establishment of those close interactions between the fruiting bodies of mushrooms and bacteria. Moreover, the ectomycorrhizal evaluated individuals demonstrated a higher diversity of bacteria, which can be explained by their ecological roles.
The results corroborate the initial hypothesis that fungi can control their biofilm communities. In summary it can be predicted that appropriate knowledge about fungi and bacteria interactions will be beneficial to determine approaches to screen for compounds exhibiting biological activities.

6.2 Compounds isolated from *Calcarisporium arbuscula*

6.2.1 Roridins

The *C. arbuscula* strain used in this work was isolated from a *Russula emetica* fruiting body and identified according to its ITS sequence. In 1955, *C. arbuscula* was already reported living in symbiosis with Ascomycotina and Basidiomycotina fruiting bodies [142, 169]. From *C. arbuscula* fermentations, several cytotoxic compounds have been isolated, like polyketides, named aureovertin D and B, [170, 171] as also trichothecenes [156]. Both aurovertins are very cytotoxic, and the mechanism of action is defined as potent inhibitors of ATP-synthesis and ATP-hydrolysis. They have been used in studies about H-translocating ATPases [172].
Trichothecenes are sesquiterpenoid metabolites, comprised of a tricyclic core. Many of those compounds have an epoxide at C-12 and C-13, crucial for their toxicity [173, 174, 175]. More than 200 trichothecenes are known, and they were classified in non-macrocyclic and macrocyclic compounds. The group of non-macrocyclic trichothecenes is divided in three types: A, B and C. Examples are T-2 toxin, nivalenol, deoxynivalenol and trichothecin, all produced by *Fusarium* [176, 177]. All of the macrocyclic trichothecenes belong to type D compounds. They possess a cyclic diester or triester ring bound to the trichothecene at C-4 and C-15. This division encloses satratoxins, verrucarins, roridins, myrotoxins and baccharinoids [176, 178].
The production of roridins is extensively reported for fungi belonging to the Hypocreaceae family. *Cylindrocarpon* sp., *Myrothecium roridum* and *Myrothecium verrucaria* are the most known producers, being the source of more than 20 roridins (table 6.1). For *C. arbuscula*, production of roridin H, roridin J, 8α-hydroxy-roridin and 8α-acetoxy-roridin H (as calcarisporin B1) was reported [156]. Herein, 6 roridins, epiisororidin E **1**, isororidin E **2**, roridin H **3**, 8α-hydroxy-roridin **4**, 8α-acetoxy-roridin H **5** and roridin J **6** produced by *C. arbuscula* were isolated and identified using NMR. Although most of these mycotoxins are already reported for this fungal species, the relative configuration at either C-6' and C-13' for roridin H, and at 4'-H for roridin J was not determined. Therefore, ^{1}H NMR data obtained from roridin H **3** was compared with 1,3-dioxolanes of erythro- and threo-10,11-dihydroxy-trans-12-nornerolidol [151]. The chemical shifts of the threo-compound 13-methyl group (δH = 1.25 ppm) together with a shielding of 11-H to δH = 3.72 ppm matched to the data obtained for roridin H **3**. Consequently, its stereochemistry at C-6' and C-13' was solved as a 6'S,13'S-configuration. ^{1}H NMR spectrum analysis of

roridin J **6** indicates a hydroxyl group at the 4' position and coupling constant of J= 6.9 Hz between 4' H and 5' H. This value requires an dihedral angle of approximately 180° among those protons, which is only achievable if the 4'- hydroxyl group is in β-position. Hence, its configuration is solved here, being 4'R.
Furthermore, the additional two roridin E isomers, epiisororidin E **1** and isororidin E **2** isolated from *C. arbuscula* were originally isolated from *M. verrucaria* and *Cylindrocarpon* sp. respectively [147,149]. It is important to emphasize that, for all of the isolated roridins within this work, the stereochemistry at C-6' was only found as 6'S configuration. None of the compounds was detected as a mixture with the C-6'R isomers. The biosynthesis of isororidin E (C-6'S and C-13'S) and epiisororidin E (C-6'S and C-13'R) by *Myrothecium* spp. occurs, together with roridin E (C-6'R and C-13'R) and epiroridin E (C-6'R and C-13'S). Generally, other roridins, e.g, roridin A were also isolated from the same fermentation processes [179]. In most of the roridins, C-6' is R whereas the C-6'S configuration occurrence is less frequent. Moreover, roridins showing a C-6'S configuration were always detected combined with their C-6'R isomers [147, 179]. The detection of only C-6'S-configuration is the first report of such a stereospecificity. It may indicate a biosynthesis which deviates from the one of *Myrothecium* sp.
Concerning trichothecenes biosynthesis, *Fusarium* spp., *Trichoderma* spp. and *M. roridium* have been used to investigate gene clusters involved in those processes [173, 174, 175, 176, 180, 181]. The first step on the trichothecenes biosynthesis is the cyclization of farnesyl pyrophospate to trichodiene by a trichodiene synthase, followed by a sequence of oxygenations, cyclizations and esterifications, originating more complex structures. It was shown that the genes involved in the biosynthesis of these compounds are organized in clusters, designated TRI [173, 176, 180, 181]. While the non-macrocyclic trichothecenes pathways are provided with more details, the macrocyclic biosynthetic pathways still remain obscure and only the last intermediates were already identified [181].
In 1982, Jarvis *et al.* [154] working with a strain of *M. verrucaria*, showed that trichoverrins and isotrichoverrins (Fig. 6.1), are the macrocyclic trichothecenes precursors. From the trichoverrins (C-6"S) or isotrichoverrins (C-6"R) to the macrocycles, ring closure results in an inversion of the configuration at the C-6". After the inversion, the resulting roridin is further transformed to other roridins. However, the sequence of the hydroxylation and esterification steps between trichodermol and trichoverrins remains unclear, as well as the further steps needed for roridins modification [176, 181]. So far, only genes controlling the initial stages of the trichothecenes macrocyclic biosynthetic pathway in *M. roridum* (MRTRI4-6) have been characterized [173, 180, 181].

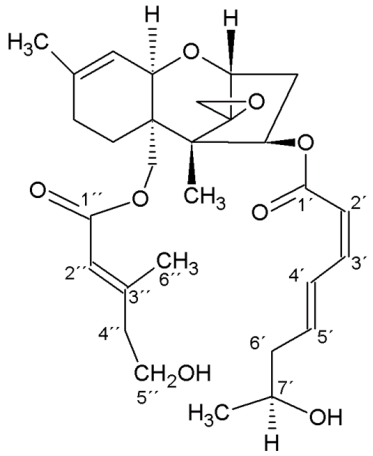

Figure 6.1: Structure of trichoverrin.

6.2.2 Fusidic acid

Fusidic acid was isolated the first time in 1962 from *Fusarium coccineum* fermentations [182]. In 2001, this same antibiotic was isolated from *Stilbella aciculosa*, a marine fungus [183]. This steroid-like antibiotic is widely used to treat infections caused by Gram-positive bacteria, including methicillin resistant *Staphylococccus aureus* [184]. A fusidic acid analogue has been isolated from *Acremonium crotocinigenum* as well as cephalosporin P1 - a triterpenoid antibiotic, related to fusidic acid, but not to cephalosporin - from *Acremonium chrysogenum (Cephalosporium acremonium)* [185, 186]. Besides demonstrating the ability of producing fusidanes antibiotics, the common feature between these 4 genera is that they all belong to the Hypocreales order. No literature correlating this order with production of fusidanes has been encountered.

6.3 Biological activities of roridins

6.3.1 Yeasts growth inhibition

Inhibition of yeast and fungal growth was shown for roridin A and 8β-acetoxy roridin H. For these two compounds, activity against *C. albicans, Tricophyton rubrum* and *Aspergillus niger* was reported. Roridin A was also demonstrated to interfere with *Kluyveromyces fragilis* growth [152, 187, 188]. Herein, fungicide and fungistatic activities of epiisororidin E **1**, isororidin E **2**, roridin H **3**, 8α-hydroxy-roridin **4** and roridin J **6** against a panel of 7 yeasts species was reported. All of these compounds were effective against *Y. lypolytica*, acting as fungistatic (roridin H **3**, 8α-hydroxy-roridin **4** and roridin J **6**) or fungicide (epiisororidin E **1**, isororidin E **1**) agents. Regarding *Candida* spp., epiisororidin E **1** inhibited the growth of all of the evaluated species, whereas isororidin E **2** was not active against *C. parapsilosis*. Additionally, roridin H **3** showed a fungistatic effect against *C. tropicalis*. Moreover, *R. glutinis* growth was inhibited only when epiisororidin E **1**, isororidin E **2** were employed. Despite roridins structural similarities, the displayed activities against yeasts demonstrate distinct features. Apparently, the ring

conformation at C-6'S and C-13'S on roridin H **3**, 8α-hydroxy-roridin 4 and roridin J **6**, conferred by the acetal moiety decreases their toxicity to yeasts cells. These observations suggest that small changes on roridins macrocyclic ring conformation can cause variations on their activity.

6.3.2 Cytotoxicity

Trichothecenes are phytotoxic and cytotoxic, causing several crop diseases and intoxications. However, antifungic and antileukemic activities are also reported [147, 152, 176, 189, 190]. Inhibition of protein, DNA and RNA synthesis, interference with mitochondrial function, effects on cell division and on membrane are some known cytotoxic responses in eukaryotic cells. Nevertheless, the exact mechanism of toxicity is not completely clear [176, 191]. Most of the investigations on trichothecenes mechanisms of toxicity are restricted to the non-macrocyclic type. Within this class, anguidin achieved phase II in clinical trials, but those investigations were discontinued due to toxic effects heterogeneity and inadequacy of the observed biological activity. Furthermore, anguidin demonstrated to be non-selective between murine and tumor cells [176, 192].
In 2003, Amagata *et al.* [192], investigated the cytotoxic effects of several trichothecenes, including non-macrocyclic (anguidin, 13'-acetyltrichoverrin B, trichoverrin A and trichoverrin B) and macrocyclic compounds (roridin A, isororidin A, epiroridin E, 3-hydroxy-roridin E, roridin L, roridin M, miophytocen C, verrucarin A and verrucarin M). Here, a disk diffusion soft agar colony formation assay and a NCI screen, consisting 60 cancer cell lines were employed. Regarding those assays, a substantial variation on the cytotoxic effects displayed by the tested compounds was observed. Here, miophytocen C showed the lowest toxicity, which is explained by the absence of the C-12 and C-13 epoxide. The epoxide ring has been shown to be essential for trichothecenes toxicity [176, 193]. Therefore, in 1984, Jarvis *et al.* [193] used a semi synthetic approach in order to introduce a 9β-10β epoxide at some trichothecenes, including roridin A, roridin J and roridin H. Their activitiy was tested *in vivo* against P388 mouse leukemia. Herein, the addition of an epoxide increased selectivity and potency for roridin A and roridin H. Contradictorily, the modified roridin J was less active against leukemia. Moreover, reported experiments using roridins imply on a broad toxicity, which is cell strain and roridin structure dependent. On a general manner, it is suggested that a 2'-OH substituent on the macrocyclic ring increases tumor cells selectivity and potency, as well as the stereochemistry at C-6' and C-13' [192]. On the other hand, Oda *et al.* 2010 [194] demonstrated that the cytotoxicity of 12$\prime$-hydroxyroridin E was more than 1000 fold reduced when compared to roridin E.
Here, the cytotoxicity of epiisororidin E **1**, isororidin E **2**, 8α-hydroxy-roridin H **4** and roridin J **6** was evaluated against a mouse fibroblast cell strain (L-929). The obtained IC_{50} values demonstrated that 8α-hydroxy-roridin H **4** and roridin J **6** displayed a higher cytotoxicity than epiisororidin E **1**, isororidin E **2**. Hitherto, the roridins showing a 13' -OH (epiisororidin E **1** and isororidin E **2**) demonstrated a decreased toxicity of approximately 10 fold when compared to 8α-hydroxy-roridin H **4** and roridin J **6**. Epiisororidin E **1** and isororidin E **2** were also subjected to an impedance measurement in order to predict their toxic mechanisms. Within this assay, both roridins clustered together, establishing a new group, not related to the standard references. This indicates a peculiar mode of action. In table 6.1, data about roridins producer organisms along with their biological

activities are summarized.
Besides of all of these observed effects on eukaryotic cells, almost no biological activity on prokaryotes was reported. In fact, these compounds showed a preference for eukaryotic systems [176]. For bacteria, studies showed de-epoxidation of the non-macrocyclic trichothecenes deoxynivalenol caused by *Clostridiales, Anaerofilum* sp., *Collinsella* sp., and *Bacillus* spp. [195, 196]. Nevertheless, data obtained within this work, revealed that epiisororidin E **1** and roridin H **3** are capable of inhibiting *S. aureus* biofilm formation. The mechanisms underlying this activity remain to be investigated.

Table 6.1: Roridins producer organisms and biological activities, together with the respective refences.

Compound	Formula	Producer organism	Biological activity	Ref.
Roridin A	$\mathbf{C_{29}H_{40}O_9}$	*Cylindrocarpon* sp. *Myrothecium roridum* *Myrothecium verrucaria*	Growth inhibition of *Candida albicans, Kluyveromyces fragilis, Tricophyton rubrum, Aspergillus niger.* Cytotoxicity against L1210, NCI-H226 NCI-H522, COLO205, M14, UACC-62 SK-MEL-2, 786-0, A498, RXF 393, MDA-N and MDA-MB-435 cell lines. Inhibition of *Arabidopsis thaliana* pollen development. *Plasmodium falciparum* Junin virus	192, 197, 198, 199, 200, 201, 202
Isororidin A	$\mathbf{C_{29}H_{40}O_9}$	*Myrothecium verrucaria* *Acremonium neo-caledoniae*	Cytotoxicity against KB, NCI-H522, COLO205, M14, UACC-62, A498, RXF 393, MDA-N and MDA-MB-435 cell lines	179, 192, 203
8β-hydroxyroridin A	$\mathbf{C_{29}H_{40}O_{10}}$	Semisynthetic	P388 mouse leukemia (*in vivo*)	193
9β, 10β - epoxyroridin A	$\mathbf{C_{29}H_{40}O_{11}}$	Semisynthetic	P388 mouse leukemia (*in vivo*)	193
8β-hydroxy-9 β,10 β - epoxyroridin A	$\mathbf{C_{29}H_{40}O_{11}}$	Semisynthetic	P388 mouse leukemia (*in vivo*)	193

Compound	Formula	Producer organism	Biological activity	Ref.
16-hydroxy-9 β,10 β -epoxyroridin A	$\mathbf{C_{29}H_{40}O_{11}}$	Semisynthetic	P388 mouse leukemia (*in vivo*)	193
Roridin D	$\mathbf{C_{29}H_{38}O_9}$	*Myrothecium roridum* *Myrothecium verrucaria*	Cytotoxicity against primary soft-tissue sarcoma cells	198, 204, 205
Roridin E	$\mathbf{C_{29}H_{38}O_8}$	*Myrothecium roridum* *Myrothecium verrucaria*	Phytotoxicity Cytotoxicity against H4TG, MDCK, NIH3T3, KA31T and primary soft-tissue sarcoma cells. Activity against *Plasmodium falciparum* Activity against Junin virus	147, 197, 198, 206, 207
Epiroridin E	$\mathbf{C_{29}H_{38}O_8}$	*Myrothecium verrucaria*	Cytotoxicity against HL-60, NCI-H226, HCT-116, M14, UACC-62, 786-0, A498, RXF 393 and MDA-MB-435 cell lines.	149, 192
Epiisororidin E	$\mathbf{C_{29}H_{38}O_8}$	*Calcarsiporium arbuscula*[a] *Myrothecium verrucaria*	Fungicide against *C. krusei, R. glutinis* and *Y. lypolytica;* Fungistatic against *C. guilliermondii, C. parapsilosis* and *C. tropicalis*[a] Phytotoxicity Cytotoxicity against L929, H4TG, MDCK, NIH3T3, KA31T and primary soft-tissue sarcoma cells.	147, 198, 207, a
Isororidin E	$\mathbf{C_{29}H_{38}O_8}$	*Calcarsiporium arbuscula*[a] *Cylindrocarpon* sp. *Myrothecium roridum* *Myrothecium verrucaria*	Fungicide against *C. krusei, C. tropicalis* and *Y. lypolytica;* *Fungistatic against C. parapsilosis* and *R. glutinis*[a] Cytotoxicity against L929 cells[a].	147, 149, a

Compound	Formula	Producer organism	Biological activity	Ref.
12,13-deoxyroridin E	$\mathbf{C_{29}H_{38}O_7}$	*Myrothecium roridum*	HL-60 and L1210 cell lines	208
7β - 8β-Epoxyisororidin E	$\mathbf{C_{29}H_{36}O_9}$	*Cylindrocarpon sp.*		149
3-hydroxy roridin E	$\mathbf{C_{29}H_{38}O_9}$	*Myrothecium verrucaria*	Cytotoxicity against HL-60, NCI-H226, HCT-116, M14, UACC-62, 786-0, A498, RXF 393 and MDA-MB-435 cell lines.	192
12'- hydroxy roridin E	$\mathbf{C_{29}H_{39}O_9}$	*Myrothecium roridum*	Cytotoxicity against cells L1210.	199
16-hydroxy roridin E	$\mathbf{C_{29}H_{39}O_9}$	*Myrothecium roridum*	Cytotoxicity against primary soft-tissue sarcoma and high-grade leiomyosarcoma tumor cells.	209
Roridin J	$\mathbf{C_{29}H_{36}O_9}$	*Calcarisporium arbuscula* *Myrothecium verrucaria*	P388 mouse leukemia (*in vivo*) Growth inhibition of Yarrowia lipolytica[a]. Cytotoxic against L-929 cellsÃć	157, 193, a
9 β,10 β-epoxyroridin J	$\mathbf{C_{29}H_{38}O_9}$	Semisynthetic		193
Roridin H	$\mathbf{C_{29}H_{36}O_8}$	*Calcarisporium arbuscula* *Myrothecium roridum* *Myrothecium verrucaria*	Phytotoxicity Cytotoxicity against H4TG, MDCK, NIH3T3, KA31T, L1210 and primary soft-tissue sarcoma cells. Cytotoxic against L-929 cells[a] P388 mouse leukemia (*in vivo*). Fungistatic against *C. tropicalis* and *Y. lipolytica*[a]	150, 193, 207
8 α - hydroxy roridin H	$\mathbf{C_{29}H_{36}O_9}$	*Myrothecium* sp. GS-17 *Calcarisporium arbuscula*	Growth inhibition of *Rhizoctonia solani Fusarium oxysporum* and *Yarrowia lipolytica*[a]. Cytotoxic against L-929 cellsa	153, 156

Compound	Formula	Producer organism	Biological activity	Ref.
8β - Acetoxy-roridin H	$C_{31}H_{38}O_{10}$	*Myrothecium* sp. Z16	Growth inhibition of*Candida albicans, Tricophyton rubrum, Aspergillus niger*	153
7β, 8β, 2', 3'- Diepoxyroridin H	$\mathbf{C_{29}H_{34}O_{10}}$	*Cylindrocarpon* sp.		149
7β - 8β- Epoxyroridin H	$\mathbf{C_{29}H_{34}O_{9}}$	*Cylindrocarpon* sp.		149
9 β,10β- epoxyroridin H	$\mathbf{C_{29}H_{38}O_{9}}$	Semisynthetic	P388 mouse leukemia (*in vivo*).	193
Isororidin K	$\mathbf{C_{29}H_{38}O_{9}}$	*Myrothecium verrucaria*		153
Roridin L	$\mathbf{C_{29}H_{38}O_{9}}$	*Myrothecium verrucaria*	Cytotoxicity against P388, NCI-H226, NCI-H522, COLO205, M14, UACC-62, SK-MEL-2, A498, MDA-N and MDA-MB-435 cell lines.	210
Roridin M	$\mathbf{C_{29}H_{36}O_{9}}$	*Myrothecium verrucaria*	Cytotoxicity against P388, NCI-H226, NCI-H522, HCT-116, HCT - 15, M14, UACC-62 SK-MEL-2, A498, RXF 393, MDA-N and MDA-MB-435 cell lines.	192, 210
Roridin Q	$\mathbf{C_{35}H_{47}O_{11}}$	*Myrothecium roridum*	Cytotoxicity against L1210 cells.	199
Roridin R	$\mathbf{C_{29}H_{39}O_{9}}$	*Myrothecium roridum*	Cytotoxicity against L1210 cells.	199

6.4 Compounds isolated from *Coprinus comatus*

Coprinus comatus, the shaggy ink cap, is an edible mushroom of cosmopolitan occurrence (Fig. 6.2). Its cultivation was established in China and Taiwan, generally in sawdust

plastic bags [215, 216]. It is known as a medicinal fungus and a number of biological activities have been reported, including anticancer, due to blocking the androgen receptor, antioxidant [216, 217], nematocidal [218, 219, 220] and analgesic activities [221]. *C. comatus* fruiting bodies have also been found possessing antimicrobial activity [222, 223] but the underlying chemical compounds have not yet been identified.

Figure 6.2: Fruiting bodies of *C. comatus*.

Within this work, a specimen of *C. comatus* was collected in Braunschweig, Germany and isolated in PDA media. The obtained mycelium was subjected to growth under different stress conditions, in order to produce bacterial biofilm modulators. Regarding this activity, (3R,4S)-2-methylene-3,4-dihydroxypentanoic acid 1,4-lactone was isolated. This compound was produced in BAF and YEM media, adjusted to pH 5.0, 7.0 and 9.0 and at both temperatures tested. No production was detected when the fungi was incubated in PDB. The aforementioned molecule was already described as synthetic derivative [159, 160], being characterized here, for the first time as a natural product. Therefore, it was denominated comatuslactone **9** (Fig. 6.3A). Moreover, a second lactone, named (2S,3R,4S)-2-methyl-3,4-dihydroxypentanoic acid 1,4-lactone **10** (Fig. 6.3B) was also isolated. Nevertheless this compound did not exhibit any of the tested biological activities. Alpha-methylene-gamma-butyrolactones are generally isolated from plants [224]. Few cases are reported for fungi, including 2-methyl-pentene-olide (Fig. 6.3C), a flavor isolated from *C. comatus* fruiting bodies [225] and (3S,4R)-3-carboxy-2-methylene-heptan-4-olide (Fig. 6.3D), produced by the plant pathogen *Lasiodiplodia theobromae*, responsible for black spots induction on bananas [226]. Tulipalin A and B (Fig. 6.3E) were first isolated from *Tulipa gesneriana*. Tulipalins are recognized as chemical self-defense compounds, acting against microbial infection and insects predation. Interestingly, tulipalin A demonstrates a higher antifungal activity than tulipalin B, whereas tulipalin B inhibits bacterial growth more efficiently than tulipalin A. Tulipalin A was also shown to cause contact allergies in mammals [227, 228, 229].

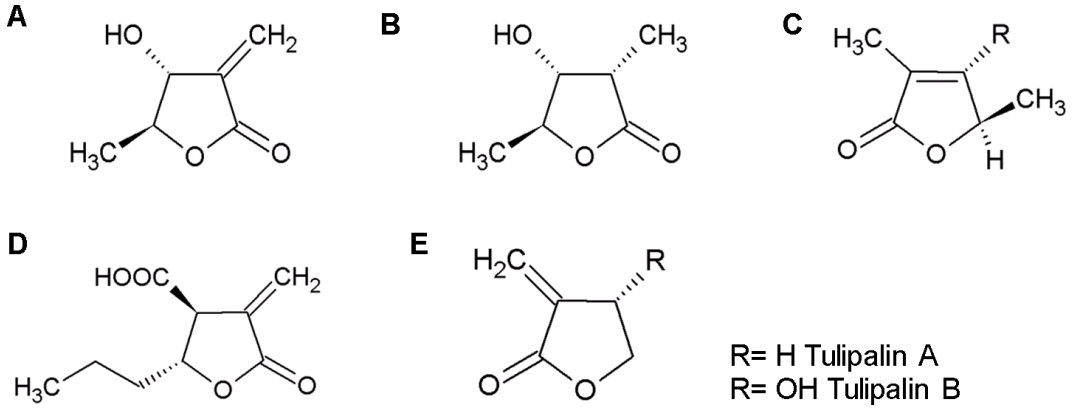

Figure 6.3: Chemical structures of: A - (3R,4S)-2-methylene-3,4-dihydroxypentanoic acid 1,4-lactone (comatuslactone 9); B - (2S,3R ,4S)-2-methyl-3,4- dihydroxypentanoic acid 1,4-lactone 10; C- 2-methyl-pentene-olide, isolated from *C. comatus*; D - (3S,4R)-3-carboxy-2-methylene-heptan-4-olide, isolated from *L. theobromae* and E- tulipalins A and B, isolated from *T. gesneriana.*

Kato *et al.* have been working on the biosynthesis of tulipalins [230, 231]. Thus, glucose esters, named tuliposides (Fig. 6.4) were identified as tulipalins precursors. So far, seven analogs have been characterized: 1 - tuliposide A and B; 6 - tuliposide A and B; and tuliposides D, E and F. Tulipalins are the result of a lactonization of a released aglycone, which can occur spontaneously as a result of a pH change, due to tuliposides instability on pH above 5.5, or as a result of enzymatic liberation [232].

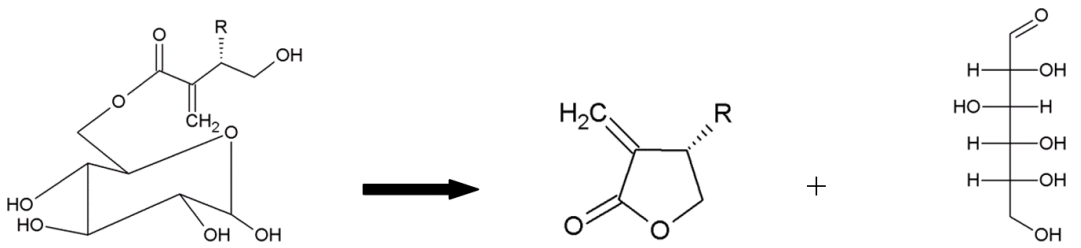

Figure 6.4: Tulipalin A synthesis. Tuliposide A is hydrolysed under alkaline conditions, or enzymatically yielding tulipalin A and glucose.

In 2012, Nomura *et al.* [227] purified a tuliposide-converting-enzyme (TgTCE1) from tulips bulbs. This enzyme belongs to the lactone forming carboxylesterases and catalyzes the reaction from 6-tuliposides A, yielding tulipalin A. It is proposed that tuliposides possess a storage function, being compartmentalized in vacuoles and acting as prodrugs. The TgTCE1 enzymes are organized in plastids, both in intact tulips tissues. Due to cellular damage by infection or wounding, those molecules are released, finally converting 6-tuliposide A to tulipalin A and glucose. Some other examples of prodrugs are the fatty acid esters of some sesquiterpenes. In this case, some *Russula* spp. produce sesquiterpene alcohols which are esterified with fatty acids. These fatty acid esters do not display strong antibiotic activities. However, when the fruiting body is injured esterases are activated which cleave the ester bond and release the free alcohols. These alcohols are either very labile and react to a number of products or they are the substrates for enzymes which

transform them into a multitude of products. These products are chemically very reactive, hence toxic on the one hand but instable on the other hand [233, 234].
Comatuslactone and tulipalins possess a very similar structure, and it would not be a surprise if both are derived from a similar precursor. Comatuslactone was always detected after 35 days of incubation, which would corroborate to a mycelial storage derived product. Moreover, due to long incubation periods, the cells are normally lysed, liberating the glycol-complex, which is hydrolysed through enzymatic activity or environmental conditions, yielding glucose and comatuslactone. No antimicrobial activity was detected in fruiting bodies and mycelia extracts.
Although bacterial community analyses from *C. comatus* fruiting bodies demonstrated an efficient infection control mechanism, it improbable that comatuslactone is responsible for those regulations. This was already demonstrated by Stadler and Sterner, 1998 [69], when several Basidiomycotina fungi were tested for biological activities before and after their respective fruiting bodies injury. In this case, *C. comatus* mushrooms did not exhibit any activity or changes in their chemical profiling after injury. Nevertheless, it is still not clear if comatuslactone **9** is a self-defense agent, stored as a glyco-complex, in the cells of *C. comatus* vegetative mycelia.

6.4.1 Biological activities

6.4.1.1 Antimicrobial activity

Comatuslactone exhibited bacteriostatic properties against both Gram-positive and Gram-negative bacteria. To provide more details about the possible mechanism of action of this compound, *P. aeruginosa* and *S. aureus* cells treated with comatuslactone were subjected to ultrastructural analysis, using TEM. Membrane damage, causing extracellular leakage, is clearly observed in *P. aeruginosa* micrographs, together with black dots of unknown origin. Regarding *S. aureus*, myelin-like structures could be seen in the treated cells, as well as a substantial reduction on the cellular diameter.
In 1982, Wecke *et al.* [235] investigated ultrastructural changes on *S. aureus* cells treated with lysozyme. Among several alterations observed, myelin-like structures were also recognized. Lysozyme catalyses the hydrolysis of the β-1-4 bond between N-acetylmuramic (NAM) acid and N-acetylglucosamine (NAG), the building blocks of the bacterial cell wall peptidoglycan. The lysozyme mechanism of action was described on 1969, by Chipman and Sharon [236].
Peptidoglycan biosynthesis is catalyzed, in its first step, by the UDP-N-acetylglucosamine 1- carboxyvinyltransferase (MurA). This enzyme has been evaluated as a target for antibacterial drug discovery. Fosfomycin is the only MurA inhibitor in clinical use [237, 238]. In 2010, Mendgen *et al.* [238] have described MurA inactivation by tulipalin B and 1-tuliposide B. Interestingly, no enzyme inhibition was detected when tulipalin A was employed. All of those compounds showed antimicrobial activity against a broad range of bacteria [239]. Further assays using a fosfomycin resistant MurA *E. coli* mutant revealed no resistance against tulipalin derivatives, demonstrating other targets than MurA [251].
Considering the ultrastuctural modifications of the bacterial cells towards the presence of comatuslactone and its similarity with tulipalin B, two mechanisms of action are proposed to comatuslactone **9**:

a Membrane destabilization. In this case, comatuslactone would interact with negatively charged lipids, causing membrane permeabilization;

b Inactivation of MurA.

Both proposed mechanisms remain to be investigated in detail.

6.4.1.2 Biofilm damaging and dispersal

S. aureus biofilms are commonly associated with osteomyelitis, periodontitis and peri-implantitis, endocarditis, chronic rhinosinusites, ocular and chronic wound infections. Furthermore, those biofilms characterize chronic polymer-associated infections, where indwelling devices are colonized, causing a chronic condition [240, 241]. Infections caused by *S. aureus* biofilms are related to a mortality rate of 25% in the USA [254].
Despite its bacteriostatic activity, comatuslactone **9** was effective in *P. aeruginosa* and *S. aureus* biofilm damage as well as in *P. aeruginosa* biofilm dispersal, although no inhibition on biofilm formation was detected. Even when concentrations below the MICs were employed, those activities were further observed.
Compared to planktonic bacterial cells, biofilms are much more resistant against antibiotics, heavy metals and disinfectants [32, 242]. Considering *S. aureus* biofilms, it was already demonstrated that oxacillin, cefotaxime and vancomycin diffusion is deficient into the matrix [243]. Moreover, in 2011, Thurlow *et al.* [244] showed that inflammatory mediator production and macrophage invasion are attenuated by *S. aureus*, when growing on biofilms.
P. aeruginosa biofilms are associated with urinary tract, ocular, ears and burned wound infections and most of the lung infections in cystic fibrosis patients. As *S. aureus*, *P. aeruginosa* also colonizes medical devices, leading to a chronic condition [245, 246]. A number of studies have been performed in order to understand the mechanisms underlying biofilms resistance against antibiotics. In 2013, Hengzhuang *et al.* [247] showed accumulation of beta-lactamases in *P. aeruginosa* biofilms matrix. Increased resistance was also demonstrated against tobramycin. In this case, extracelluar DNA was suggested to bind the aminoglycosides, decreasing their penetration into the biofilm [28, 248]. Moreover, the low growth rates of the cells embedded in the lowest biofilm layers, also contributed to an increased resistance against antibiotics [1, 28, 32].
One novel approach to control biofilm infections is the interference with the QS systems, *quorum quenching* (QQ), which have been correlated with virulence factors production as well as biofilm formation [53, 61]. Following this rational, a number of natural products which exhibit the capacity of inhibiting or dispersing bacterial biofilms were already identified. Furanones from the macroalga *Delisea pulchra* (Rhodophyta) are such QQ compounds and are capable of inhibiting a number of QS-controlled phenotypes, including virulence factors. Moreover, those compound scaffolds inspired a number of research for their synthetic derivatives [53, 54, 55, 56, 57]. Plants such as carrots, garlic, habanero (chili), and water lily also produce compounds that interfere with bacterial QS systems. Garlic extracts were demonstrated to be able to clear pulmonary *P. aeruginosa* infections in mouse models, and ajoene was recognized as the major QS inhibitor [62, 63, 64, 65, 66]. Therefore, comatuslactone **9** *quorum quenching* properties was evaluated using two mutants: (a) *E. coli* MT102 (pSB403) - a reporter for genes *lux*, responding to short chain

AHLs [130] and (b) *P. putida* F117 (pKR-C12) - based on the *las* QS-system of *P. aeruginosa*, responding to long chain AHLs [131]. Our results showed an inhibition of both QS systems. Additionally, it was demonstrated that comatuslactone **9** inhibits the QS products pyocyanin and rhamnolipid B, in an assay using *P. aeruginosa* PA14.
P. aeruginosa AHL-mediated QS system is based on the V. fisheri luxIR homologous system, consisting of LasI and LasR (responding to 3-oxo-C12-HSL) and and RhlI and RhlR (responding to responsive to C4-HSL). Those systems control the expression of several virulence genes, such as alkaline protease (aprA), exotoxin A (toxA), pyocyanin, pyoverdine, the Xcp translocation machinery, cyanide, lipase, rpoS, twitching motility, azurin (azu), alginate and chitinase, as well as catalase and superoxide dismutase (katA, sodA and sodB) [249, 250]. Biofilm formation is essential for *P. aeruginosa* pathogenicity and persistence. However, its relation with QS systems is not yet fully understood. Davey *et al.* 2003 [251], working with a *P. aeruginosa* PAO1 mutant strain uncapable of synthesize rhamnolipids, demonstrated that those molecules regulate biofilm architecture, without affecting initial biofilm formation. Furthermore, rhamnolipid B displayed hemolytic and biosurfactant properties. In 2007, it was demonstrated by Jensen *et al.* [252] that rhamnolipid B affects polymorphonuclear leukocytes (PMNs), causing necrosis and enabling *P. aeruginosa* persistence in the lungs. HPLC-MS-MS experiments using *P. aeruginosa* cultures treated with comatuslactone **9** demonstrated rhamnolipid B production inhibition. 3D reconstructions of the *in vitro* treated biofilms showed a volume decrease of approximately 85% with the employment of 37.5 μg/ml of comatuslactone. Besides QS and rhamnolipid B inhibition, no initial biofilm inhibition was detected.
Moreover, inhibition of pyocyanin production was also investigated using comatuslactone. Pyocyanin causes alterations of calcium concentrations in the cytoplasmic matrix of the epithelial cells, inhibiting their ciliary activity and leading to lung damage. It was demonstrated that pyocyanin also inhibits the expression of interleukin (IL)-2 and its receptor and stimulates IL-8 release in human epithelial cells [253]. Usually, a spectrophotometric method, described by Essar *et al.* [254] is used to perform this assay. Here, a HPLC-MS-MS method was developed for pyocyanin quantification in culture media. Comatuslactone **9** inhibited pyocyanin production by 80%. Synthetic autoinducer-mimics were investigated by Morkunas *et al.* 2012 [255] who found that most compounds antagonized pyocyanin production, whereas no structure activity relations could be established. Raloxifene, an oral selective oestrogen receptor modulator was also reported to inhibit pyocyanin biosynthesis [256].
The results of interference with QS systems were dispersed and thinner biofilms, together with the decrease of virulence factor expression. Hence, biofilms become more accessible to antibiotic therapies and to the host immune system.

6.4.1.3 Cytotoxicity to eukaryotic cells

Results obtained with an impedance method assay, showed no cytotoxic mechanisms associated with comatuslactone. Moreover, cell morphology visualized by fluorescence microscopy suggested that comatuslactone acts as a cytostatic compound. Interestingly, despite their structural similarities, it was reported that tulipalin A possesses an IC_{50} value of 0.8 μg ml^{-1} [257]. This compound is known for causing contact allergies among workers in the tulip fields. Guinea pigs have been used for sensitization against aller-

genic compounds and both (+)-tulipalin A, and (-)-tulipalin A showed positive reactions. On the other hand, when tulipalin B was evaluated, the positive reactions were enantiospecific, while (-)-tulipalin B showed no such effect. The synthetic (+)- and (-)-beta-hydroxy-gamma-methyl-alpha-methylene-gamma-butyrolactones were also evaluated by Papageorgiou *et al.* 1988 [228]. Here it is critical to emphasize that (-)-beta-hydroxy-gamma-methyl-alpha-methylene-gamma-butyrolactone was isolated in this work as the natural product comatuslactone **9**. As (-)-tulipalin B it did not sensitize the tested animals [228, 229].
Nevertheless, further characterization of comatuslactone **9** regarding its impact on eukaryotic systems is required in order to evaluate possible applications concerning human health.
Moreover, with the data obtained within this work in combination with the literature reports about tulipalins on their biological activities it is possible to propose:

a The hydroxy group decreases the toxicity of tulipalin B and comatuslactone against fungi and increases at the same time the toxicity against bacteria; on the other hand, the lack of this hydroxyl-group (tulipalin A) increases the toxicity against eukaryotic cells.

b The methylene group is essential for the biological activities, since (2S, 3R, 4S)-2-methyl-3,4-dihydroxypentanoic acid 1,4-lactone did not show any of the evaluated activities.

Chapter 7

Concluding remarks

Fungi are known as a rich source of bioactive compounds. Therefore the present study aimed the use of those organisms to produce metabolites with biofilm modulatory properties. The rationale employed was based on fungal self-defense mechanisms, since their sporocarps offer ideal substrata for bacterial colonization with subsequent biofilm formation. Moreover, fungal vegetative mycelia share ecological niches with bacteria, insects and other fungi, which imposes successful competition strategies for survival. Here, for the first time, bacterial communities associated with mushrooms were evaluated addressing biofilm modulators compounds research. The obtained results demonstrated interesting data, as the lack of bacterial attachment on the surface of certain fungi, particularly *C. comatus*. From this species, a compound, named comatuslactone, showing bacteriostatic, biofilm and *quorum sensing* modulating properties was successfully isolated. Comatuslactone was demonstrated to be cytostatic against eukaryotic cells. Nevertheless, its effects on such cells should be further characterized in order to evaluate its possible uses in the clinics. Regarding the interactions of fungi with their bacterial neighbours, the exploitation of such synergies may be a valuable approach on drug discovery programs. Additionally, 6 roridins and fusidic acid were purified from the parasitic fungus *C. arbuscula*. Roridins have been evaluated as anticancer compounds and show selectivity for eukaryotic organisms. However, their applicability on human therapy is still not clear, since the exact mechanism of cytotoxicity is unknown. Nevertheless, a number of roridins show specificity against cancer cell lines, but again the structure requirements which could improve such feature are still unidentified. Studies on their structure activity relationships are highly recommended. All of the roridins produced by *C. arbuscula* possessed C-6'S-configuration. This is the first report of such stereospecificity. *C. arbuscula*, which parasites other fungi, shows two faces: it produces at the same time compounds responsible for human and animal intoxications and crop diseases, as well as an antibiotic already used in the clinics, especially against methicillin resistant *S. aureus*. These findings demonstrate that ecological considerations can be useful in drug discovery.

Chapter 8

Supplementary material

8.1 Screening

Figure 8.1: Fruiting bodies of some mushrooms used in this work. A-*Macrolepiota fuliginosa*, B-*Laetiporus sulphureus*, C-*Pholiota lenta* and D-*Russula emetica*.

Figure 8.2: Fruiting bodies used for the SSCP fingerprint analysis. A-*Boletus edulis*, B-*Boletus edulis*, C-*Coprinopsis atramentaria* and D-*Boletus edulis*.

8.2 Quantitavive HPLC-MS/MS

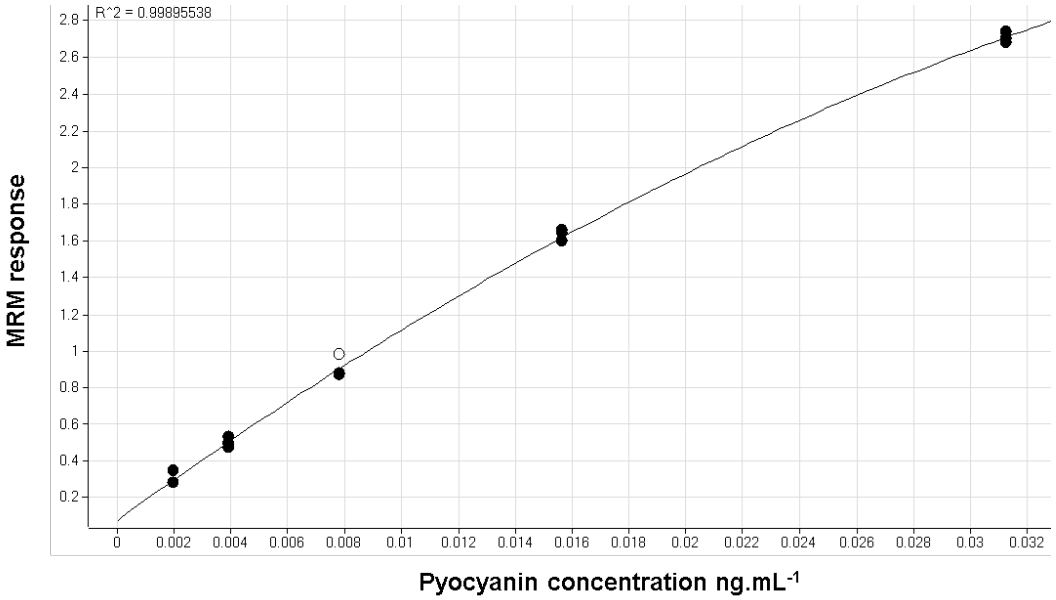

Figure 8.3: Pyocyanin standard curve.

Bibliography

[1] Stewart, P. S. and M. J. Franklin. Physiological heterogeneity in biofilms. Nature Reviews Microbiology 6 (3): 199-210 (2008).

[2] Costerton, J. W., Z. Lewandowski, *et al.* Microbial biofilms. Annual Review of Microbiology 49: 711-745 (1995).

[3] Costerton, J. W., P. S. Stewart, *et al.* Bacterial biofilms: a common cause of persistent infections. Science 284 (5418): 1318-1322 (1999).

[4] O'Toole, G., H. B. Kaplan, *et al.* Biofilm formation as microbial development. Annual Review of Microbiology 54: 49-79 (2000).

[5] Donlan, R. M. Biofilms: microbial life on surfaces. Emerging Infectious Diseases 8 (9): 881-890 (2002).

[6] Abraham, W.-R. Controlling pathogenic Gram-negative bacteria by interfiring with their biofilm formation. Drug Design Reviews 2 (1): 1-21 (2005).

[7] Karatan, E. and P. Watnick. Signals, regulatory networks, and materials that build and break bacterial biofilms. Microbiology and Molecular Biology Reviews 73 (2): 310-347 (2009).

[8] McDougald, D., S. A. Rice, *et al.* Should we stay or should we go: mechanisms and ecological consequences for biofilm dispersal. Nature Reviews. Microbiology 10 (1): 39-50 (2012).

[9] Flemming, H. C. and J. Wingender. The biofilm matrix. Nature Reviews. Microbiology 8 (9): 623-633 (2010).

[10] Branda, S. S., A. Vik , *et al.* Biofilms: the matrix revisited. Trends in Microbiology 13 (1): 20-26 (2005).

[11] Monroe, D. Looking for chinks in the armor of bacterial biofilms. PLoS Biology 5 (11): e307 (2007).

[12] Nealson, K. H., T. Platt, *et al.* Cellular control of the synthesis and activity of the bacterial luminescent system. Journal of Bacteriology 104 (1): 313-322 (1970).

[13] Eberhard, A., A. L. Burlingame, *et al.* Structural identification of autoinducer of Photobacterium fischeri luciferase. Biochemistry 20 (9): 2444-2449 (1981).

[14] Fuqua, W. C., S. C. Winans, *et al. Quorum sensing* in bacteria: the LuxR-LuxI family of cell density-responsive transcriptional regulators. Journal of Bacteriology 176 (2): 269-275 (1994).

[15] Taga, M. E. and B. L. Bassler. Chemical communication among bacteria. Proceedings of the National Academy of Sciences of the United States of America 100 (2): 14549-14554 (2003).

[16] Choudhary, S. and C. Schmidt-Dannert. Applications of *quorum sensing* in biotechnology. Applied Microbiology and Biotechnology 86 (5): 1267-1279 (2010).

[17] Fuqua, C. and E. P. Greenberg. Listening in on bacteria: acyl-homoserine lactone signalling. Nature Reviews. Molecular Cell Biology 3 (9): 685-695 (2002).

[18] Churchill, M. E., H. M. Sibhatu, *et al.* Defining the structure and function of acyl-homoserine lactone autoinducers. Methods in Molecular Biology 692: 159-171 (2011).

[19] Abraham, W. R. Controlling biofilms of Gram-positive pathogenic bacteria. Current Medicinal Chemistry 13 (13): 1509-1524 (2006).

[20] Waters, C. M. and B. L. Bassler. *Quorum sensing*: cell-to-cell communication in bacteria. Annual Review of Cell and Developmental Biology 21: 319-346 (2005).

[21] Hentzer, M. and M. Givskov. Pharmacological inhibition of *quorum sensing* for the treatment of chronic bacterial infections. The Journal of Clinical Investigation 112 (9): 1300-1307 (2003).

[22] Fux, C. A., J. W. Costerton, *et al.* Survival strategies of infectious biofilms. Trends in Microbiology 13 (1): 34-40 (2005).

[23] Burmolle, M., T. R. Thomsen, *et al.* Biofilms in chronic infections - a matter of opportunity - monospecies biofilms in multispecies infections. FEMS Immunology and Medical Microbiology 59 (3): 324-336 (2010).

[24] Hall-Stoodley, L. and P. Stoodley. Evolving concepts in biofilm infections. Cellular Microbiology 11 (7): 1034-1043 (2009).

[25] Parsek, M. R. and P. K. Singh. Bacterial biofilms: an emerging link to disease pathogenesis. Annual Review of Microbiology 57: 677-701 (2003).

[26] Macfarlane, S. and J. F. Dillon. Microbial biofilms in the human gastrointestinal tract. Journal of Applied Microbiology 102 (5): 1187-1196 (2007).

[27] von Rosenvinge, E. C., G. A. O'May, *et al.* Microbial biofilms and gastrointestinal diseases. Pathogens and Disease 67 (1): 25-38 (2013).

[28] Hall-Stoodley, L., J. W. Costerton, *et al.* Bacterial biofilms: from the natural environment to infectious diseases. Nature Reviews. Microbiology 2 (2): 95-108 (2004).

[29] Fux, C. A., P. Stoodley, *et al.* Bacterial biofilms: a diagnostic and therapeutic challenge. Expert Review of Anti-infective Therapy 1 (4): 667-683 (2003).

[30] Hall-Stoodley, L., P. Stoodley, *et al.* Towards diagnostic guidelines for biofilm-associated infections. FEMS Immunology and Medical Microbiology 65 (2): 127-145 (2012).

[31] Stewart, P. S. Mechanisms of antibiotic resistance in bacterial biofilms. International Journal of Medical Microbiology 292 (2): 107-113 (2002).

[32] Hoiby, N., T. Bjarnsholt, *et al.* Antibiotic resistance of bacterial biofilms. International Journal of Antimicrobial Agents 35 (4): 322-332 (2010).

[33] Mah, T. F., B. Pitts, *et al.* A genetic basis for *Pseudomonas aeruginosa* biofilm antibiotic resistance. Nature 426 (6964): 306-310 (2003).

[34] Bjarnsholt, T. The role of bacterial biofilms in chronic infections. Acta Pathologica, Microbiologica et Imunologica Scandinavica 136: 1-58 (2013).

[35] Macedo, A. and W.R. Abraham. Can infectious biofilm be controlled by blocking bacterial communication? Medicinal Chemistry 5 (6): 517-528 (2009).

[36] Kostakioti, M., M. Hadjifrangiskou, *et al.* Bacterial biofilms: development, dispersal, and therapeutic strategies in the dawn of the postantibiotic era. Cold Spring Harbor Perspectives in Medicine 3 (4): a010306 (2013).

[37] Batoni, G., G. Maisetta, *et al.* Use of antimicrobial peptides against microbial biofilms: advantages and limits. Current Medicinal Chemistry 18 (2): 256-279 (2011).

[38] Richards, J. J. and C. Melander. Controlling bacterial biofilms. Chembiochem: a European Journal of Chemical Biology 10 (14): 2287-2294 (2009).

[39] Ranall, M. V., M. S. Butler, *et al.* Resolving biofilm infections: current therapy and drug discovery strategies. Current Drug Targets 13 (11): 1375-1385 (2012).

[40] Kolodkin-Gal, I., S. Cao, *et al.* A self-produced trigger for biofilm disassembly that targets exopolysaccharide. Cell 149 (3): 684-692 (2012).

[41] Parra-Ruiz, J., C. Vidaillac, *et al.* Activities of high-dose daptomycin, vancomycin, and moxifloxacin alone or in combination with clarithromycin or rifampin in a novel *in vitro* model of *Staphylococcus aureus* biofilm. Antimicrobial Agents and Chemotherapy 54 (10): 4329-4334 (2010).

[42] Allison, K. R., M. P. Brynildsen, *et al.* Metabolite-enabled eradication of bacterial persisters by aminoglycosides. Nature 473 (7346): 216-220 (2011).

[43] Favre-Bonte, S., T. Kohler, *et al.* Biofilm formation by *Pseudomonas aeruginosa*: role of the C4-HSL cell-to-cell signal and inhibition by azithromycin. The Journal of Antimicrobial Chemotherapy 52 (4): 598-604 (2003).

[44] Gillis, R. J. and B. H. Iglewski. Azithromycin retards *Pseudomonas aeruginosa* biofilm formation. Journal of Clinical Microbiology 42 (12): 5842-5845 (2004).

[45] Clardy, J. and C. Walsh. Lessons from natural molecules. Nature 432 (7019): 829-837 (2004).

[46] Beghyn, T., R. Deprez-Poulain, *et al.* Natural compounds: leads or ideas? Bioinspired molecules for drug discovery. Chemical Biology & Drug Design 72 (1): 3-15 (2008).

[47] Butler, M. S. The role of natural product chemistry in drug discovery. Journal of Natural Products 67 (12): 2141-2153 (2004).

[48] Baker, D. D., M. Chu, *et al.* The value of natural products to future pharmaceutical discovery. Natural Product Reports 24 (6): 1225-1244 (2007).

[49] Newman, D. J. Natural products as leads to potential drugs: an old process or the new hope for drug discovery? Journal of Medicinal Chemistry 51 (9): 2589-2599 (2008).

[50] Chin, Y. W., M. J. Balunas, *et al.* Drug discovery from natural sources. The AAPS Journal 8 (2): E239-253 (2006).

[51] Kingston, D. G. Modern natural products drug discovery and its relevance to biodiversity conservation. Journal of Natural Products 74 (3): 496-511 (2011).

[52] Rasmussen, T. B. and M. Givskov. *quorum sensing* inhibitors as anti-pathogenic drugs. International Journal of Medical Microbiology 296 (2-3): 149-161 (2006).

[53] Hentzer, M., K. Riedel, *et al.* Inhibition of *quorum sensing* in *Pseudomonas aeruginosa* biofilm bacteria by a halogenated furanone compound. Microbiology 148 (1): 87-102 (2002).

[54] Hentzer, M., H. Wu, *et al.* Attenuation of *Pseudomonas aeruginosa* virulence by *quorum sensing* inhibitors. The EMBO Journal 22 (15): 3803-3815 (2003).

[55] de Nys, R., A. D. Wright, *et al.* New halogenated furanones from the marine alga *Delisea pulchra* (cf. fimbriata). Tetrahedron 49 (48): 11213-11220 (1977).

[56] Wu, H., Z. Song, *et al.* Synthetic furanones inhibit *quorum sensing* and enhance bacterial clearance in *Pseudomonas aeruginosa* lung infection in mice. The Journal of Antimicrobial Chemotherapy 53 (6): 1054-1061 (2004).

[57] Borchardt, S. A., E. J. Allain, *et al.* Reaction of acylated homoserine lactone bacterial signaling molecules with oxidized halogen antimicrobials. Applied and Environmental Microbiology 67 (7): 3174-3179 (2001).

[58] Cavallito, J.C and J. H. Bailey. Allicin, the antibacterial principle of *Allium satioum.* I. Isolation, physical properties and antibacterial action. Journal of the American Chemical Society 66: 1950-1951 (1944).

[59] Rasmussen, T. B., T. Bjarnsholt, *et al.* Screening for *quorum sensing* inhibitors (QSI) by use of a novel genetic system, the QSI selector. Journal of Bacteriology 187 (5): 1799-1814 (2005).

[60] Rasmussen, T. B. and M. Givskov. *quorum sensing* inhibitors: a bargain of effects. Microbiology 152 (4): 895-904 (2006).

[61] Jakobsen, T. H., M. van Gennip, *et al.* Ajoene, a sulfur-rich molecule from garlic, inhibits genes controlled by *quorum sensing*. Antimicrobial Agents and Chemotherapy 56 (5): 2314-2325 (2012).

[62] Persson, T., T. H. Hansen, *et al.* Rational design and synthesis of new *quorum sensing* inhibitors derived from acylated homoserine lactones and natural products from garlic. Organic & Biomolecular Chemistry 3 (2): 253-262 (2005).

[63] Bjarnsholt, T., P. O. Jensen, *et al.* Garlic blocks *quorum sensing* and promotes rapid clearing of pulmonary *Pseudomonas aeruginosa* infections. Microbiology 151 (12): 3873-3880 (2005).

[64] Yamanaka, A., R. Kimizuka, *et al.* Inhibitory effects of cranberry juice on attachment of oral streptococci and biofilm formation. Oral Microbiology and Immunology 19 (3): 150-154 (2004).

[65] LaPlante, K. L., S. A. Sarkisian, *et al.* Effects of cranberry extracts on growth and biofilm production of *Escherichia coli*and *Staphylococcus* species. Phytotherapy Research 26 (9): 1371-1374 (2012).

[66] Worthington, R. J., J. J. Richards, *et al.* Small molecule control of bacterial biofilms. Organic & Biomolecular Chemistry 10 (37): 7457-7474 (2012).

[67] O'Brien, J. and G. D. Wright. An ecological perspective of microbial secondary metabolism. Current Opinion in Biotechnology 22 (4): 552-558 (2011).

[68] Spiteller, P. Chemical defence strategies of higher fungi. Chemistry 14 (30): 9100-9110 (2008).

[69] Stadler, M. and O. Sterner. Production of bioactive secondary metabolites in the fruit bodies of macrofungi as a response to injury. Phytochemistry 49 (4): 1013-1019 (1998).

[70] Brase, S., A. Encinas, *et al.* Chemistry and biology of mycotoxins and related fungal metabolites. Chemical Reviews 109 (9): 3903-3990 (2009).

[71] Keller, N. P., G. Turner, *et al.* Fungal secondary metabolism - from biochemistry to genomics. Nature Reviews. Microbiology 3 (12): 937-947 (2005).

[72] Aly, A. H., A. Debbab, *et al.* Fifty years of drug discovery from fungi. Fungal Diversity 50 (1): 3-19 (2011).

[73] Dias, D. A., S. Urban, *et al.* A historical overview of natural products in drug discovery. Metabolites 2 (4): 303-336 (2012).

[74] Hoffmeister, D. and N. P. Keller. Natural products of filamentous fungi: enzymes, genes, and their regulation. Natural Product Reports 24 (2): 393-416 (2007).

[75] Simpson, T. J. and R. J. Cox. Polyketide biosynthesis: fungi. In: Wiley Encyclopedia of Chemical Biology: 1-11 (2008).

[76] Cox, R. J. Polyketides, proteins and genes in fungi: programmed nano-machines begin to reveal their secrets. Organic & Biomolecular Chemistry 5 (13): 2010-2026 (2007).

[77] Raistrick, H. and C. E. Stickings. Chemistry of the fungi. Annual Review of Biochemistry 25: 225-256 (1956).

[78] Lee, I. K. and B. S. Yun. Styrylpyrone-class compounds from medicinal fungi *Phellinus* and *Inonotus* spp., and their medicinal importance. The Journal of Antibiotics 64 (5): 349-359 (2011).

[79] Osmanova, N., W. Schultze, *et al.* Azaphilones: a class of fungal metabolites with diverse biological activities. Phytochemistry Reviews 9 (2): 315-342 (2010).

[80] Robbins, W. J., F. Kavanagh, *et al.* Antibiotics from basidiomycetes: II. *Polyporus biformis*. Proceedings of the National Academy of Sciences of the United States of America 33 (6): 176-182 (1947).

[81] Zjawiony, J. K. Biologically active compounds from Aphyllophorales (polypore) fungi. Journal of Natural Products 67 (2): 300-310 (2004).

[82] Bauerle, J., T. Anke, *et al.* Antibiotics from basidiomycetes. 16. Antimicrobial and cytotoxic polyines from *Mycena viridimarginata* Karst. Archives of Microbiology 132 (2): 194-196 (1982).

[83] Jente, R., F. Bosold, *et al.* Tetra-acetylenic metabolites from *Mycena viridimarginata*. Phytochemistry 24 (3): 553-559 (1985).

[84] Lorenzen, K. and T. Anke. Basidiomycetes as a source for new bioactive natural products. Current Organic Chemistry 2 (4): 329-364 (1998).

[85] Kavanagh, F., A. Hervey, *et al.* Antibiotic substances from basidiomycetes: VI. *Agrocybe dura*. Proceedings of the National Academy of Sciences of the United States of America 36 (2): 102-106 (1950).

[86] Rosa, L. H., E. M. Souza-Fagundes, *et al.* Cytotoxic, immunosuppressive and trypanocidal activities of agrocybin, a polyacetylene produced by *Agrocybe perfecta* (Basidiomycota). World Journal of Microbiology & Biotechnology 22 (6): 539-545 (2006).

[87] Nair, M. S. R. and M. Anchel. Frustulosinol, an antibiotic metabolite of *Stereum frustulosum* - revised structure of frustulosin. Phytochemistry 16 (3): 390-392 (1977).

[88] Goddard, M. L. and R. Tabacchi. Total synthesis of bioactive frustulosin and frustulosinol. Tetrahedron Letters 47 (6): 909-911 (2006).

[89] Ali, N. A. A., R. Jansen, *et al.* Hispolon, a yellow pigment from *Inonotus hispidus*. Phytochemistry 41(3): 927-929 (1996).

[90] Ali, N. A. A., R. A. A. Mothana, *et al.* Antiviral activity of Inonotus hispidus. Fitoterapia 74 (5): 483-485 (2003).

[91] Closse, A. and D. Hauser. Isolierung und konstitutionsermittlung von Chrysodin. Helvetica Chimica Acta 56 (8): 2694-2698 (1973).

[92] Haraguchi, H., M. Taniguchi, *et al.* Chrysodin, an antifungal antimetabolite. Agricultural and Biological Chemistry 54 (8): 2167-2168 (1990).

[93] Anke, T., F. Oberwinkler, *et al.* The strobilurins - new antifungal antibiotics from the basidiomycete *Strobilurus tenacellus*. The Journal of Antibiotics 30 (10): 806-810 (1977).

[94] Stadler, M., V. Hellwig, *et al.* Novel analgesic triglycerides from cultures of *Agaricus macrosporus* and other basidiomycetes as selective inhibitors of neurolysin. The Journal of antibiotics 58 (12): 775-786 (2005).

[95] Stadler, M., H. Anke, *et al.* Novel bioactive azaphilones from fruit bodies and mycelial cultures of the ascomycete *Bulgaria inquinans* (Fr). Natural Product Letters 7 (1): 7-14 (1995).

[96] Hayashi, M., K. Wada, *et al.* New nematocidal metabolites from a fungus, *Irpex lacteus*. Agricultural and Biological Chemistry 45 (6): 1527-1529 (1981).

[97] Cavill, G. W. K., P. S. Clezy, *et al.* The chemistry of mould metabolites. III. Tetrahedron 5 (4): 275-280 (1959).

[98] Smania, E. D. A., A. Smania, *et al.* Cinnabarin synthesis by *Pycnoporus sanguineus* strains and antimicrobial activity against bacteria from food products. Revista de Microbiologia 30 (1): 89-89 (1999).

[99] Walsh, C. T. Polyketide and nonribosomal peptide antibiotics: modularity and versatility. Science 303 (5665): 1805-1810 (2004).

[100] Schwarzer, D., R. Finking, *et al.* Nonribosomal peptides: from genes to products. Natural Product Reports 20 (3): 275 (2003).

[101] Saboulard, D., A. Gaspar, *et al.* New antiherpetic nucleoside from a basidiomycete. Comptes Rendus de L Academie des Sciences Serie III- Sciences de la Vie- Life Sciences 321 (7): 585-591 (1998).

[102] Weber, D., G. Erosa, *et al.* Cylindrocyclin A, a new cytotoxic cyclopeptide from *Cylindrocarpon* sp. The Journal of Antibiotics 59 (8): 495-499 (2006).

[103] Guo, H. J., B. D. Sun, *et al.* Diketopiperazines from the *Cordyceps* colonizing fungus *Epicoccum nigrum*. Journal of Natural Products 72 (12): 2115-2119 (2009).

[104] Guimaraes, D. O., W. S. Borges, *et al.* Diketopiperazines produced by endophytic fungi found in association with two Asteraceae species. Phytochemistry 71 (11-12): 1423-1429 (2010).

[105] de Carvalho, M. P. and W. R. Abraham. Antimicrobial and biofilm inhibiting diketopiperazines. Current Medicinal Chemistry 19 (21): 3564-3577 (2012).

[106] Abraham, W. R. Bioactive sesquiterpenes produced by fungi: are they useful for humans as well? Current Medicinal Chemistry 8 (6): 583-606 (2001).

[107] Simon, B., T. Anke, *et al.* Collybial, a new antibiotic sesquiterpenoid from *Collybia confluens* (basidiomycetes). Zeitschrift Fur Naturforschung C-a Journal of Biosciences 50 (3-4): 173-180 (1995).

[108] Yamamoto, T., N. Izumi, *et al.* Wickerols A and B: novel anti-influenza virus diterpenes produced by *Trichoderma atroviride* FKI-3849. Tetrahedron 68 (45): 9267-9271 (2012).

[109] Stadler, M., T. Anke, *et al.* Phellodonic acid, a new biologically active hirsutane derivative from *Phellodon melaleucus* (Thelephoraceae, basidiomycetes). Zeitschrift für Naturforschung. C, Journal of Biosciences 48 (7-8): 545-549 (1993).

[110] Paterson, R. R. Ganoderma - a therapeutic fungal biofactory. Phytochemistry 67 (18): 1985-2001 (2006).

[111] Kupka, J., T. Anke, *et al.* Antibiotics from basidiomycetes .14. Isolation and biological characterization of hypnophilin, pleurotellol, and pleurotellic acid from *Pleurotellus hypnophilus* (Berk). Archives of Microbiology 130 (3): 223-227 (1981).

[112] Abate, D. and W. R. Abraham. Antimicrobial metabolites from *Lentinus crinitus*. The Journal of Antibiotics 47 (11): 1348-1350 (1994).

[113] Souza-Fagundes, E. M., B. B. Cota, *et al.* In vitro activity of hypnophilin from *Lentinus strigosus*: a potential prototype for Chagas disease and leishmaniasis chemotherapy. Brazilian Journal of Medical and Biological Research 43 (11): 1054-1061 (2010).

[114] Stadler, M., H. Anke, *et al.* 6 new antimicrobial and nematocidal bisabolanes from the basidiomycete *Cheimonophyllum candidissimum*. Tetrahedron 50 (44): 12649-12654 (1994).

[115] Ishikawa, N. K., Y. Fukushi, *et al.* Antimicrobial cuparene-type sesquiterpenes, enokipodins C and D, from a mycelial culture of *Flammulina velutipes*. Journal of Natural Products 64 (7): 932-934 (2001).

[116] Opatz, T., H. Kolshorn, *et al.* . Sterelactones: new isolactarane type sesquiterpenoids with antifungal activity from *Stereum* sp. IBWF 01060. Journal of Antibiotics 61 (9): 563-567 (2008).

[117] Stark, A., T. Anke, *et al.* Antibiotics from basidiomycetes. 27. Lentinellic acid, a biologically-active protoilludane derivative from *Lentinellus* species (basidiomycetes). Zeitschrift Für Naturforschung C-a Journal of Biosciences 43 (3-4): 177-183 (1988).

[118] Scopel, M., W. R. Abraham, *et al.* Dipeptide cis-cyclo(Leucyl-Tyrosyl) produced by sponge associated *Penicillium* sp. F37 inhibits biofilm formation of the pathogenic *Staphylococcus epidermidis*. Bioorganic & Medicinal Chemistry Letters 23 (3): 624-626 (2013).

[119] Rasmussen, T. B., M. E. Skindersoe, *et al.* Identity and effects of *Quorum sensing* inhibitors produced by *Penicillium* species. Microbiology 151(5): 1325-1340 (2005).

[120] Zhu, H., S. Wang, *et al.* Inhibiting effect of bioactive metabolites produced by mushroom cultivation on bacterial *quorum sensing* regulated behaviors. Chemotherapy 57 (4): 292-297 (2011).

[121] Bruns, T. D., R. Fogel, *et al.* Amplification and sequencing of DNA from fungal herbarium specimens. Mycologia 82 (2): 175-184 (1990).

[122] Schwieger, F. and C. C. Tebbe. A new approach to utilize PCR single strand conformation polymorphism for 16S rRNA gene-based microbial community analysis. Applied and Environmental Microbiology 64 (12): 4870-4876 (1998).

[123] Wos-Oxley, M. L., I. Plumeier, *et al.* A poke into the diversity and associations within human anterior nare microbial communities. The ISME Journal 4 (7): 839-851 (2010).

[124] Bassam, B. J., G. Caetano-Anolles, *et al.* Fast and sensitive silver staining of DNA in polyacrylamide gels. Analytical Biochemistry 196 (1): 80-83 (1991).

[125] Bauer, A. W., W. M. Kirby, *et al.* Antibiotic susceptibility testing by a standardized single disk method. American Journal of Clinical Pathology 45 (4): 493-496 (1966).

[126] Spurr, A. R. A low-viscosity epoxy resin embedding medium for electron microscopy. Journal of Ultrastructure Research 26 (1): 31-43 (1969).

[127] Yakimov, M. M., P. N. Golyshin, *et al. Alcanivorax borkumensis* gen. nov., sp. nov., a new, hydrocarbon degrading and surfactant producing marine bacterium." International Journal of Systematic Bacteriology 48 (2): 339-348 (1998).

[128] Reynolds, E. S. The use of lead citrate at high pH as an electron-opaque stain in electron microscopy. The Journal of Cell Biology 17: 208-212 (1963).

[129] Merritt, J. H., D. E. Kadouri, *et al.* Growing and analyzing static biofilms. Current Protocols in Microbiology Chapter 1: Unit 1B (2005).

[130] Steidle, A., K. Sigl, *et al.* Visualization of N-acylhomoserine lactone mediated cell-cell communication between bacteria colonizing the tomato rhizosphere. Applied and Environmental Microbiology 67 (12): 5761-5770 (2001).

[131] Winson, M. K., S. Swift, *et al.* Construction and analysis of luxCDABE-based plasmid sensors for investigating N-acyl homoserine lactone mediated *quorum sensing*. FEMS Microbiology Letters 163 (2): 185-192 (1998).

[132] Cramer, N., S. Helbig, *et al.* Synthesis and biological properties of cylindramide derivatives: evidence for calcium-dependent cytotoxicity of tetramic acid lactams. Chembiochem: a European journal of chemical biology 9 (15): 2474-2486 (2008).

[133] Solly, K., X. Wang, *et al.* Application of real-time cell electronic sensing (RT-CES) technology to cell-based assays. Assay and Drug Development Technologies 2 (4): 363-372 (2004).

[134] Atienza, J. M., N. Yu, *et al.* Dynamic and label-free cell-based assays using the real-time cell electronic sensing system. Assay and Drug Development Technologies 4 (5): 597-607 (2006).

[135] Abassi, Y. A., B. Xi, *et al.* Kinetic cell-based morphological screening: prediction of mechanism of compound action and off-target effects. Chemistry & Biology 16 (7): 712-723 (2009).

[136] W. N. Venables & B. D. Ripley. Modern Applied Statistics with S (4th ed.). 508pp. Springer New York (2002).

[137] G. R. Warnes. Gplots: Various R programming tools for plotting data. Retrieved from http://cran.r-project.org/package=gplots (2010).

[138] Ke, N., B. A. Xi, *et al.* Screening and identification of small molecule compounds perturbing mitosis using time-dependent cellular response profiles. Analytical Chemistry 82 (15): 6495-6503 (2010).

[139] Schneider, T., Y. Muthukumar, *et al.* Deciphering intracellular targets of organochalcogen based redox catalysts. MedChemComm 3 (7): 784-787 (2012).

[140] Clarke, K. R. Non-parametric multivariate analyses of changes in community structure. Austral Ecology 18 (1): 117-143 (1993).

[141] Clarke, K. R. and R. M. Warwick. A further biodiversity index applicable to species lists: variation in taxonomic distinctness. Marine Ecology Progress Series 216: 265-278 (2001).

[142] Watson, P. *Calcarisporium arbuscula* living as endophyte in apparently healthy sporophores of *Russula* and Lactarius. Transactions of the British Mycological Society 38 (4):409-414 (1955).

[143] Cole, J. R., Q. Wang, *et al.* The Ribosomal Database Project: improved alignments and new tools for rRNA analysis. Nucleic Acids Research 37: D141-145 (2009).

[144] Gouy, M., S. Guindon *et al.* SeaView version 4: a multiplatform graphical user interface for sequence alignment and phylogenetic tree building. Molecular Biology and Evolution 27 (2): 221-224 (2010).

[145] Tamura, K., D. Peterson, *et al.* MEGA5: molecular evolutionary genetics analysis using maximum likelihood, evolutionary distance, and maximum parsimony methods. Molecular Biology and Evolution 28 (10): 2731-2739 (2011).

[146] Scheithauer, B. K., M. L. Wos-Oxley, *et al.* Characterization of the complex bacterial communities colonizing biliary stents reveals a host-dependent diversity. The ISME Journal 3 (7): 797-807 (2009).

[147] Jarvis, B. B. and S. Wang. Stereochemistry of the roridins. Diastereomers of roridin E. Journal of Natural Products 62 (9): 1284-1289 (1999).

[148] Saikawa, Y., H. Okamoto, *et al.* Toxic principles of a poisonous mushroom *Podostroma cornu-damae*. Tetrahedron 57 (39): 8277-8281 (2001).

[149] Matsumoto, M. M., H.; Tori, K.; Ueyama, M. Strucutres of isororidin E, epoxyisororidin E, and epoxy- and diepoxyroridin H, new metabolites isolated from *Cylindrocarpon* species determined by Carbon- 13 and Hydrogen- 1 NMR spectroscopy. Tetrahedron Letters 47: 4093-4096 (1977).

[150] Traxler, P. and C. Tamm. 215. Die struktur des Antibioticums Roridin H. Verrucarine und Roridine, 20. Mitteilung. Helvetia Chimica Acta 53: 1846-1869 (1970).

[151] Abraham, W.-R. and B. Stumpf. Enzymatic acyloin condensation of acyclic aldehydes. Zeitschrift für Naturforschung 42c: 559-566 (1987).

[152] Wagenaar, M. M. and J. Clardy. Two new roridins isolated from *Myrothecium* sp. The Journal of Antibiotics 54 (6): 517-520 (2001).

[153] Zhang, S. Y., Z. L. Li, *et al.* Structure determination of two new trichothecenes from a halotolerant fungus *Myrothecium* sp. GS-17 by NMR spectroscopy. Magnetic Resonance in Chemistry 50 (9): 632-636 (2012).

[154] Kupchan, S. M., D. R. Streelman, *et al.* Isolation of potent new antileukemic trichothecenes from *Baccharis megapotamica*. The Journal of Organic Chemistry 42 (26): 4221-4225 (1977).

[155] Jarvis, B. B., G. P. Stahly, *et al.* Isolation and characterization of the trichoverroids and new roridins and verrucarins. The Journal of Organic Chemistry 47: 1117-1124 (1982).

[156] Yu, N. J., S. X. Guo, *et al.* Cytotoxic macrocyclic trichothecenes from the mycelia of *Calcarisporium arbuscula* Preuss. Journal of Asian Natural Products Research 4 (3): 179-183 (2002).

[157] Jarvis, B. B., G. P. Stahly, *et al.* Structure of roridin J, a new macrocyclic trichothecene from *Myrothecium verrucaria*. The Journal of Antibiotics 33 (2): 256-258 (1980).

[158] Rastrup-Andersen, N. and T. Duvold. Reassignment of the1H NMR spectrum of fusidic acid and total assignment of1H and13C NMR spectra of some selected fusidane derivatives. Magnetic Resonance in Chemistry 40 (7): 471-473 (2002).

[159] Barbier, P. and C. Benezra. Allergenic alpha-methylene-gamma-butyrolactones. Beta-Hydroxy-alpha-methylene-gamma-butyrolactones. 2. Syntheses from ethyl 2-(phenylthio)propionate and .alpha.-acetoxy aldehydes. The Journal of Organic Chemistry 48(16): 2705-2709 (1983).

[160] Bernardi, A., M. G. Beretta, *et al.* Synthetic opportunities offered by anti alpha-methylene-beta-hydroxy-gamma-alkoxy esters: stereoselective reactions at the double bond. The Journal of Organic Chemistry 50 (23): 4442-4447 (1985).

[161] Lorenzo, M., I. Brito, et al.. 13C NMR-based empirical rules to determine the configuration of fatty acid butanolides. Novel gamma-dilactones from Pterogorgia spp. Organic Letters 8 (22): 5001-5004 (2006).

[162] Boer, W., L. B. Folman, *et al.* Living in a fungal world: impact of fungi on soil bacterial niche development. FEMS Microbiology Reviews 29 (4): 795-811 (2005).

[163] Warmink, J. A., R. Nazir, *et al.* Universal and species-specific bacterial 'fungiphiles' in the mycospheres of different basidiomycetous fungi. Environmental Microbiology 11 (2): 300-312 (2009).

[164] Kumari, D., M. S. Reddy, *et al.* Diversity of cultivable bacteria associated with fruiting bodies of wild Himalayan *Cantharellus* spp. Annals of Microbiology 63 (3): 845-853 (2012).

[165] Sbrana, C., M. Agnolucci, *et al.* Diversity of culturable bacterial populations associated to *Tuber borchii* ectomycorrhizas and their activity on *T. borchii* mycelial growth. FEMS Microbiology Letters 211 (2): 195-201 (2002).

[166] Voronina, E. Y., L. V. Lysak, *et al.* The quantity and structure of the saprotrophic bacterial complex of the mycorhizosphere and hyphosphere of symbiotrophic basidiomycetes. Biology Bulletin 38 (6): 622-628 (2011).

[167] Zagriadskaia, Y. A., L. V. Lysak, *et al.* Bacterial complexes of the fruiting bodies and hyphosphere of certain basidiomycetes. Biology Bulletin 40 (4): 358-364 (2013).

[168] Dahm H, W. WrÃştniak, *et al.* Diversity of culturable bacteria associated with fruiting bodies of ectomycorrhizal fungi. Phytopathologia Polonica 38: 51-62 (2005).

[169] Kataoka, R., T. Taniguchi, *et al.* Comparison of the bacterial communities established on the mycorrhizae formed on *Pinus thunbergii* root tips by eight species of fungi. Plant and Soil 304 (1-2): 267-275 (2008).

[170] Scheublin, T. R., I. R. Sanders, *et al.* Characterisation of microbial communities colonising the hyphal surfaces of arbuscular mycorrhizal fungi. The ISME Journal 4 (6): 752-763 (2010).

[171] Warmink, J. A. and J. D. van Elsas. Selection of bacterial populations in the mycosphere of *Laccaria proxima*: is type III secretion involved? The ISME Journal 2 (8): 887-900 (2008).

[172] Galan, J. E. and A. Collmer. Type III secretion machines: bacterial devices for protein delivery into host cells. Science 284 (5418): 1322-1328 (1999).

[173] Watson, P. Further observations on *Calcarisporium arbuscula*. Transactions of the British Mycological Society 48 (1): 9-17 (1965).

[174] Mulheirn, L.J., R.B. Beechey, *et al.* Aurovertin B, a metabolite of *Calcarisporium arbuscula*. Journal of the Chemical Society, Chemical Communications 21: 874-876 (1974).

[175] Osselton, M.D., H.Baum, *et al.* Isolation, purification and characterization of aurovertin B Biochemical Society Transactions, 544th Meeting 2: 200-202 (1974).

[176] Steyn, P.S., R. Vleggaar, *et al.* Biosynthesis of the Aurovertins B and D. The role of methionine and propionate in the simultaneous operation of two independent biosynthetic pathways. Journal of the Chemical Society, Perkin Transactions 1 1:1298-1308 (1981).

[177] Trapp, S.C., T.M. Hohn, *et al.* Characterization of the gene cluster for biosynthesis of macrocyclic trichothecenes in *Myrothecium roridum*. Molecular and General Genetics 257 (4): 421-432 (1998).

[178] McCormick, S.P., A.M. Stanley, *et al.* Trichothecenes: from simple to complex mycotoxins. Toxins 3 (7): 802-814 (2011).

[179] Desjardins, A.E., T. M. Hohn, *et al.* Trichothecenes biosynthesis in Fusarium species: Chemistry, genetics, and significance. Microbiological Reviews 57: 595-604 (1993).

[180] Shank, R.A., N.A. Foroud, *et al.* Current and future experimental strategies for structural analysis of trichothecenes mycotoxins - a prospectus. Toxins 3: 1518-1553 (2011).

[181] Li, Y., Z. Wang, *et al.* T-2 toxin, a trichothecene mycotoxin: review of toxicity, metabolism, and analytical methods. Journal of Agricultural and Food Chemistry 59 (8): 3441-3453 (2011).

[182] Jarvis, B.B., J.O Midiwo, *et al.* The mystery of trichothecene antibiotics in *Baccharis* species. Journal of Natural Products 51 (4): 736-744 (1988).

[183] Jarvis, B.B., J.O Midiwo, *et al.* Stereochemistry of the roridins. Journal of Natural Products, 45 (4): 440-448 (1982).

[184] Cardoza, R. E., M. G. Malmierca, *et al.* Identification of loci and functional characterization of trichothecene biosynthesis genes in filamentous fungi of the genus *Trichoderma*. Applied and Environmental Microbiology 77 (14): 4867-4877 (2011).

[185] Grove, J. F. The trichothecenes and their biosynthesis. In: Progress in the Chemistry of Organic Natural Products 88: 63-130 (2007).

[186] Godtfredsen, W. O., S. Jahnsen, *et al.* Fusidic acid: a new antibiotic. Nature 193: 987 (1962).

[187] Kuznetsova, T. A., O. F. Smetanina, *et al.* The identification of fusidic acid, a steroidal antibiotic from marine isolate of the fungus *Stilbella aciculosa*. Biochemical Systematics and Ecology 29 (8): 873-874 (2001).

[188] Pfaller, M. A., M. Castanheira, *et al.* Evaluation of the activity of fusidic acid tested against contemporary Gram-positive clinical isolates from the USA and Canada. International Journal of Antimicrobial Agents 35 (3): 282-287 (2010).

[189] Evans, L., J. N. Hedger, *et al.* An antibacterial hydroxy-fusidic acid analogue from Acremonium crotocinigenum. Phytochemistry 67 (19): 2110-2114 (2006).

[190] O'Neill, A. J., J. M. Bostock, *et al.* Antimicrobial activity and mechanisms of resistance to cephalosporin P1, an antibiotic related to fusidic acid. The Journal of Antimicrobial Chemotherapy 50 (6): 839-848 (2002).

[191] Schappert, K.T.K., H.A. Koshinsky, *et al.* Growth inhibition of yeast by T-2, HT-2, T-2 triol, T-2 tetraol, diacetoxyscirpenol, verrucarol, verrucarin A, and roridin A mycotoxins. Journal of the American College of Toxicology 5 (2): 181-187 (1986).

[192] Liu, J.Y., L.L. Huang, *et al.* Antifungal and new metabolites of *Myrothecium* sp. Z16, a fungus associated with white croaker *Argyrosomus argentatus*. Journal of Applied Microbiology 100 (1):195-202 (2006).

[193] Bennett, J.W. and M. Klich. Mycotoxins. Clinical Microbiology Reviews 16 (3): 497-516 (2003).

[194] Ueno, Y. The toxicology of mycotoxins. Critical Reviews in Toxicology 14 (2): 99-132 (1985).

[195] Rocha, O., K . Ansari, *et al.* Effects of trichothecene mycotoxins on eukaryotic cells: a review. Food Additives and Contaminants, 22 (4):369-378 (2005).

[196] Amagata, T., C. Rath, *et al.* Structures and cytotoxic properties of trichoverroids and their macrolide analogues produced by saltwater culture of *Myrothecium verrucaria*. Journal of Medicinal Chemistry, 46 (20):4342-4350 (2003).

[197] Jarvis, B.B., J.O. Midiwo, *et al.* Antileukemic compounds derived by chemical modification of macrocyclic trichothecenes. 2. Derivatives of roridins A and H and verrucarins A and J. Journal of Medicinal Chemistry, 27 (2):239-244 (1984).

[198] Oda, T., J. Xu, *et al.* 12'-hydroxyl group remarkably reduces roridin E cytotoxicity. Mycoscience 51 (4): 317-320 (2010).

[199] Volkl, A., B. Vogler, *et al.* Microbial detoxification of mycotoxin deoxynivalenol. Journal of Basic Microbiology 44 (2):147-156 (2004).

[200] Karlovsky, P. Biological detoxification of the mycotoxin deoxynivalenol and its use in genetically engineered crops and feed additives. Applied Microbiology and Biotechnology 91 (3): 491-504 (2011).

[201] Böhner, B. And C. Tamm. Die konstitution von Roridin A. Verrucarine und Roridine, 11. Mitteilung. Helvetia Chimica Acta 49 (8): 2527-2546 (1966).

[202] Tamm, C. The antibiotic complex of the verrucains and roridins. Fortschritte der Chemie Organische Naturstoffe 31: 66-117 (1974).

[203] Xu, J., A. Takasaki, *et al.* Four new macrocyclic trichothecenes from two strains of marine-derived fungi of the genus *Myrothecium*. Journal of Antibiotics 59 (8): 451-455 (2006).

[204] Shimada, A., S.Takeuchi, *et al.* Roridin A and verrucarin A, inhibitors of pollen development in *Arabidopsis thaliana*, produced by *Cylindrocarpon* sp. Plant Science 166: 1307-1312 (2004).

[205] Isaka, M., J. Punya, *et al.* Antimalarial activity of macrocyclic trichothecenes isolated from the fungus *Myrothecium verrucaria*. Journal of Natural Products 62 (2): 329-331(1999).

[206] Garcia, C.C., M.L. Rosso, *et al.* Evaluation of the antiviral activity against Junin virus of macrocyclic trichothecenes produced by the hypocrealean epibiont of *Baccharis coridifolia*. Planta Medica 68 (3): 209-212 (2002).

[207] Laurent, D., G. Guella, *et al.* Cytotoxins, mycotoxins and drugs from a new deuteromycete, *Acremonium neo-caledoniae*, from the southwestern lagoon of New Caledonia. Planta Medica 66: 63-66 (2000).

[208] Böhner, B. and C. Tamm. Die konstitution von Roridin D. Verrucarine und Roridine, 12. Mitteilung. Helvetia Chimica Acta 49 (8): 2547-2554 (1966).

[209] Böhner, B., E. Fetz, *et al.* Über die isolierung von Verrucarin H, Verrucarin J, Roridin D und Roridin E aus Myrothecium - arten. Verrucarine und Roridine, 8. Mitteilung. Helvetia Chimica Acta 48 (5): 1079-1087 (1965).

[210] Traxler, P., W. Zurcher, *et al.* Die struktur des Antibiotikums Roridin E. Verrucarine und Roridine, 21. Mitteilung. Helvetia Chimica Acta 53 (8): 2071-2085 (1970).

[211] Abbas, H.K., B.B. Johnson, *et al.* Phytotoxicity and mammalian cytotoxicity of macrocyclic trichothecene mycotoxins from *Myrothecium verrucaria*. Phytochemistry 59 (3): 309-313 (2002).

[212] Namikoshi, M., K. Akano, *et al.* A new macrocyclic trichothecene, 12,13-deoxyroridin E, produced by the marine-derived fungus *Myrothecium roridum* collected in Palau. Journal of Natural Products 64 (3): 396-398 (2001).

[213] Alvi, K.A., J. Rabenstein, *et al.* 14'-Hydroxymytoxin B and 16-hydroxyroridin E, two new cytotoxic trichothecenes from *Myrothecium roridum*. Journal of Natural Products, 65 (5):742-744 (2002).

[214] Murakami, Y., T. Okuda, *et al.* Roridin L, M and verrucarin M, new macrocyclic trichothecene group antitumor antibiotics, from *Myrothecium verrucaria*. The Journal of Antibiotics 54 (11): 980-983 (2001).

[215] Ju, Y. M., H. M. Hsieh, *et al. Xylaria coprinicola*, a new species that antagonizes cultivation of *Coprinus comatus* in China. Mycologia 103 (2): 424-430 (2011).

[216] Tsai, S.Y., H.L. Tsai, *et al.* Antioxidant properties of *Coprinus comatus*. Journal of Food Biochemistry 33 (3): 368-389 (2009).

[217] Li, B., F. Lu, *et al.* Antioxidant properties of cap and stipe from *Coprinus comatus*. Molecules 15 (3): 1473-1486 (2010).

[218] Luo, H., M. Mo, *et al. Coprinus comatus*: A basidiomycete fungus forms novel spiny structures and infects nematode. Mycologia 96 (6): 1218-1224 (2004).

[219] Dotan, N., S. P. Wasser, *et al.* The culinary medicinal mushroom *Coprinus comatus* as a natural antiandrogenic modulator. Integrative Cancer Therapies 10 (2): 148-59 (2011).

[220] Zaidman, B.Z., S. P. Wasser, *et al. Coprinus comatus* and *Ganoderma lucidum* interfere with androgen receptor function in LNCaP prostate cancer cells. Molecular Biology Reports 35 (2):107-117 (2008).

[221] Ren, J., J. L. Shi, *et al.* Isolation and biological activity of triglycerides of the fermented mushroom of *Coprinus comatus*. BMC Complementary and Alternative Medicine 12: 52 (2012).

[222] Stojkovic, D., F.S. Reis, *et al.* Nutrients and non-nutrients composition and bioactivity of wild and cultivated *Coprinus comatus* (O.F.Müll.) Pers. Food and Chemical Toxicology 59: 289-296 (2013).

[223] Vamanu, E. In vitro antioxidant and antimicrobial activities of two edible mushroom mycelia obtained in the presence of different nitrogen sources. Journal of Medicinal Food 16 (2):155-166 (2013).

[224] Kitson, R. R. A., A. Millemaggi, *et al.* The renaissance of alpha-methylene-gamma-butyrolactones: new synthetic approaches. Angewandte Chemie International Edition 48 (50): 9426-9451 (2009).

[225] Dijkstra, F. Y. and T. O. Wiken. Studies on mushroom flavours 2. Flavour compounds in *Coprinus comatus*. Zeitschrift für Lebensmittel Untersuchung und Forschung 160 (3): 263-269 (1976).

[226] He, G., H. Matsura, *et al.* Isolation of an alpha-methylene-gamma-butyrolactone derivative, a toxin from the plant pathogen *Lasiodiplodia theobromae*. Phytochemistry 65 (20): 2803-2807 (2004).

[227] Nomura, T., S. Ogita, *et al.* A novel lactone forming carboxylesterase: molecular identification of a tuliposide A converting enzyme in tulip. Plant Physiology 159 (2): 565-578 (2012).

[228] Papageorgiou, C., J. L. Stampf, *et al.* Allergic contact dermatitis to tulips: an example of enantiospecificity. Archives of Dermatological Research 280 (1): 5-7 (1988).

[229] Lepoittevin, J. P., V. Berl, *et al.* Alpha-methylene-gamma-butyrolactones: versatile skin bioactive natural products. Chemical Record 9 (5): 258-270 (2009).

[230] Kato, Y., K. Shoji, *et al.* Purification and characterization of a tuliposide converting enzyme from bulbs of *Tulipa gesneriana*. Bioscience, Biotechnology, and Biochemistry 73 (8): 1895-1897 (2009).

[231] Kato, Y., H. Yoshida, *et al.* A facile method for the preparation of alpha-methylene-gamma-butyrolactones from tulip tissues by enzyme-mediated conversion. Tetrahedron Letters 50 (33): 4751-4753 (2009).

[232] van Rossum, M. W. P. C., M. Alberda, *et al.* Tulipaline and tuliposide in cultured explants of tulip bulb scales. Phytochemistry 49 (3): 723-729 (1998).

[233] Sterner, O., R. Bergman, *et al.* The sesquiterpenes of *Lactarius vellereus* and their role in a proposed chemical defense system. Journal of Natural Products 48 (2): 279-288 (1985).

[234] Sterner, O., O. Bergendorff, *et al.* The isolation of a guaiane sesquiterpene from fruit bodies of *Lactarius sanguifluus*. Phytochemistry 28 (9): 2501-2502 (1989).

[235] Wecke, J., M. Lahav, *et al.* Cell wall degradation of *Staphylococcus aureus* by lysozyme. Archives of Microbiology 131 (2): 116-123 (1982).

[236] Chipman, D. M. and N. Sharon. Mechanism of lysozyme action. Science 165 (3892): 454-465 (1969).

[237] Bachelier, A., R. Mayer, *et al.* Sesquiterpene lactones are potent and irreversible inhibitors of the antibacterial target enzyme MurA. Bioorganic & Medicinal Chemistry Letters 16 (21): 5605-5609 (2006).

[238] Mendgen, T., T. Scholz, *et al.* Structure-activity relationships of tulipalines, tuliposides, and related compounds as inhibitors of MurA. Bioorganic & Medicinal Chemistry Letters 20 (19): 5757-5762 (2010).

[239] Shigetomi, K., K. Shoji, *et al.* The antibacterial properties of 6-tuliposide B. Synthesis of 6-tuliposide B analogues and structure-activity relationship. Phytochemistry 71 (2-3): 312-324 (2010).

[240] Archer, N. K., M. J. Mazaitis, *et al. Staphylococcus aureus* biofilms: properties, regulation, and roles in human disease. Virulence 2 (5): 445-459 (2011).

[241] Götz, F. *Staphylococcus* and biofilms. Molecular Microbiology 43 (6): 1367-1378 (2002).

[242] Bridier, A., R. Briandet, *et al.* Resistance of bacterial biofilms to disinfectants: a review. Biofouling 27 (9): 1017-1032 (2011).

[243] Singh, R., P. Ray, *et al.* Penetration of antibiotics through *Staphylococcus aureus* and *Staphylococcus epidermidis* biofilms. The Journal of Antimicrobial Chemotherapy 65 (9): 1955-1958 (2010).

[244] Thurlow, L. R., M. L. Hanke, *et al. Staphylococcus aureus* biofilms prevent macrophage phagocytosis and attenuate inflammation *in vivo*. Journal of Immunology 186 (11): 6585-6596 (2011).

[245] Tseng, B. S., W. Zhang, *et al.* The extracellular matrix protects *Pseudomonas aeruginosa* biofilms by limiting the penetration of tobramycin. Environmental Microbiology: DOI: 10.1111/1462-2920.12155 (2013).

[246] Hoiby, N., O. Ciofu, *et al. Pseudomonas aeruginosa* biofilms in cystic fibrosis. Future Microbiology 5 (11): 1663-1674 (2010).

[247] Hengzhuang, W., O. Ciofu, *et al.* High beta-lactamase levels change the pharmacodynamics of beta-lactam antibiotics in *Pseudomonas aeruginosa* biofilms. Antimicrobial Agents and Chemotherapy 57 (1): 196-204 (2013).

[248] Chiang, W. C., M. Nilsson, *et al.* Extracellular DNA shields against aminoglycosides in *Pseudomonas aeruginosa* biofilms. Antimicrobial Agents and Chemotherapy 57 (5): 2352-2361 (2013).

[249] Jakobsen, T. H., T. Bjarnsholt, *et al.* Targeting *quorum sensing* in *Pseudomonas aeruginosa* biofilms: current and emerging inhibitors. Future Microbiology 8 (7): 901-921 (2013).

[250] Rumbaugh, K. P., J. A. Griswold, *et al.* The role of *quorum sensing* in the *in vivo* virulence of *Pseudomonas aeruginosa*. Microbes and Infection 2 (14): 1721-1731 (2000).

[251] Davey, M. E., N. C. Caiazza, *et al.* Rhamnolipid surfactant production affects biofilm architecture in *Pseudomonas aeruginosa* PAO1. Journal of Bacteriology 185 (3): 1027-1036 (2003).

[252] Jensen, P. O., T. Bjarnsholt, *et al.* Rapid necrotic killing of polymorphonuclear leukocytes is caused by *quorum sensing* controlled production of rhamnolipid by *Pseudomonas aeruginosa*. Microbiology 153 (5): 1329-1338 (2007).

[253] Fuse, K., S. Fujimura, *et al.* Reduction of virulence factor pyocyanin production in multidrug-resistant *Pseudomonas aeruginosa*. Journal of Infection and Chemotherapy 19 (1): 82-88 (2013).

[254] Essar, D. W., L. Eberly, *et al.* Identification and characterization of genes for a second anthranilate synthase in *Pseudomonas aeruginosa*: interchangeability of the two anthranilate synthases and evolutionary implications. Journal of Bacteriology 172 (2): 884-900 (1990).

[255] Morkunas, B., W. R. Galloway, *et al.* Inhibition of the production of the *Pseudomonas aeruginosa* virulence factor pyocyanin in wild-type cells by *quorum sensing* autoinducer-mimics. Organic & Biomolecular Chemistry 10 (42): 8452-8464 (2012).

[256] Ho Sui, S. J., R. Lo, *et al.* Raloxifene attenuates *Pseudomonas aeruginosa* pyocyanin production and virulence. International Journal of Antimicrobial Agents 40 (3): 246-251 (2012).

[257] Perry, N. B. and N. J. Brennan. Antimicrobial and cytotoxic phenolic glycoside esters from the New Zealand tree *Toronia toru*. Journal of Natural Products 60 (6): 623-626 (1997).